MACHINE LEARNING & DATA ANALYTICS

FRIEDRICH-ALEXANDER UNIVERSITÄT ERLANGEN-NÜRNBERG
TECHNISCHE FAKULTÄT

Influence of Acute Psychosocial Stress on Body Posture and Movement

Master's Thesis in Medical Engineering

submitted
by

Veronika Koch

born 07.05.1996 in Tegernsee

Written at

Machine Learning and Data Analytics Lab
Department Artificial Intelligence in Biomedical Engineering
Friedrich-Alexander-Universität Erlangen-Nürnberg (FAU)

Advisors:
Robert Richer M.Sc., Arne Küderle M.Sc., Dr.-Ing. Felix Kluge, Prof. Dr. Bjoern Eskofier
(Machine Learning and Data Analytics Lab, FAU Erlangen-Nürnberg)
Prof. Dr. Nicolas Rohleder
(Chair of Health Psychology, FAU Erlangen-Nürnberg)

Started: 15.02.2021

Finished: 16.08.2021

Ich versichere, dass ich die Arbeit ohne fremde Hilfe und ohne Benutzung anderer als der angegebenen Quellen angefertigt habe und dass die Arbeit in gleicher oder ähnlicher Form noch keiner anderen Prüfungsbehörde vorgelegen hat und von dieser als Teil einer Prüfungsleistung angenommen wurde. Alle Ausführungen, die wörtlich oder sinngemäß übernommen wurden, sind als solche gekennzeichnet.

Die Richtlinien des Lehrstuhls für Bachelor- und Masterarbeiten habe ich gelesen und anerkannt, insbesondere die Regelung des Nutzungsrechts.

Erlangen, den 16. August 2021

Übersicht

Akuter psychischer Stress tritt auf wenn eine Situation unkontrollierbar ist, die Anpassungsfähigkeit einer Person übersteigt oder wenn eine Situation mit einer sozialen Bewertung droht. Als Reaktion auf akuten Stress aktiviert der Körper die beiden wichtigsten Stresskanäle, das sympathische Nervensystem und die Hypothalamus-Hypophysen-Nebennierenrinden-Achse. Beide lösen starke physiologische Reaktionen aus, die das Arbeitsgedächtnis und die kognitive Flexibilität beeinträchtigen. Daher sind Stress und seine Folgen eines der wichtigsten sozialen Probleme in den Industrienationen, da sie das tägliche Leben und die berufliche Leistungsfähigkeit einschränken. Die Messung von Stress ist daher von steigendem Interesse, denn herkömmlichen Methoden beruhen auf komplexen und oft invasiven Laborverfahren. Daher sind neue BewertungsmodalitätenbenÃ¶tigt. Die Beobachtung von Makrobewegungen des Körpers könnte eine alternative Möglichkeit darstellen um eine akute Stressreaktion zu erfassen.

Daher wurde die Körperhaltung und -bewegung von 21 Teilnehmern mit einem Motion-Capture-Anzug unter dem Einfluss von Stress, induziert durch den Trier social stress test (TSST) und unter Kontrollbedingungen (friendly-TSST) erfasst. Anschließend wurden die unterschiedlichen Bewegungsmuster anhand von 181 Bewegungsmerkmalen analysiert. Zusätzlich wurden mehrere rückwärts gerichtete mehrfache lineare Regressionsanalysen durchgeführt, um die Beziehung zwischen Körperhaltung und Bewegung und den traditionellen Verfahren zur Stressbewertung wie Biomarkern und Selbsteinschätzungen zu bestimmen.

Zunächst wurde eine rückwärts gerichtete mehrfache lineare Regression durchgeführt, um festzustellen, ob stressbedingte Bewegungsänderungen durch Veränderungen von Cortisol und psychologischen Zustandsvariablen erklärt werden können. Bei der Vorhersage eines PCA-ermittelten Bewegungsfaktors durch die Biomarker und Selbstberichte wurde der PASA-Threat, ein bedrohungsassoziierter Score, als signifikanter Prädiktor für den PCA-ermittelten Bewegungsfaktor identifiziert. Der Score sagte 19,7% der Gesamtvarianz des PCA-Bewegungsfaktors voraus. Diese Ergebnisse bestätigen die Annahme, dass bedrohungsbezogene Bewegungsmuster gemessen wurden.

Zudem wurde die Regressionsanalyse umgekehrt, um zu untersuchen, inwiefern traditionelle Verfahren zur Stressbewertung durch Veränderungen der Körperhaltung und Bewegung verschiedener Körperteile vorhergesagt werden können. Bei der Durchführung mehrerer Regressionsanalyse waren die PCA-Bewegungsfaktoren, die aus verschiedenen Körperteilen ermittelt wurden, in der Lage, den PANAS-Negativ-Affekt (26,5% der Varianz), den PANAS-Positiv-Affekt (61,8% der Gesamtvarianz) und den PASA-Threat (79,6% der Gesamtvarianz) vorherzusagen. Die anschließende Vorhersage der Selbsteinschätzungen und Biomarker durch die extrahierten

Merkmale der einzelnen Körperteile zeigte, dass die Selbsteinschätzungen besser vorhergesagt werden konnten als die Biomarker. Zusätzlich wurde festgestellt, dass die Merkmale des Kopfes den höchsten Prozentsatz der Gesamtvarianz der Selbsteinschätzungen und Biomarker vorhersagen konnten. Allerdings waren nur die Merkmale der Arme in der Lage alle berücksichtigten Biomarker und Selbsteinschätzungen signifikant vorherzusagen.

Die Ergebnisse sind durch den starken Positions- und Rotationsdrift in den Mocap-Daten und der geringen Teilnehmerzahl an der Studie limitiert.

Abstract

Acute psychological stress occurs when a situation is uncontrollable, exceeds the ability of a person to adapt, or in a situation with a social evaluation threat. As a response to acute stress, the body activates the two main stress pathways, the sympathetic nervous system and the hypothalamic-pituitary-adrenocortical axis. Both induce strong physiological reactions that affect working memory and cognitive flexibility. Hence, stress and its consequences are one of the key social problems in industrialized nations as they limit daily life and working functions. Thus, stress measurement is a growing area of interest, but traditional methods are based on complex, often invasive, laboratory procedures. Hence, novel assessment modalities are required. An alternative way of capturing an acute stress reaction might be given by observing body macro-movements.

Thus, the body posture and movement of 21 participants was measured with a motion capture suit during the exposure of stress, conducted with the Trier social stress test (TSST) and in a control condition (friendly-TSST). Afterwards, the different movement patterns were analyzed using 181 movement features. Additionally, several backward multiple linear regression analyses were performed to determine the relationship between body posture and movement and the traditional stress assessment modalities, such as biomarkers and self-reports.

Firstly, a backward multiple linear regression was performed to assess whether stress-induced movement alterations can be explained by changes in cortisol and psychological state variables. By predicting a PCA obtained motion factor by the biomarkers and self-report, the PASA-Threat, a threat-associated score, was identified as a significant predictor for the PCA obtained motion factor. The score predicted 19.7% of the total variance of the PCA motion factor. These findings validate the assumption that threat-related movement patterns were measured.

Secondly, the regression analysis was inverted to examine to which extent traditional stress assessment modalities can be predicted by changes of body posture and movement of different body parts. While performing multiple regression analysis, PCA movement factors obtained from different body parts were able to predict the PANAS-Negative-Affect (26.5% of variance), PANAS-Positive-Affect (61.8% of total variance), and the PASA-Threat (79.6% of total variance).

Afterwards, prediction of the self-reports and biomarkers by the extracted features of single body parts showed that the self-reports could be predicted better than the biomarkers. Additionally, it was obtained, that features of the head were able to predict the highest percentage of the total variance of the self-reports and biomarkers. Just the features of the arms were able to predict all obtained biomarkers and self reports significantly. The reported results are limited by strong positional and rotational drift in the mocap data and a low number of participants.

Contents

Chapter 1

Introduction

Stress and its consequences are one of the key social problems in industrialized nations. Nowadays, most people have stressful events, and it not only limits their well-being but also has measurable effects on their health. Stressful events cause negative affective states such as feelings of anxiety and depression, which trigger biological processes that increase disease risk [Coh07]. These biological processes also affect working memory and cognitive flexibility, which are essential functions for daily life [Shi16]. These findings also have economic consequences as almost 50 percent of individuals indicated in a US study that stress has a negative influence on their working productivity [Coh07]. In 2017, the European Commission reported that work-related stress is one of the "most challenging - and growing - occupational safety and health problems" [Eur17]. Additionally, stress accounts for about half of absence days at work and leads to reduced work performance, which can increase the risk of accidents up to five times [Eur17].

Acute stress, such as psychosocial stress, occurs when a situation is uncontrollable, exceeds the ability to adapt, or in a situation with a social evaluation threat. Stressful situations are for example job interviews or exams. Acute stress induces strong physiological reactions that affect the whole body. As a response to acute psychosocial stress, the body activates the two main stress pathways. First, the sympathetic nervous system (SNS) induces the release of adrenaline as an immediate response, which affects the cardiovascular, pulmonary, skeletal muscle, and immune systems. These induce several physiological changes, like increased heart rate and blood pressure. As a second delayed response to stress, the hypothalamic-pituitary-adrenocortical (HPA) axis is activated, leading to the secretion of cortisol [Ulr09]. Cortisol modulates a large part of physiological processes, including anti-inflammatory reactions, the metabolism of carbohydrates, fats, and proteins. The activation of immune and inflammatory processes by repeated stress potentially affects depression, infectious, autoimmune, and coronary heart diseases [Coh07].

An acute stress reaction is typically assessed by "wet markers" such as saliva and blood samples as well as electrophysiological measurements, such as electrocardiograms and self-reports. These traditional methods are the gold standard for many years, but they are based on complex, often invasive, laboratory procedures, which limit biopsychological research. Hence, it is not feasible to measure stress in regular intervals. In addition, most of these methods induce additional stress, like taking a blood sample. Hence, novel and non-invasive, potentially even contactless, assessment modalities are required.

Another way of capturing an acute stress reaction might be given by observing body macro-movements. Such movements are often expressions of human emotion and, hence, have the potential to reflect acute psychosocial stress. Previous work has shown that humans can easily identify negative emotions just from body posture and movements, such as dropping the head, bringing hands to the face or the head, and crossing or bringing their hands in front of the body [Atk04]. Recent studies showed that individuals who were exposed to stress showed a reduction in hand movements [Pis18] and body sway [Dou18], which resulted in defensive "freezing behavior". Both studies assessed motion using Inertial Measurement Units (IMU). However, they only investigated a single movement parameter with IMUs and did not capture entire body posture and movements, which might provide additional insights for the assessment of acute psychosocial stress.

For that reason, this thesis attempts to investigate the influence of acute stress on body posture and movement with an IMU-based motion capture system. Thus, a stress study was conducted with 21 healthy subjects undergoing the Trier Social Stress Test (TSST) as a stress condition and the friendly version of the Trier Social Stress Test (f-TSST) as a non-stress condition. This study resulted in a dataset consisting of IMU-based motion capture data, salivary cortisol, alpha-amylase levels, and self-report questionnaire data. Based on the resulted dataset, a data processing pipeline was developed to extract measures for characterizing body posture and movement. Additionally, it was explored whether body posture and movement can be used to predict the magnitude of an endocrinological stress response.

The thesis is structured as follows: Chapter 2 presents the medical background, which is useful for understanding this thesis. Afterwards, the Related work (no. 3) is dealing with acute stress induction and stress-related motion changes. Chapter 4 shows the fundamentals of different motion capture systems. The methods chapter (no. 5) explains the data acquisition, data cleaning, and feature extraction, followed by the Evaluation chapter (no. 6), which is about the performed statistical methods. The obtained results of the thesis (Chapter 7) are discussed in Chapter 8. Finally, Chapter (no. 9) presents the Conclusions and Outlook of the conducted work.

Chapter 2

Medical Background

This chapter will give an introduction to the medical background which is needed for understanding the topic of this thesis. In the first part, the stress system and its consequences will be presented. In the second part, the consequences of stress are explained.

2.1 Stress Fundamentals

Stress is a well-known problem, however, it is difficult to precisely define. A famous definition is given by Hans Selye: “Stress is the nonspecific response of the body to any demand.” [Fin16]. Fink et al. discussed whether the term non-specificmay now be redundant since there is now extensive literature on the specificity of stressors and their physiological responses [Fin16]. Common stressors are situations involving social evaluation threat, such as job interviews or exams. Thus, possibly a more specific description of psychological stress is provided by Cohen et al. as “Psychological stress occurs when an individual perceives that environmental demands tax or exceed his or her adaptive capacity.” [Coh07].

As a physiological response to acute stress, the body activates the main stress pathways the *hypothalamic-pituitary-adrenocortical (HPA)* axis and the *sympathetic nervous system (SNS)*, both pathways originated in the hypothalamus. The SNS is the immediate stress response, and one main part of the autonomous nervous system (ANS) [Roh12]. The whole stress system is shown in Figure 2.1, on the left side the response of the HPA axis is given, and on the right one of the ANS. The ANS plays an important role in maintaining vital functions, like the regulation of blood pressure, the gastrointestinal response to food, thermoregulation, and additionally, the ANS is involved in many systematic diseases like heart failure. It contains two anatomically and functionally distinct systems, the SNS, and the parasympathetic nervous system (PSNS). These

two systems react as antagonists, where the SNS is responsible for the “fight-or-flight” response in emergency conditions. In contrast, the PSNS represents the “rest-and-digest response” and is activated during rest [McC07]. During exposure to stress, the SNS is immediately activated through the posterior hypothalamus, by sending signals through the sympathetic nerves to activate the body for the upcoming challenge [Che17]. These signals are stimulating the adrenal medulla to release the hormone adrenaline [Fol10] (Figure 2.1, left). The presence of adrenaline in the bloodstream leads to several physiological changes, like increased heart rate, heart rate variability and blood pressure [Ant17]. Adrenaline also has effects on the cardiovascular, pulmonary, skeletal muscle, and immune systems. The SNS activity can be measured by restricted (electro-) physiological measurements, such as skin conductance and heart rate or plasma measurements of adrenaline and noradrenaline [Roh04].

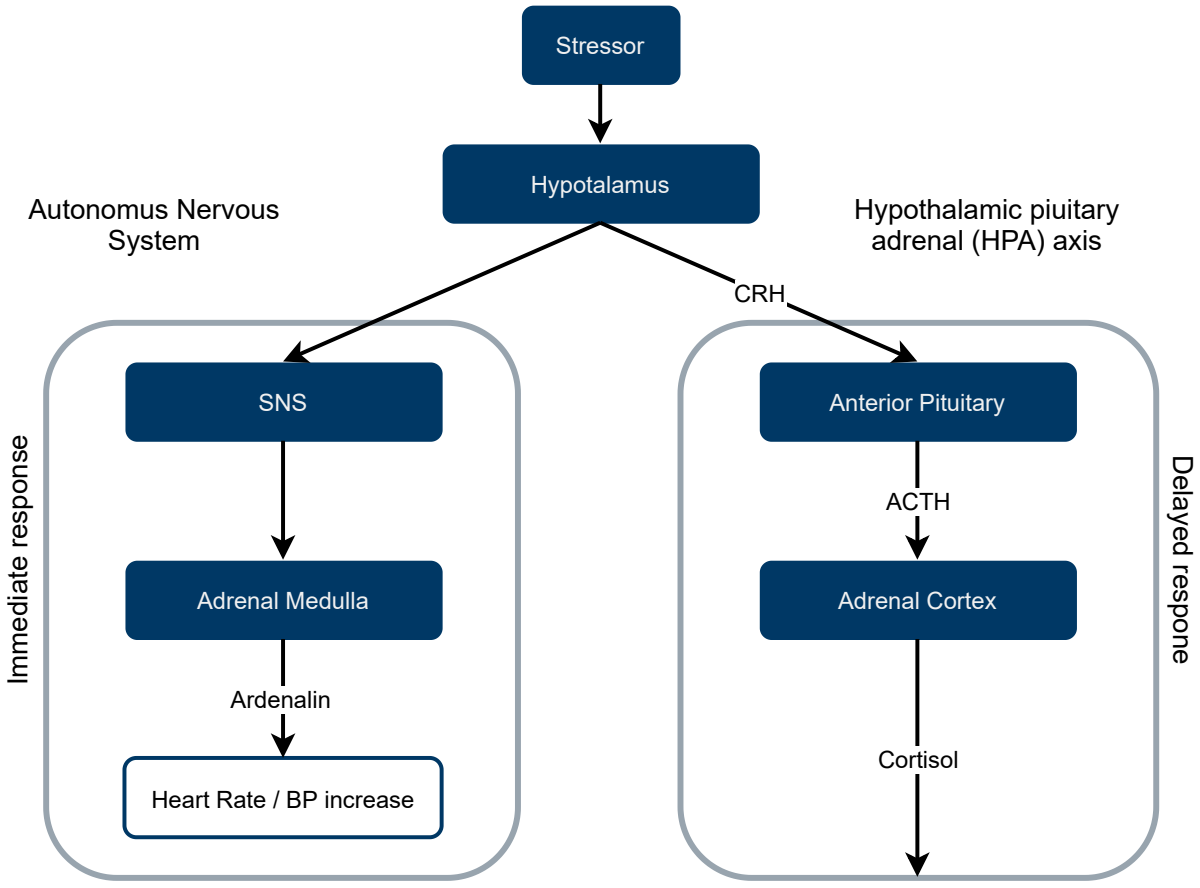

Figure 2.1: Schematic representation of the Stress System.
SNS: sympatic nervous system, CRH: corticotrophin-releasing hormone, ACTH: adrenocorticotropin hormone, BP: blood pressure; modified from [Ant17]

In contrast to this, the HPA axis is the delayed stress response and is activated by the medial hypothalamus to possibly compensate, enhance or suppress the consequences of the previous SNS activation [Che17]. Thus, the medial hypothalamus increases the release of the peptide corticotropin-releasing hormone (CRH), which is the hypothalamic regulator of the HPA axis. The increasing concentration of CRH stimulates the anterior pituitary to the secretion of adrenocorticotropin hormone (ACTH). Due to the ACTH in the systemic circulation, the adrenal cortex is stimulated to release glucocorticoids like cortisol into the bloodstream [Ulr09]. The cortisol concentration itself is regulated by a negative feedback loop to the hypothalamus (secretion of CRH) and the anterior pituitary (secretion of ACTH) [Cha05]. The HPA axis plays a central role in the generation of stress-associated diseases. Measuring the HPA is a useful tool to differentiate between patients and healthy persons. Cortisol is known as the "stress hormone" and is the best characterized HPA axis activation marker for an acute psychological stress response [Fol10]. The concentration of cortisol usually increases within a few minutes after exposure to stress and reaches its maximum concentration 10-30 min after stress occurrence [Fol10]. The increased cortisol concentration in the bloodstream then promotes mobilization of energy resources to activate the body for upcoming challenges [Ulr09]. The Cortisol concentration can be measured in blood or saliva samples, although saliva samples are usually used as sampling is stress-free and less invasive [Kir94].

2.2 Manifestations and Consequences of Stress

Normally, the response to acute psychosocial stress has a short duration over a couple of minutes to a few hours. If acute stress is repeatedly experienced over longer periods as days, weeks, or months, it might become chronic stress [Epe18]. Stress can be divided into acute and chronic stress, as acute stressors differ from chronic stressors. Acute stressors are short-term, for example, job interviews, public talks, or exams. In contrast to this, chronic stressors are long-term stressors, like caregiving, financial strain, or being in a conflictual relationship [Epe18]. Chronic stress results in long-term repeated activation of the stress system [Coh07]. As the activation of the HPA axis and the SNS can influence the cardiovascular, pulmonary, hepatic, skeletal muscle, anti-inflammation response, and immune systems, repeated activation can result in an increased risk for physical and psychiatric disorders. During acute stress the adrenaline and cortisol concentration increases, due to the activation of the stress system, which results in heart rate and blood pressure increase and in an inflammatory response. During chronic stress, the effects on the inflammatory process and the immune system can influence depression, coronary artery disease, or diabetes.

It can also influence allergic manifestations like asthma or eczema, autoimmune diseases, upper respiratory tract infections and wound healing [Coh07, Che17]. Due to the influence of the stress system on the skeletal muscle system, stress also induces changes in body movement and postural behavior, as a decrease in hand movement [Pis18, Zit19].

Chapter 3

Related Work

This chapter provides an overview of the related work about acute stress induction with laboratory stress protocols and motion data measurement to assess inner processes.

3.1 Acute Stress Induction

In the last 30 years, the research on stress highly increased, which resulted in a variety of well-described stress protocols to induce psychosocial stress in a laboratory setting. Dickerson and Kemeny conducted a meta-analysis of 208 laboratory studies of acute psychological stressors to find conditions that reliably activate the HPA axis. They conclude that tasks containing uncontrollable and social-evaluative elements result in the highest HPA axis activation and thus, the largest cortisol secretion [Dic04].

Two of the commonly used methods to induce acute psychological stress, both including uncontrollable and social-evaluative elements, are the *Montreal Imaging Stress Task (MIST)* [Ded05] and the *Trier Social Stress Test (TSST)* [Kir93]. The MIST was originally designed by Dedovic et al. based on the Trier Mental Challenge Test. It consists of solving mental arithmetic challenges with negative feedback. The main part of the MIST is a computer program that displays the arithmetic tasks. While participants solve the arithmetic problems, the remaining time is displayed as a progress bar on the screen. If the time limit has been reached, feedback is given before the next task starts. In addition, a bar comparing the individual performance of the participants to the average performance is displayed. The stress test is divided into three parts, after each task, the investigator provides negative feedback to the participant's performance [Ded05]. The MIST can also be carried out as a "control" condition, in which no time limit and feedback is presented, to remove the social-evaluative stressor components.

The *Trier Social Stress Test (TSST)* is the most popular protocol for inducing acute psychosocial stress in a laboratory environment and is the current gold standard [Bal15, All14]. The original version of the TSST protocol was developed by Kirschbaum et al. in 1993. It originally consisted of two periods, a preparation period (10 min) and a test period (10 min). In most TSST studies conducted nowadays, the preparation time is reduced to 5 minutes [Che17, Het09]. During the test period, the participants have to perform two tasks. First, they have to give a free speech (5 min), which they prepared right before the beginning of the TSST. Subsequently, they have to solve a mental arithmetic problem (5 min) [Kir93]. Both tasks are performed while standing in front of a committee of two people dressed in white coats [Het09]. During the procedure, a microphone and a video camera are pointed directly at the participant to induce additional pressure. Before the two periods, they are informed about the procedure and are told that the committee is specially trained in analyzing verbal and nonverbal behavior. They are additionally informed that video and audio recordings are captured to perform a voice frequency analysis afterwards [Kir93]. The free speech task is performed like an interview with standardized additional questions if the duration of the presentation was shorter than 5 minutes. During the mental arithmetic task, participants have to continuously subtract a two-digit (e.g. 17) number from a four-digit number (e.g 2043) and speak out loud [Bal15, Het09]. If the participant has made a mistake, the investigator makes him/her aware of it, and the participant has to start from the beginning. This procedure is repeated until 5 minutes are over. During the TSST procedure, salivary cortisol levels rise two to threefold in about 70-80 % of the tested subjects [Kud07].

As a control condition for the TSST, Wiemers et al. developed a friendly version of the Trier Social Stress Test (f-TSST). It is also divided into a preparation period (5 min) and a test period (10 min). During the preparation period, participants get a sheet of paper with questions about their curriculum vita, hobbies, favorite book, etc. After the preparation period, they have to talk about the prepared questions in front of the committee. In this condition, the committee does not wear white coats and behaves in a friendly manner, unlike during the TSST, to help participants feel safe. Due to this procedure, the f-TSST does not activate the HPA axis in contrast to the TSST [Wie13b, Wie15].

3.2 Assessment of inner processes by movement data

As illustrated in Chapter 1, psychological stress and its consequences are one of the key social problems in industrialized nations. Therefore, stress assessment is of great importance, but traditional methods are based on complex, often invasive laboratory procedures. Another possibility of

capturing an acute stress response could be by observing macro movements of the body. These movements are often expressions of human emotions. For that reason, they have the potential to be used for the detection of acute psychosocial stress. Previous work has shown that humans can identify negative emotions just from body posture and movements. Atkinson et al. showed that people easily recognize emotions from dynamic and static body expressions in point-light and full-light display movies. First, different emotions were captured in these movies by actors, afterwards, participants had to identify these emotions. From this study, the authors concluded that sadness can be characterized by three types of movements: Dropping the head, bringing the hands to the face, and crossing their arms in front of the body [Atk04]. Even though stress is not a specific emotion, stress creates negative emotions that affect body posture and movement.

Lasselin et al. conducted a study intending to determine the effect of inflammation on gait and motion in humans. For that, they induced systematic inflammation with an intravenous injection of lipopolysaccharide. Afterwards, biological movement parameters and inflammatory symptoms were assessed while walking and compared to a placebo group. Their results showed that participants with acute systematic inflammation walked more slowly, had a more downward tilted head than those without inflammation, and generally had a more rigid walking pattern. In the study, a step-wise backward multiple linear regression analysis was performed to predict LPS-induced motion alterations. Their results showed that during inflammation, sickness symptoms are related to higher motion alterations [Las20].

The work of Doumas et al. shows the strong correlation between stress and movement. They aimed to investigate if people show a reduction in body sway during an increasing exposure to stress. Psychological stress was triggered using a combination of an arithmetic task and a social evaluative threat (SET). Their results showed a significant reduction in body sway during exposure to stress [Dou18]. To investigate the different responses to the stress of healthy subjects and patients with functional movement disorders, Zito et al. induced stress with the TSST. They evaluated that their healthy controls showed a defensive “freezing behavior” which represents a reduction of body sway over time during exposure to stress. Their results also showed that the change in cortisol for the controls negatively correlated with the change in body sway over time, which was not the case for the patients with functional movement disorders [Zit19]. The topic of freezing in humans is well investigated. Participants who were looking at angry faces or affective films while standing on a stabilometric platform showed a significant reduction in body sway and freezing-like response [Roe10, Hag14].

Another study that shows the correlation of stress and movement during the TSST was conducted by Pisanski et al. They hypothesized that a multi-modal measurement could improve

stress detection. Therefore, they conducted a stress study collecting voice, polygraph, and saliva samples, before, during, and after stress induction via TSST. Their results showed remarkable systematic increases in voice pitch, cortisol level, and decreases in skin temperature and hand movement during exposure to psychosocial stress. The reduction in hand movement was measured with finger sensors [Pis18]. These results show that it is possible to measure stress-indicating behaviors with IMU-sensors.

The work of van der Zee et al. also deals with movement measurement. They used a motion capture approach to detect deceit. They used a full-body motion capture suit for data collection, which can record the position, velocity, and orientation of 23 joints. In their study, they compared the full-body movement of interviewees while lying or telling the truth. Before the interview, they instructed half of their participants to lie. For comparing the full-body movement they calculated the absolute movement of the whole participant's body. The absolute movement is the sum of joint displacements between two-time points. Their results are indicating that liars generally moved more than truth-tellers. They also were able to correctly classify 74.4% as truth-tellers or lairs using a binary logistic regression with two predictors [van19]. Aigrain et al. conducted a study for automatic stress detection from micro and macro movements. They conducted a stress study containing a time-constrained arithmetic task. Afterwards, they extracted features using video processing and depth data of the Microsoft Kinect. Using Support Vector Machine (SVM) they were able to detect stress with an accuracy of 77% [Aig15].

Chapter 4

Fundamentals

This chapter presents the fundamentals of motion capture (mocap). Motion capture is an approach to capture the movement of a real-world object (usually humans) and transfer it into a three-dimensional model [Sha19]. Currently, motion capturing is a growing and challenging area. Many mocap systems were developed in the last years, such as optical, image-based, or Inertial Measurement Units (IMU)-based. Mocap systems are widely employed in film-making, video gaming, sports, medicine, and many more areas.

Motion capture systems can be divided into optical motion capture systems and non-optical motion capture systems, whether a camera is used or not. As non-optical mocap systems, IMU-based mocap systems are mainly used, where a few IMU-sensors are attached to the body. Later, the orientations and positions are evaluated by the raw sensor data. Optical mocap systems can further be classified as marker-based and marker-less systems. While using marker-based systems, markers are placed on the human body with cameras tracking the positions of the markers. In contrast to the first two approaches, using optical marker-less systems, the participants do not have to wear any devices, as the human motion is only tracked by cameras. Because of their high accuracy, optical motion capture systems are still preferred in medical approaches to other mocap systems [Ser20, Zho08]. Table 4.1 compares the most commonly used motion capture types regarding accuracy, compactness, cost, and drawbacks.

Table 4.1: Comparison of different motion capture systems, modified [Zhou]

Systems	**Accuracy**	**Compactness**	**Coast**	**Drawbacks**
IMU-based	High	High	Low	Drifts
Maker-based	High	Low	Medium	Occlusion
Maker-less	High	High	Low	Occlusion

4.1 Optical Motion Capture Systems

In optical systems, cameras and image sensors capture 3D motion. Optical mocap systems can further be divided into marker-based systems and marker-less systems, depending on whether or not markers were attached to the body [Zhu16].

4.1.1 Marker-Based Motion Capture Systems

In optical marker-based motion capture systems, cameras are utilized to track human movement with the help of markers, placed on the human body. Afterwards, the 3D marker positions are computed by surrounding cameras with the help of triangulation methods [Vla07]. These systems are usually used in computer animation and film-making, because of their high accuracy and fast update rates. An example setup for a marker-based mocap system is provided in Figure 4.1. On top of the picture, cameras are placed around the room and the reflective markers are placed all over the human body. One disadvantage of these systems is the potential overlapping of body parts with markers, due to the complex rotations of the human joints.

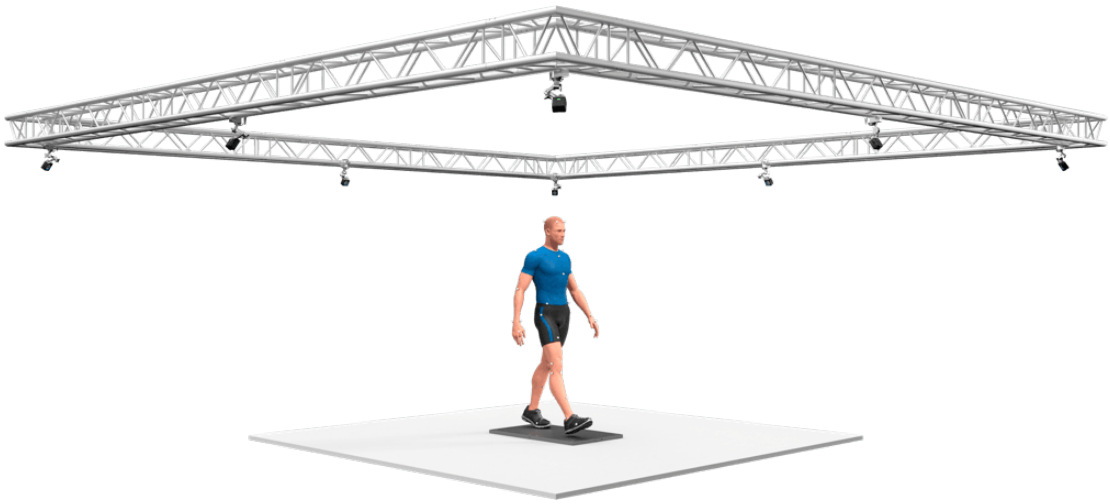

Figure 4.1: Example setup for a marker-based Motion Capture System. [Nat21]

The gold standard system is *VICON* (Soest, Germany). Because of the accurate position estimation, it is also popular in applications in medicine [Zhu16]. The *VICON* uses infrared cameras to track reflective markers on the human body. It was specially designed for virtual environments, but it is also often used in medical science for gait analysis to calculate joint center and segment orientations of the human body. Another maker-based mocap system is *Qualisyis* (Göteborg, Schweden) [Zho08], which also uses infrared cameras and reflective markers.

4.1.2 Marker-less Motion Capture

In contrast to marker-based systems, marker-less optical systems do not require markers or other additional equipment. The 3D position is only calculated from the camera data. Because of this, the systems are portable and low-cost. A well-known low cost example is *Microsoft's Kinect* (Redmond, Washington, USA) [Sha19], a sensor add-on for the Xbox 360. The *Kinect* was developed for video gaming to capture the movements of players interacting with the game without wearing controllers. The *Kinect v1* (Kinect Xbox 360) includes an infrared camera, a light projector, and an RGB video camera [Pfi14]. It uses 3D depth mapping to evaluate the 3D positions. Thus, the depth data is evaluated of the reflected infrared light and afterwards calibrated with the RGB camera (Figure 4.2) [Pfi14]. In contrast to this, the *Kinect v2* (Kinect Xbox One) includes infrared emitters and detectors and uses time-of-flight for estimating the depth data, providing a higher accuracy [Nae19]. With this, the Microsoft Kinect is one of the most successful human motion capture systems system [Dut12, Nae19].

(a) Microsoft's Kinect v1 [Wik21] **(b)** Mocap with Kinect [Rea21]

Figure 4.2: Microsoft's Kinect as a human motion capture system.; **(a)** Microsoft Kinect v1, **(b)** Mocap with the Kinect.

4.2 Non-Optical Systems (IMU-based)

In non-optical motion capturing, Inertial Measurement Units (IMU) are often used for recording human motion data. Most IMU-sensors include an accelerometer, gyroscope, and magnetometer. The IMU-based mocap systems are low-cost, small, and easy to use for full-body human motion

detection. One drawback of IMU-based mocap systems is that they often deal with drift over extended periods. The main advantage of these systems is the portability [Ser20]. Most mocap systems include a mocap suit containing IMU-sensors placed on each body limb [Zho08, Vla07], which fixes the occlusion problem of the other mocap systems. A very well-known mocap system is from *Xsens* (AN ENSCHEDE, Netherlands). The *Xsens* suit contains 17 wireless sensors which are placed on the body and fixed to straps [Xse21]. Another commercially available IMU-based mocap suit comes from Noitom Ltd. (Beijing, China), developed for gaming and virtual reality applications. The Perception Neuron mocap system is cost-efficient, easy to use, and it is a valid motion capture method [Ser20]. The *Perception Neuron mocap suit* is presented on the left side of Figure 4.3. The right side of the Figure provides the suit during data recording with the axis neuron software.

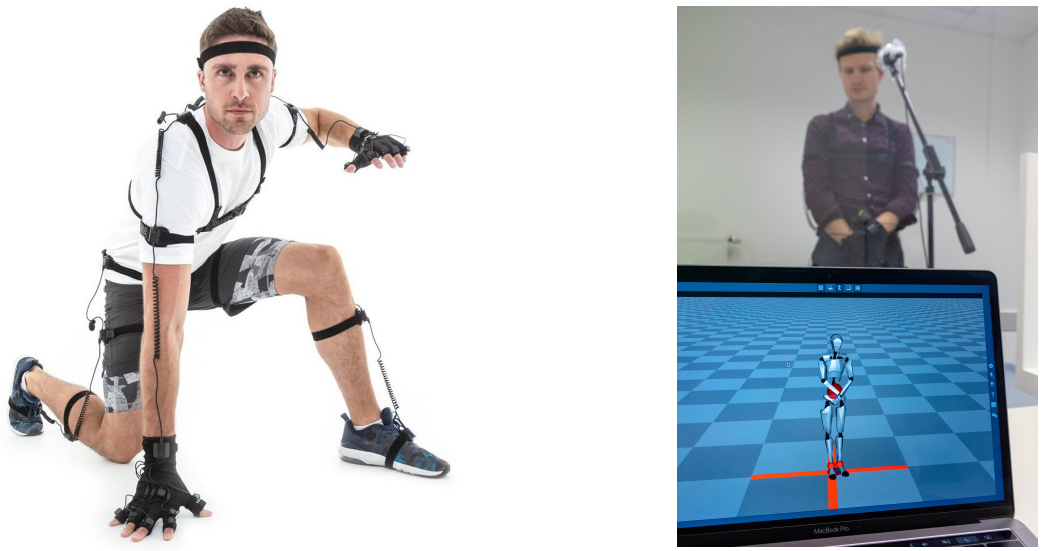

(a) Mocap suit sensor placement[Noi21] **(b)** Mocap suit with Axis Neuron Software

Figure 4.3: Perception Neuron mocap suit.; **(a)** exemplary placement of the Axis Neuron sensor on the human body, **(b)**, mocap suit during human motion tracking.

The suite of Perception Neuron contains 31 sensor nodes (“Neuron”) for full-body motion capture. It also has different operating modes, where a lower number of Neurons is used to capture different parts of the body as a single arm or the upper body. Each Neuron (12.5 mm x 13.1 mm x 4.3 mm) includes an IMU-sensor comprising a 3-axis gyroscope, a 3-axis accelerometer, and a 3-axis magnetometer [Ser20]. The Neurons are attached to the body by straps and are connected via cables. While collecting the data, the mocap suit is connected to a computer via USB, or the measured data is transferred wireless via TCP/IP. During data acquisition, the mocap

suit is controlled by the Axis Neuron software [Noi21]. The collected data can be streamed and displayed in real-time in the software. For providing accurate results the software includes two options. As a first option, it is possible to create body size models according to the participant's body dimensions, and second, the software provides a calibration procedure, which helps the sensors to orient.

Chapter 5

Methods

The methods chapter first presents the data acquisition with the study design, procedure, and the collected parameters of the study. Afterwards, the data cleaning of the collected motion data is explained. Finally, the calculation of the features of the cleaned motion data is presented. The evaluation of the extracted features will be presented in Chapter 6.

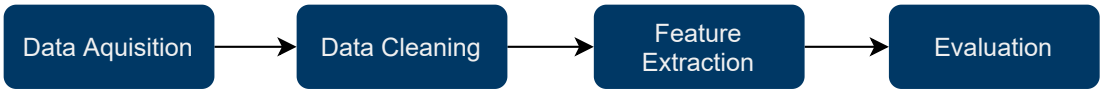

Figure 5.1: General pipeline of the methods of the thesis.

5.1 Data Acquisition

The data acquisition took place at the *Chair of Health Psychologie of the Friedrich-Alexander Universität Erlangen-Nürnberg (FAU)* from January to February 2021. The stress protocol used for the data acquisition is the TSST, which was introduced in Section 3.1. The TSST was most suitable for the study design since it is the gold standard for acute stress induction. Additionally, participants have to stand throughout the whole procedure and do not have to interact with a computer, allowing to collect data without limiting the natural movement of the subjects. The f-TSST was used as the control condition. The IMU-based motion capture suite Perception Neuron was used to collect body movement data. The suit was used in full-body mode, containing 31 “Neuron” sensors. During data collection, it was connected to a computer via USB. Selected body measurements of the participants were measured to create an individual body size model for each participant. Due to COVID-19 regulations, all people had to wear mouth-nose protection.

Additionally, the participants had to provide a COVID-19 rapid test before participating in the study. Because of the COVID-19 rapid test, participants were allowed to remove their mouth-nose protection for the duration of the f-TSST and TSST ((f-)TSST) interview.

5.1.1 Study Design

For the study, 21 healthy participants were recruited, 18 females and 3 males. Before they were included in the stress study, they had to fill out a screening questionnaire. That included criteria, which are known to influence salivary hormone levels or the psychosocial stress response. For participating in this study, they had to be older than 18 years and non-smokers. Additional exclusion criteria were the physical or mental illness of any kind, intake of medication, adiposity, and former participation in the TSST. Recruiting was performed using flyers at the university and via social media. All of the study participants were university students, with the majority being psychology students. As compensation for the participation in the study, participants had the option to either receive 4 VPN (for psychology students) or 30 €. The most important demographic and anthropometric data are shown in table 5.1.

Table 5.1: Demographic and anthropometric data of the participants, (18 female, 3 male)

Age [years]	**Height [cm]**	**Weight [kg]**
22.62 ± 4.01	170.19 ± 6.74	63.52 ± 8.98

The data acquisition took place between 9:00 am and 9:00 pm on different days. Each participant took part in the f-TSST and the TSST on two consecutive days at similar times of the day. The participants were instructed to wake up in the morning at least 2 hours before the beginning of the study. In the laboratory, they were advised not to eat and only to drink water throughout the study. They were also asked not to use their smartphones because the content could affect their emotions. The data collection was carried out by five persons, whereas one person was serving as study instructor and two persons were serving as a committee for both TSST and f-TSST. The condition order (i.e., whether f-TSST or TSST was conducted first), as well as the instructor and committee members, were randomized for both conditions.

5.1.2 Procedure

Day 1

On the first day, the COVID-19 rapid test was conducted after the manufacturer's instructions. After obtaining a negative COVID-19 rapid test, the participants were allowed to enter the laboratory and were guided into the waiting room, where they got instructed about the study procedure and had to provide written consent for the study. This was followed by the collection of the first saliva sample (S0), which occurred at t= -20 min relative to (f-)TSST start. After that, the participants had to fill out the first set of a questionnaire assessing pre-state variables and a few additional variables. After finishing the questionnaire, they were taken to the corridor between the waiting room and the TSST room, where they were equipped with the mocap suit. Subsequently, some relevant body size measures were collected in the Axis Neuron software for the creation of a participant-specific body size model. The body measurements were height, shoulder width, upper arm width, lower arm width, palm width, and hip-width. Putting on the mocap suit was followed by the calibration procedure. The procedure required four different calibration poses (Figure 5.2): 1) *Steady pose*: sitting on a chair steadily while putting the hands on the knees; 2) *A-pose*: standing with palms facing to the body and parallel feet; 3) *T-pose*: standing with arms at the same high and palms facing down; 4) *S-pose*: A half-squat with the arms positioned straight in front of the body and palms facing downwards [Noi20].

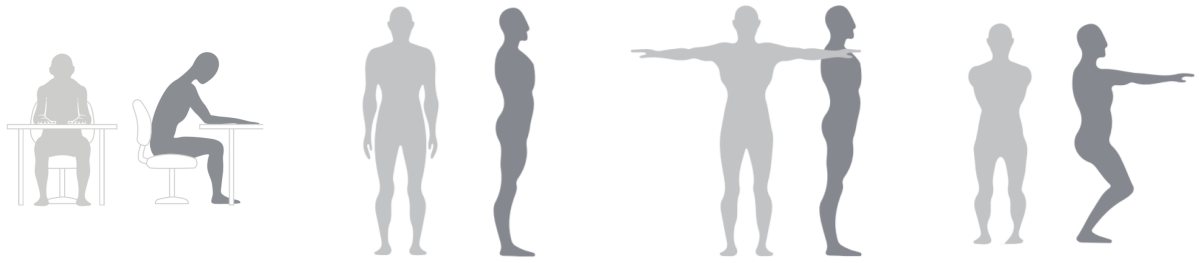

(a) *Steady pose* **(b)** *A-pose* **(c)** *T-pose* **(d)** *S-pose*

Figure 5.2: Perception Neuron mocap suit calibration poses.; **(a)** *steady pose*: sitting on a chair steadily while putting the hands on the knees; **(b)** *A-pose*: standing with palms facing to the body and parallel feet; **(c)** *T-pose*: standing with arms at the same high and palms facing down; **(d)** *S-pose*: A half-squat with the arms positioned straight in front of the body and palms facing downwards [Noi21].

After calibration, the second saliva sample (S1) was taken before entering the TSST room at time point t= -1 relative to (f-)TSST start. In Figure 5.3 the TSST setup is presented. In contrast to a standard TSST setup, additional two plexiglass panels were added due to COVID-19 regulations.

One panel was placed between the two committee members, the other was placed between the committee and the participant.

Figure 5.3: TSST setting with mocap suit, Note: The TSST room was equipped with additional added plexiglas panels due to COVID-19 regulations.

At this point, the (f-)TSST procedure started as explained in Chapter 3.1. Additional changes to the standard procedure consisted of informing the subjects that they were recruited to test the mocap suit under different conditions, as the mocap suit is still very new. Before the beginning of the (f-)TSST interview, recording of the mocap data was started. Afterwards, they had to clap in their hands for the synchronization of the mocap and video data. The data recording ended right after the end of the (f-)TSST. Immediately after, the participants were taken back to the corridor and the third saliva sample (S2) was collected at t= +20 min after (f-)TSST start. Then they pulled off the suit and returned to the waiting room, where the participants were asked to fill out post-state variables. In between, they had to give the fourth saliva sample (S3) at time t= +30 min after (f-)TSST start. After finishing the post-test state variables, they were handed out a medicine magazine against boredom. Subsequently, before the end of the first day, they had to give additional saliva samples. The fifth (S4) at t= +40 min after (f-)TSST start and the sixth saliva sample (S5) at time point t= +65 min after (f-)TSST start. After the last saliva sample was collected, the first study day ended. Participants were discharged from the laboratory and reminded of the next day's second study appointment

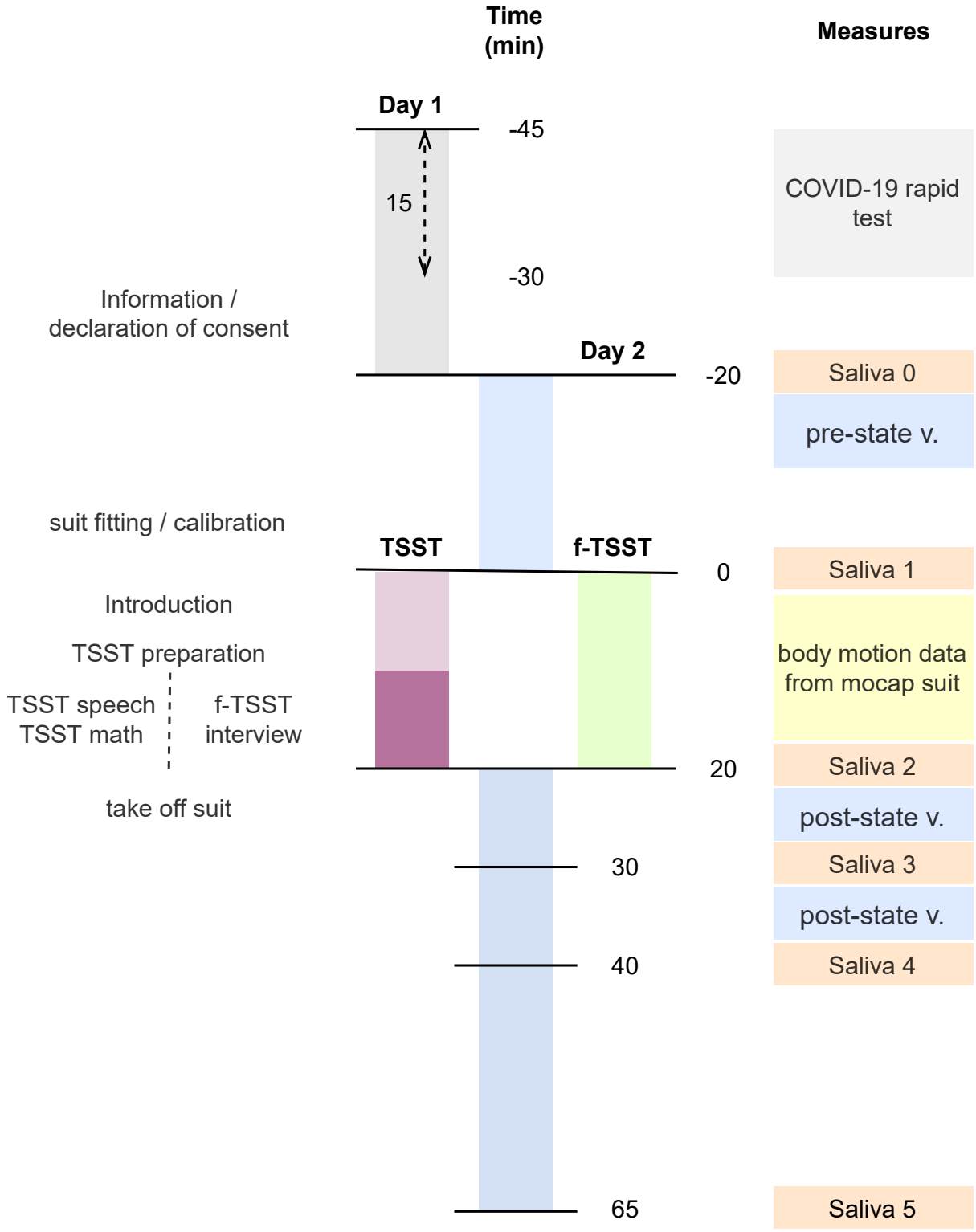

Figure 5.4: Protocol of the data acquisition process for both collection days. *Note*: (pre) post-test state v. : set of questionnaires assessing (pre) post-state variables

Day 2

On the second day, the participants did not have to provide a negative COVID-19 rapid test result, as the test result from the first day was still valid. They were directly guided into the waiting room for the first saliva sample (S0). Afterwards, the procedure was fulfilled, as on the first day. After the collection of the last saliva sample (S5), the participants were debriefed and either received 4 VPN (for psychology students) or 30 €.

5.1.3 Measures

During the study, data was collected from three different sources: body movement data by the mocap suit, biomarkers of saliva data, and questionnaire-based self-report. The collected data is explained in the section below.

Motion Data

The acquired motion capture data was exported using the manufacturer's software *Axis Neuron*[1]. Among other possible file formats, the software offers the possibility to export the recorded data as Biovision Hierarchy character animation file format (BVH) (.bvh) and the Calculation file format (CALC) (.calc). For the study, data were exported as BVH files and CALC files per participant and condition. Furthermore, the center-of-mass file (.txt) was exported, including the position data of the center-of-mass of the participant. Listing 5.1 presents an example of a calculation file, it includes the velocity (unit: m/s), acceleration (unit: g), angular velocity (unit: radians/s), position, and quaternion data for each joint. The data is coded as e.g. *01-X-x*: 01 denotes the body ID, *X* the position data and x the channel. Additionally, the velocity is denoted by *V*, quaternions by *Q*, acceleration by *A* and the angular velocity by *W*. The manual of the axis neuron software provides a bone mapping, where e.g. body ID 01 represents the hips or body ID 02 the RightUpLeg [Noi21].

Listing 5.1: Example CALC file.

```
1 bones:  59
2
3
4 01-X-x  01-X-y  01-X-z  01-V-x  01-V-y  01-V-z  01-Q-s  01-Q-x  01-Q-y  01-Q-z  01-A-x  01-A-y
      01-A-z  01-W-x  01-W-y  01-W-z   ...    59-W-x  59-W-y  59-W-z
5 -0.0014 -0.0111 -0.0161 0.0031  0.0031  -0.0039 0.4492  ...
```

[1] Axis Neuron Version: 3.8.42.8591, https://neuronmocap.com/content/axis-neuron

The BVH file contains the local rotation in Euler angles and the local position for each joint, in a hierarchical data structure. The file is divided into two parts, the first part includes the hierarchical information, and the second part the motion data (Listing 5.2).

Listing 5.2: Example BVH file.

```
HIERARCHY
ROOT Hips
{
    OFFSET 0.000 98.429 0.000
    CHANNELS 6 Xposition Yposition Zposition Yrotation Xrotation Zrotation
    JOINT RightUpLeg
    {
        OFFSET -10.000 -1.689 0.000
        CHANNELS 6 Xposition Yposition Zposition Yrotation Xrotation Zrotation
        JOINT RightLeg
        {
            OFFSET 0.000 -44.370 0.000
            CHANNELS 6 Xposition Yposition Zposition Yrotation Xrotation Zrotation
            JOINT RightFoot
            {
                OFFSET 0.000 -44.370 0.000
                CHANNELS 6 Xposition Yposition Zposition Yrotation Xrotation Zrotation
                End Site
                {
                    OFFSET 0.000 -8.000 18.200
                }
            }
        }
    }
    JOINT LeftUpLeg
    {
        ...
    }
    JOINT Spine
    {
        ...
    }
}
MOTION

Frames: 38312
Frame Time: 0.017
42.314823 100.187111 39.775772 46.877846 -3.699605 0.643386 -10.030867  ...
```

The hierarchical parts start with the keyword *HIERACHY*, afterwards, the *ROOT* (Hips) of the skeletal hierarchy is described. The other body parts are followed by the keyword *JOINT*. Each joint section consists of the name of the joint, the *OFFSET*, the *CHANNELS* and the name of the child item. The *OFFSET* describes the translation of the bone with respect to the parent's bone. The *CHANNELS* keyword is followed by the degree of freedoms (DOFs) of the current joint.

The second part of the file starts with the keyword *MOTION* and is followed by *FRAMES* and *FRAME TIME*. Afterwards, the rest of the file contains the channel data for each joint [Mer01]. For the feature extraction, the global positions and rotations were additionally evaluated of the local positions and rotations of the BVH file.

Saliva Data

During both conditions ((f-)TSST), six saliva samples were taken to measure the HPA axis response. Two saliva samples before the beginning of each (f-)TSST and four afterwards (Table 5.2). The collection times relative to the beginning of the (f-)TSST are given in Table 5.2. The saliva samples were collected with the help of Salivettes (Sarstedt AG & Co. KG, Nümbrecht, Germany). Participants were instructed to keep the cotton pad in their mouth for one minute but not chew on it. The Salivettes were then kept at room temperature until the end of the session. Afterwards, the Salivettes were stored in a refrigerator at a temperature of $-18\,^{\circ}\mathrm{C}$ until later analysis in the laboratory.

Due to COVID-19 regulations, saliva samples were stored at room temperature for three weeks before laboratory analysis to minimize the potential risk of COVID-19 infection from contaminated saliva samples. In the laboratory, the saliva samples were centrifuged for five minutes at 2000 g, and the cortisol concentration was measured using chemiluminescence immunoassay (CLIA, IBL, Hamburg, Germany) [Jan17].

Table 5.2: Saliva collection times relative to (f-)TSST start.

Saliva IDs	S0	S1	S2	S3	S4	S5
time [min]	-20	-1	+20	+30	+40	+65

Self-reports

In addition, a set of questionnaires and the health information of the participants were collected. The set of questionnaires included the *Positive and Negative Affect Schedule (PANAS)*, *State-Trait Anxiety-Depression Inventory (STADI)* and the *Primary Appraisal Secondary Appraisal Questionnaire (PASA)*, which are listed in Table 5.3.

The *PASA* questionnaire had to be filled only during the TSST condition, between the preparation and the test period. The PASA was designed to assess anticipatory cognitive stress appraisal [Het09] and was originally proposed by Gaab et al. [Gaa05]. With the *PASA* four subscales can be evaluated: “Threat”, “Challenge”, “Self Concept of Own Abilities” and “Control Expectancy”.

Table 5.3: Measured self-reports with collection times and conditions.

Short Form	Name	Condition	Time
PANAS	Positive and Negative Affect Schedule	(f-)TSST	Pre / Post
STADI	State-Trait Anxiety-Depression Inventory	(f-)TSST	Pre / Post
PASA	Primary Appraisal Secondary Appraisal Questionnaire	TSST	During

The participants had to rate each of the 16 questions on a scale from “Strongly agree” to “Strongly disagree” [Het09].

Additionally, the *PANAS*, originally proposed by Watson et al. [Wat88] was used to measure the positive and negative affect. The *PANAS* consists of 20 items from which two subscales can be derived to assess positive and negative affect, respectively. The questionnaire was collected before and after both conditions. The *PANAS* was assessed pre and post of the (f-)TSST interview.

The *STADI* proposed by Laux et al. [Lot13] measures state and trait anxiety and depression, where the state component represents the temporal feelings based on situational state and trait component the general anxiety levels [Osw04]. The questionnaire contains 40 items that can be used to derive four subscales assessing state and trait anxiety and depression, respectively. For this thesis, the subscales “State Anxiety” and “State Depression” was used and both were assessed pre and post (f-)TSST.

5.2 Data Cleaning

The collected motion capture data was corrupted by sensor data drifts, in both position and rotation. For that reason, the data were first preprocessed in an attempt to remove these drifts.

Position correction

The position data was filtered with a third-order high-pass Butterworth filter to remove baseline position drift. For filtering the butter function of python package *SciPy* [2] was used.

Listing 5.3: Possition correction method.

```
import scipy.signal as ss
import pandas as pd

def filter_displacement(mocapBvh, wn):
    # extract position data of the bvhFile object containing the motion data
    pos_data = mocapBvh.data.Hips.filter(like="pos")
```

[2] SciPy Version:1.7.1, https://docs.scipy.org/doc/scipy/index.html

```
7
8       # set the model to the origin
9       pos_data.Xposition = pos_data.Xposition - pos_data.Xposition[0]
10      pos_data.Zposition = pos_data.Zposition - pos_data.Zposition[0]
11
12      # filter data using butterwoth filter
13      b, a = ss.butter(N=3, Wn=wn, fs=1/0.017, btype='high')
14      filt_pos = ss.filtfilt(b=b, a=a, x=pos_data, axis=0)
15      filt_pos = pd.DataFrame(filt_pos, columns=pos_data.columns)
16
17      # add the position of time point zero
18      filt_pos = filt_pos.add(pos_data.iloc[0, :])
19      return filt_pos
```

The Butterworth filter's cutoff frequency (Wn) was set to 0.01 frames/s. In some datasets with strong positional drifts, Wn was set to 0.02 frames/s. Due to the hierarchical structure of the BVH file formate, only the hip joint was filtered, as it is the root joint. The position data for the other joints are evaluated by applying the offset between the joints to the position data of the parent joint. In figure 5.5 in the left subplot, the raw position data of one participant is shown, with the positional drift being presented in the y and y-axis. In the subplot on the right side, the filtered position data of the same subject is given.

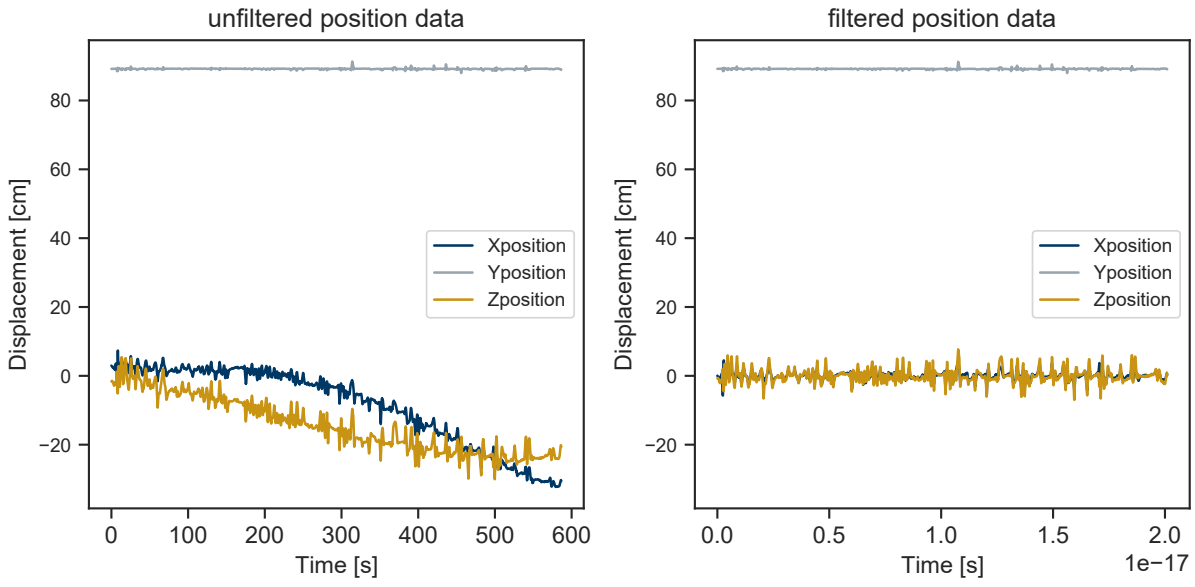

Figure 5.5: Position drift filtering. The left side shows he data with positional drift, the right side presenst the data after the filtering process.

Rotation correction

For correction of the rotational drift, the Euler angle data was unwrapped first to avoid jumps. Afterwards, the Euler angles were transformed to quaternions and the rotational drift was approximated and the drift was removed from the rotational data. In the end, the quaternion data was transformed back to quaternions, Figure 5.6 illustrates the rotational drift correction process.

Figure 5.6: Rotation drift filtering process.

First, the Euler angles were unwrapped. Unwrapping is a method in signal processing for evaluating a continuous curve out of a wrapped signal. The Euler angles are defined inside a certain range: roll -180/+180, pitch -90/+90, and yaw -180/+180. While performing more than one turn around a single axis the angle will go from -180 to 180 and then jump back to -180 and 180 again and so on. After unwrapping the data, the angle is continuously increasing after 180 to 720 for two turns and does not jump back to -180. The unwrapping and the whole correction process are illustrated in Figure 5.7, as an example for the Euler angle data from the hip.

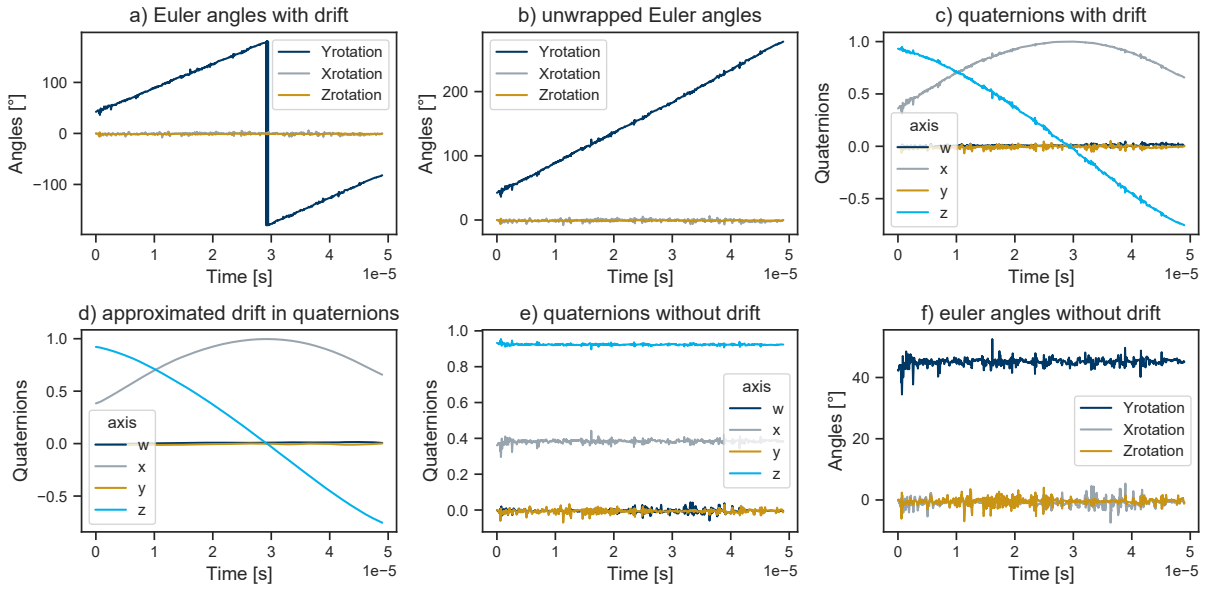

Figure 5.7: Rotation drift filtering of the hip.
(a) hip data with rotation drift; (b)-(e) showing the compensation process (f) filtered rotational data

The unwrapped Euler angles were then transformed into quaternions, using the python package SciPy [3]. The quaternion rotation data were filtered with a first-order high-pass Butterworth filter, with critical frequency (Wn) being set to 0.01 frames/s. For datasets with large drifts, Wn had to be increased for improved drift compensation. The Wn parameter was determined empirically per body part according to the magnitude of the rotational drift. Unlike position drift, rotation drift requires all body parts to be filtered, because every body part has its own rotational data. The quaternion drift was approximated by the difference between the unfiltered quaternion data and the filtered quaternion data (Listing 5.4).

Listing 5.4: Drift approximation method.

```
import pandas as pd
import scipy.signal as ss

def get_approximated_drift(body_parts, quat_df,Wn):
    drift = quat_df.copy()
    quat_before = drift.copy()
    # loop over body parts
    for i in body_parts:
        # apply butterworth filter
        b, a = ss.butter(N=1, Wn=Wn, fs=1/0.017, btype='high')
        drift[i] = ss.filtfilt(b=b, a=a, x=drift[i], axis=0)
    drift = pd.DataFrame(data=drift, columns=quat_before.columns)
    # difference between original quat data and filtered quat data, to approximate the drift
    drift = quat_before - drift
    return drift
```

Afterwards, the unfiltered quaternion data was multiplied by the inverse drift quaternion to remove the rotational drift (Listing 5.5).

Listing 5.5: Rotation correction method.

```
from pyquaternion import Quaternion
import pandas as pd

def quat_remove_drift(body_parts,quat_df, drift):
    quat_df_neu = quat_df.copy()
    # loop over body parts
    for j in body_parts:
        result = []
        # save the initial quaternion
        start = Quaternion(drift[j].loc[0]).unit

        # loop over quaternion data
        for i in range(0, len(drift)):
            # get unit quaternions
            rot_quat = Quaternion(quat_df[j].loc[i])
```

[3] SciPy Version:1.7.1, https://docs.scipy.org/doc/scipy/index.html

```
            rot_quat = rot_quat.unit
            rot_drift = Quaternion(drift[j].loc[i])
            rot_drift = rot_drift.unit
            # evaluate inverse drift quaternion
            rot_drift = rot_drift.inverse
            # multiply the original data by the drift quaternion
            corrected_quat = rot_quat * rot_drift
            # multiply by initial quaternion
            corrected_quat = corrected_quat * start
            result.append(list(corrected_quat))

        quat_df_neu[j] = pd.DataFrame(data=result, columns=quat_df[j].columns)
    return quat_df_neu
```

In the end, the quaternion data was transformed back into Euler angles, using the python package *SciPy* [4]. An example, where the Wn parameter was changed to 0.04 frames/s is ilustrated in Figure 5.8.

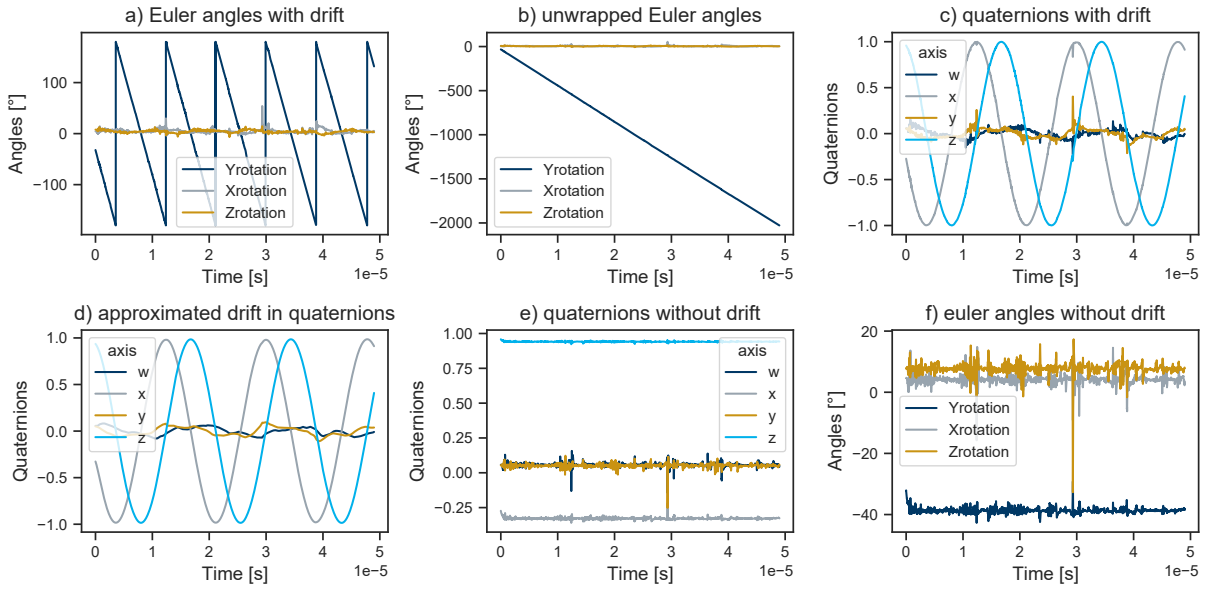

Figure 5.8: Rotation drift filtering of the right shoulder.
(a) hip data with rotation drift; (b)-(e) showing the compensation process (f) filtered rotational data; *Note:* Wn was set to 0.04

[4]SciPy Version:1.7.1, https://docs.scipy.org/doc/scipy/index.html

5.3 Feature Calculation

After drift correction was completed, features were calculated. The features can be divided into the expert and generic ones. Generic features require no previous domain knowledge, they include statistic features like mean or standard deviation and simple signal characteristics, like the maximum or the energy of a signal. In contrast, expert features are based on previous domain knowledge and were specially designed for the approach, like evaluating the times where the participants brought their hands together.

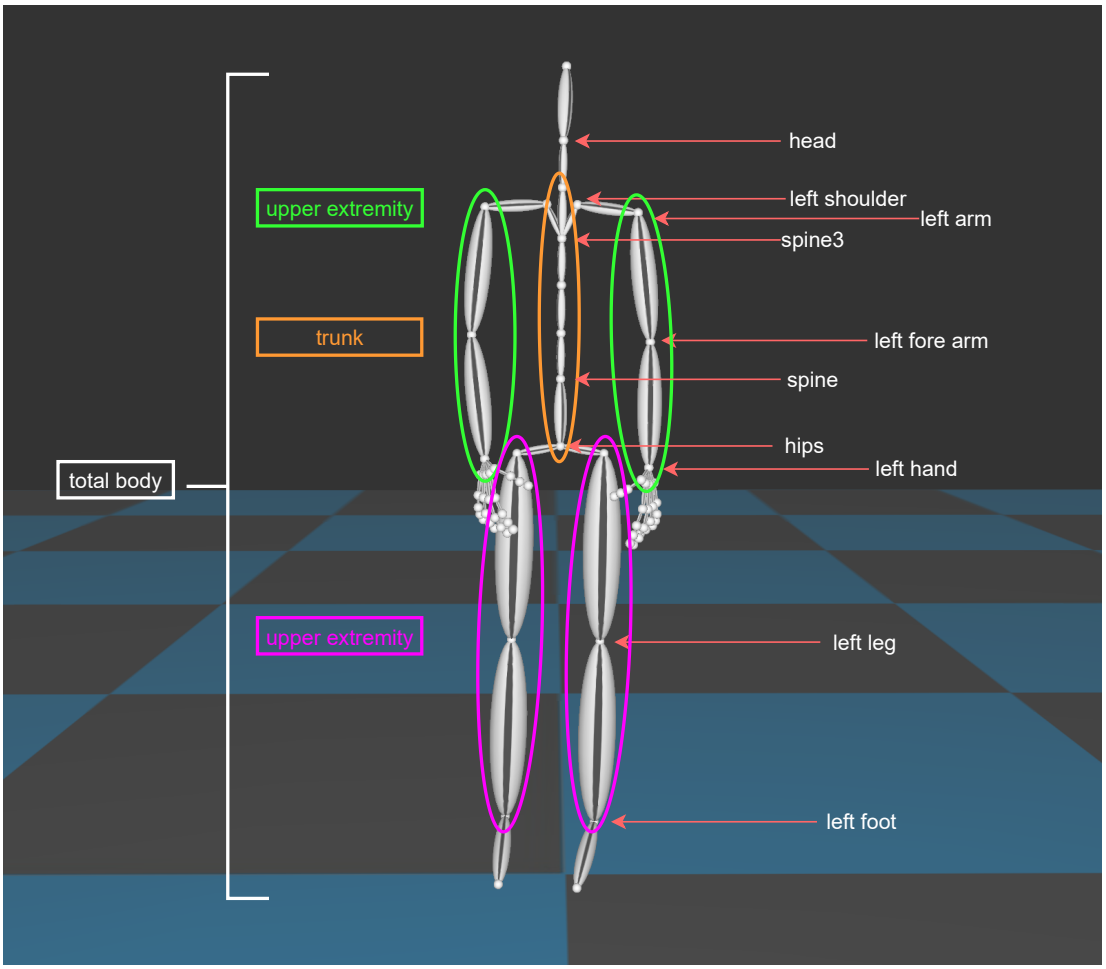

Figure 5.9: Skeletal structure of the BVH file.

Both the generic and the expert features were calculated from specific body parts or aggregate body part groups. Figure 5.9 illustrates the skeletal structure of the BVH file and the aggregate body part groups. The body part group total body contains the data of all measured body parts of the mocap suit. The upper extremity includes the data for the shoulder, arms, and hands for both

arms. The lower extremity consists of the upper leg, leg, and foot for both legs, whereas the trunk is defined as hips, spine, and neck. All features were calculated of the Euclidean norm of rotation, position, and velocity of specific body parts. The specified body parts and body part groups were determined based on characteristics mentioned in the literature and based on the results of a video data analysis. For a few body parts, the features were additionally evaluated across the three axes.

5.3.1 Generic Features

The generic features are listed in Table 5.4.

Table 5.4: Evaluated generic features.

Short From	Name	Channel
mean	Mean	center-of-mass, rotation, vel
Std	Standard Deviation	center-of-mass, rotation, vel
CV	Coefficient of Variation	center-of-mass, rotation, vel
max-abs	Absolute maximum	rotation, vel
NumCross0	Number crossing 0	vel
entropy	Entropy	rotation, vel
SamEn	Sample-Entropy	rotation, vel
abs-energy	Absolute energy	vel

The generic features mean, standard deviation (Std), coefficient of variation (CV), and absolute maximum (max-abs) ($\max_{abs} = max(|x|)$) were calculated of the same body parts and body part groups. The mean (μ), Std (σ), and CV were calculated as

$$\mu = \frac{1}{n}\sum_{i=1}^{n} x_i, \tag{5.1}$$

$$\sigma = \sqrt{\frac{1}{n-1}\sum_{i=1}^{n}(x_i - \mu)^2}, \tag{5.2}$$

$$CV = \frac{\sigma}{\mu}, \tag{5.3}$$

where the CV represents the ratio of the Std to the mean.

Higher CV values thus indicate greater dispersion around the mean. The four features for the velocity (vel), were calculated of the head, total body, upper-extremity, lower-extremity, trunk, spine3, right-hand, left-hand, and center-of-mass. For the rotation, the features were calculated for the head, right-fore-arm, left-fore-arm, right-leg, and left-leg. The features were calculated of single upper extremity body parts because a reduction in hand movement was already evaluated in literature [Pis18]. Spine3 and center-of-mass were included as they can represent the reduction of body sway, which was mentioned in previous studies [Dou18, Zit19]. The movement of the head was measured because changes in the movement were detected while analyzing the video data of the TSST and f-TSST interviews. For a detailed analysis of these body parts, the four features: mean, Std, CV, and max-abs, were also assessed across the three axes of velocity. In addition, for the head, features were also calculated over the three rotation axes.

For the calculation of the features absolute energy (abs-energy), sample entropy (SamEn), and number crossing 0 (NumCross0), the functions of the python package *tsfresh* [5] were used. The abs-energy was estimated of the body parts: total body, upper-extremity, right-arm, left-arm, and head, because of the same reason as mentioned before. The lower extremities were not included, as the motion change between TSST and f-TSST was very low. The abs-energy (E) is the sum over the squared values of a time series, described by the formula:

$$E = \sum_{i=1}^{n} x_i^2. \tag{5.4}$$

The entropy, sample-entropy, and NumCross0 were only evaluated for the head due to the strong changes in motion data, that were recognized by the video data analysis. During the TSST interview, some participants moved their head slowly diagonal upwards and downwards. This finding possibly results in a similar movement pattern with a lower number of velocity zero crossings. In the *tsfresh* function, a zero-crossing was defined as two sequential values, where the first one is lower than zero and the second one bigger, and the other way, respectively. For evaluating if the head movement contains a similar movement pattern, the features entropy, and sample entropy were calculated.

The sample entropy is a statistical method for measuring the complexity and regularity of physiological time-series data. More frequent and regular patterns result in a lower value [Ric00]. SamEn is the negative natural logarithm of the conditional probability, which shows that two sequences that are similar at m points, will be similar at the next point, not taking self-matches into account when estimating the probability [Ric00].

[5] tsfresh, https://tsfresh.readthedocs.io/en/latest/index.html

For evaluating the entropy of the head velocity and rotation, a function of the python page *scipy* [6] was used. The entropy, often called Shannon entropy can be used to differentiate between a random signal and a periodic signal. For periodic signals the entropy values will be lower than for random signals [Ric00]. With this, it could be possible to detect if similar movement patterns occur in the movement of the head. The entropy (H) was evaluated as

$$H = \sum_{i=1}^{n} p_i \log_2(p_i), \tag{5.5}$$

where p is a given probability distribution.

5.3.2 Expert Features

The evaluated expert features are given in Table 5.5.

Table 5.5: Evaluated expert features.

Short Form	Feature	Type	Channel
AbsMov	Absolute movement	-	pos-global
StatMom	Static moments of the hands	count	vel
		max	vel
		mean	vel
		percent	vel
distance	Distance of the hands	mean	pos-global
		std	pos-global
		var	pos-global
TimeTogether	Time of hand together	count	pos-global
		max	pos-global
		mean	pos-global
		percent	pos-global

Absolute Movement (AbsMov)

The *absolute movement (AbsMov)* feature was evaluated of the head, total body, upper extremity, lower extremity, and trunk. The feature was calculated according to the paper of van der Zee et al. [van19]. The absolute movement was estimated using the calculated global position of the body parts. First, the absolute difference, between all successive time frames was calculated.

[6] SciPy Version:1.7.1, https://docs.scipy.org/doc/scipy/index.html

This difference resulted in the absolute movement for each time frame. Afterwards, the mean difference for each joint was calculated and summed up for all considered joints. The AbsMov was calculated in the following way:

$$AbsMov = \frac{1}{m}\sum_{j=1}^{m-1}\left(\sum_{t=1}^{n}\left|\|x_{tj}\|_2 - \|x_{t-1j}\|_2\right|\right), \tag{5.6}$$

where x is the global position, n the number of body parts and m the number of frames.

Static Moments (StatMom)

Based on the *Static Moments (StatMom)*, four specific features were derived from the velocity of both hands and the head, as these body parts had the biggest change in motion between the two conditions. For evaluating the four features, first, the static moments had to be determined. A static moment for the head was defined as a period with a velocity smaller than 0.04 m/s. The same applied for the hands with a cutoff at 0.4 m/s.

Listing 5.6: Static moments method.

```
import numpy as np

def detect_static_moments(body, mocap_data):
    # check weather static moments for head od hands will ve evaluated
    if body == 'hands':
        # evaluate euclidean norm for both hands
        norm_left = np.linalg.norm(mocap_data.LeftHand.vel, axis=1)
        norm_right = np.linalg.norm(mocap_data.RightHand.vel, axis=1)
        # set array value to 1.0 for static moments
        stat_mom = np.zeros(len(norm_left))
        for j in range(0, len(norm_left)):
            if norm_left[j] < 0.4 and norm_right[j] < 0.4:
                stat_mom[j] = 1.0
    if body == 'head':
        # evaluate euclidean norm for the head
        norm = np.linalg.norm(mocap_data.Head.vel, axis=1)
        # set array value to 1.0 for static moments
        stat_mom = np.zeros(len(norm))
        for j in range(0, len(norm)):
            if norm[j] < 0.04:
                stat_mom[j] = 1.0
    return stat_mom
```

The method given in Listing 5.6, resulted in an array containing 0 for frames “with movement” and 1 for frames “without” motion. Afterwards, all consecutive “ones” were summed up to

get the length of the periods without motion, the results were stored in an array. These two arrays were used to calculate the four static moments features. The Static Moments Percent (StatMomPercent) gives the percentage of time without motion, and Static Moments Count (StatMomCount) determines the number of periods without movement. The other two features were Static Moments Max (StatMomMax) which estimates the maximum time without motion, and Static Moments Mean (StatMomMean), which evaluates the meantime without motion.

Distance of the Hands

Based on the distance between the hands, the two generic features: mean and STD of the distance, were evaluated. The distance between the hands for each time frame was estimated as the euclidean distance of the global position of the two hands. The euclidean distance (d) in three dimensions was evaluated as

$$d(\boldsymbol{x}^{left}, \boldsymbol{x}^{right}) = \sqrt{(x_x^{left} - x_x^{right})^2 + (x_y^{left} - x_y^{right})^2 + (x_z^{left} - x_z^{right})^2}, \tag{5.7}$$

where $\boldsymbol{x}^{left}$ denoted the global position of the left hand and $\boldsymbol{x}^{right}$ of the right hand.

Time Together

In addition, four features were evaluated based on the Time Together feature. First, the time where the hands were together was calculated based on the Euclidean distance between the two hands. Hands together were defined as the minimum distance between the two hands plus some deviation. This was evaluated using a similar approach as for the static moments and resulted in an array containing a 1 for “hands together” and a 0 for “not together”. Then all consecutive values were summed again to get the length of time the hands are together and stored in an array. TimeTogetherPercent is the percentage of time the hands were together. TimeTogetherCount is the number of times the hands were together. In addition, the mean and maximum time the hands were together was calculated.

Chapter 6

Evaluation

This chapter presents the statistical methods which were applied to assess the influence of acute psychosocial stress on body posture and movement, as well as on-ground truth biomarker and self-report data. First, the statistic methods for the assessment of the (f-)TSST responses are given. Afterwards, the statistical methods for the evaluation of the stress-induced movement changes are presented. At last, the methods for determining the relationship between biomarker and self-report data and movement changes are given by performing a stepwise backward multiple linear regression.

6.1 Responses to TSST and f-TSST

The first part of the evaluation chapter presents the cortisol and self-report derived features and the statistics, for evaluating the significance levels of both features, for the interpretation of the TSST and f-TSST responses.

Cortisol Response

For analyzing the cortisol responses to the (f-)TSST, only the cortisol samples S1-S5 were considered since sample S0 was only taken for the baseline cortisol concentration and was excluded from further analysis. From the raw cortisol values, two features reflecting the cortisol response, and, thus, HPA axis activity, were computed: maximum cortisol increase (Δc_{max}) and area under the curve with respect to ground (AUG_g).

The Δc_{max} represents the maximum cortisol increase as a response to the (f-)TSST and is computed as the difference between the maximum cortisol level after and before (f-)TSST ($\Delta c_{max} = max(S2, S3, S4, S5) - S1$).

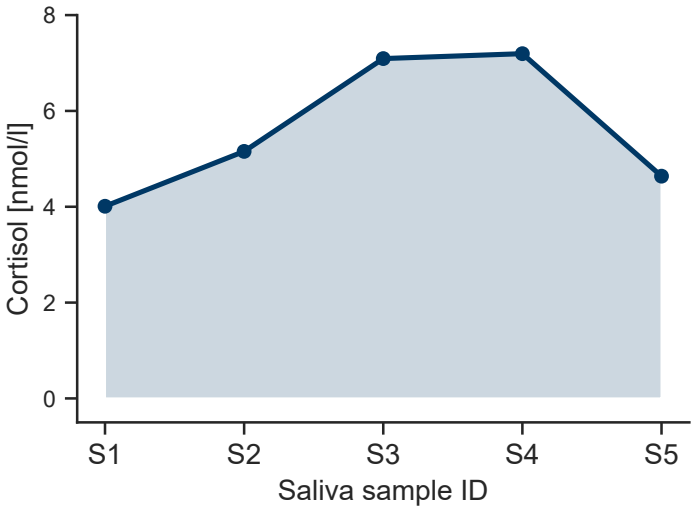

Figure 6.1: Area under the curve with respect to ground (AUC_g) with saliva sample S1-S5

The AUG_g is a tool to asses the total cortisol release over time. It is computed as the area under the cortisol curve using the trapezoidal rule according to Equation 6.2 [Pru03], where S_i is the salivary cortisol value and Δt_i is the sampling time difference between the two consecutive samples S_i and S_{i+1} in minutes.

$$AUC_g = \sum_{i=1}^{n-1} \frac{(S_{i+1} + S_i) * \Delta t_i}{2} \tag{6.1}$$

Self-Report scores

From the assessed self-reports, only questionnaires that assess state changes induced by acute psychosocial stress were considered (as reported in Table 5.3). From those questionnaire scores, the differences between pre and post (f-)TSST were computed, to assess (f-)TSST-induced changes in state variables.

For the *PASA* questionnaire, the scores *PASA-Threat* and *PASA-Challenge* were evaluated. Because the PASA was evaluated during the TSST, the scores directly show the treat and challenge during the TSST. For the *PANAS*, the two scores *PANAS-Positive-Affect (PANAS-PosAffect)* and *PANAS-Negative-Affect (PANAS-NegAffect)* were evaluated.

Statistics

For statistical analyses, the data were first tested for normal distribution (*Shapiro-Wilk* test). Then a *paired T-test* for parametric samples and a *Wilcoxon* test for non-parametric samples was performed to compare the cortisol response and self-report score changes between the conditions. The *paired T-test* and *Wilcoxon* were used because of the dependent samples (same participant for both conditions). All statistical analyses were performed using the *Pingouin* Python module [1] at a significance level of $\alpha = 0.05$. The effect sizes of *paired T-test* and *Wilcoxon* were for both reported as Hedge's g. To indicate statistical significance in Figures and Tables, the the following notation was used: $^{*}p < 0.05$, $^{**}p < 0.01$, $^{***}p < 0.001$.

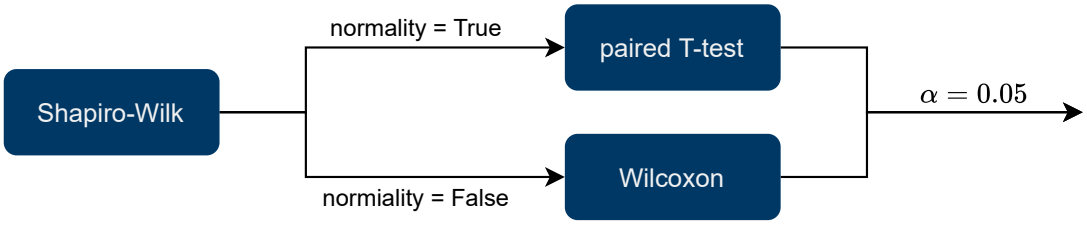

Figure 6.2: Statistical analyses pipeline. α: significance level

6.2 Psychosocial Stress-induced Movement changes

Statistical analyses were performed according to the presented pipeline in Section 6.1. First, the data of all generic and expert features was tested for normal distribution (*Shapiro-Wilk* test). Afterwards, the *pairwise T-test* for parametric samples and the *wilcoxon* for non-parametric samples was performed to compare the movement changes between the conditions (f-TSST and TSST). To correct for multiple testing, the Benjamini-Hochberg procedure for controlling the False Discovery Rate was applied. The significance level α was set to 0.05 and effect sizes were again reported as Hedge's g.

6.3 Relationship of Stress-induced variables and Movement

The following section presents the methods for assessing the relationship between stress-induced biomarker and self-report changes, and stress-induced movement changes. The analysis was divided into two parts. Firstly, a stepwise backward multiple linear regression was performed

[1] pingouin 0.3.12, https://pingouin-stats.org/index.html

to assess whether stress-induced movement alterations can be explained by changes in cortisol and psychological state variables. Secondly, the regression analysis was inverted to examine to which extent traditional stress assessment modalities, such as biomarkers and self-reports, can be predicted by changes of body posture and movement of different body parts.

6.3.1 Prediction of PCA Motion Factor using Biomarkers and Self-Reports

The first part of the analysis is inspired by the work of Lasselin et al. [Las20]. Their goal was to determine which inflammation symptoms can predict a general inflammation-related movement alteration pattern. In this thesis, the analysis approach was modified to determine which biomarker and self-report variables can predict a general stress-related movement alteration pattern. The general process of predicting the self-reports and biomarkers is visualized in Figure 6.3.

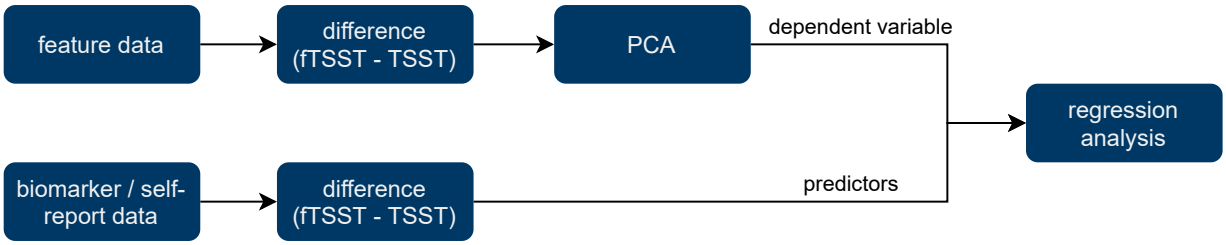

Figure 6.3: Evaluation progress for predicting a PCA movement factor using the biomarkers and self-resports

The first step for computing the stress-induced movement alteration factor was computing the difference between TSST and f-TSST for each movement feature and participant, respectively. Afterwards, features were filtered to only contain features with statistically significant differences between the two conditions (assessed by paired T-tests, controlled with the Benjamini/Hochberg procedure). Afterwards, all features were normalized by means of z score normalization, using the *sklearn* [2] class `StandardScaler`. In the end, all remaining and normalized features were reduced to one single factor reflecting stress-induced movement alteration, using Principal Component Analysis (PCA). PCA is a method for linear dimensionality reduction by using Singular Value Decomposition. The approach is fulfilled by creating new uncorrelated variables with a maximum amount of the variance [Jol16]. The `PCA` class of the Python package *sklearn* [3] was applied to determine the movement factor. The pipeline for computing the stress-induced movement alteration factor is depicted in Listing 6.1.

[2] sklearn 0.24, https://scikit-learn.org/stable/modules/generated/sklearn.decomposition.PCA.html
[3] sklearn 0.24, https://scikit-learn.org/stable/modules/generated/sklearn.decomposition.PCA.html

Listing 6.1: PCA movement factor pipeline.

```
import pingouin as pg
from sklearn.preprocessing import StandardScaler
from sklearn.decomposition import PCA
import pandas as pd

# apply benjamini/hochberg procedure
x,y =pg.multicomp(list(result['p-unc']), method="fdr_bh")
sig_values_bh = sig_values.copy()
sig_values_bh['p-unc'] = y

# extract significant features
sig_values_only_bh = sig_values_bh[sig_values_only_bh['p-unc']<0.05]
# get significant feature data
data_sig =get_significant_feature_data(sig_values_only_bh,feature_data)

# prepare data for PCA
feature_unstack = data_sig.unstack(level=list(range(2, data_sig.index.nlevels)))
feature_unstack .columns = ["_".join(col) for col in feature_unstack ["data"].columns]
# evalaute difference between TSST and f-TSST
diff_feature = feature_unstack .groupby("subject").diff().dropna().droplevel("condition")

# normalize data
diff_feature_scale = StandardScaler().fit_transform(diff_feature)
diff_feature_scale = pd.DataFrame(diff_feature_scale, index=diff_feature.index, columns=
    diff_feature.columns)

# performe PCA
pca = PCA(n_components=1)
pca_motion_factor = pca.fit_transform(diff_feature_scale)
pca_motion_factor = pd.DataFrame(pca_motion_factor, index=diff_feature_scale.index, columns=['
    pca'])
```

Before statistical analysis, the resulting PCA movement factors were inspected for outliers using the IQR (interquartile range) method. Outliers, are values outside the interval [Median - 1.5 x Q1, Median + 1.5 x Q3] [Igl93].

Listing 6.2: IQR method.

```
import numpy as np
import pandas as pd

def outliers_iqr(ys):
    # evaluate quantiles
    [quartile_1, quartile_3] = ys.quantile([0.25, 0.75])
    iqr = quartile_3 - quartile_1
    # define the range
    lower_bound = quartile_1 - (iqr * 1.5)
    upper_bound = quartile_3 + (iqr * 1.5)
    return np.where((ys > upper_bound) | (ys < lower_bound))
```

Using this method, one participant was detected as a potential outlier. After visual inspection of the video data, it was observed that this participant was considerably different from the other and did not reflect the behavior of the general study population. For that reason, the data of this participant was excluded from further analysis, and the PCA was computed again on the remaining data. For the biomarkers and self-reports, also the difference between TSST and f-TSST was computed. The obtained score differences were used as predictors for the regression analysis. During this, one participant had to be excluded because of missing questionnaire data. For better interpretability and as the independent variables were measured in different units, the self-reports biomarkers, and the PCA movement factor were z-transformed. Using z-score normalized independent variables, allowed obtaining standardized regression coefficients from the regression analysis [Lew04]. Before performing a backward multiple linear regression (Listing 6.3), the predictors were checked for multicollinearity, by evaluating the pairwise correlation coefficients. The cut-off value for the correlation coefficients was set at 0.80. Predictors with a higher correlation coefficient were excluded from the regression analysis. This value is a typically used coefficients cut-off value reported in literature [P. 16]. Afterwards, a stepwise backward multiple linear regression was performed to determine which biomarkers and self-reports were predictive for the PCA movement factor.

Listing 6.3: Backward multiple linear regression..

```
import pingouin as pg
import pandas as pd
import scipy.stats as stats

# prepare predictors and merge with pca factor
data_regression_raw = prepare_self_report_and_biomarker_data(path, file)
data_regression = data_regression_raw.merge(pca_motion_factor, left_on='subject', right_on='
    subject')

# detect multicollinearity and drop correlated predictor
corr =data_regression_raw.corr().round(2)
...
data_regression = data_regression.drop(columns='cortisol_auc_g')

# zscore evaluation for standardizied regression coeficients
zvalues = stats.zscore(data_regression, axis=0)
data_regression_zscore = pd.DataFrame(zvalues, columns = data_regression.columns, index =
    data_regression.index)

# performe backward multiple lineare regression
x=data_regression_zscore[['STADI_State_Diff', 'PANAS_NegativeAffect_Diff', '
    PANAS_PositiveAffect_Diff','PASA_Challenge', 'PASA_Threat', 'cortisol_max_inc']]
y=data_regression_zscore['pca']
lm1 = pg.linear_regression(x, y,remove_na=True)
```

To find the best-fitted model for the regression, the adjusted-R^2 value was maximized as a stopping rule. The `linear regression` function of the Python package *pingouin* [4] was applied. The PCA movement factor was utilized as the independent variable and the self-reports and biomarkers as dependent variables.

6.3.2 Prediction of Biomarkers and Self-Reports using PCA Motion Factors

To predict the biomarkers and self-report scores using the obtained movement changes, a PCA was performed for each body part to reduce the number of features. An overview of the the evaluation process is presented by Figure 6.4.

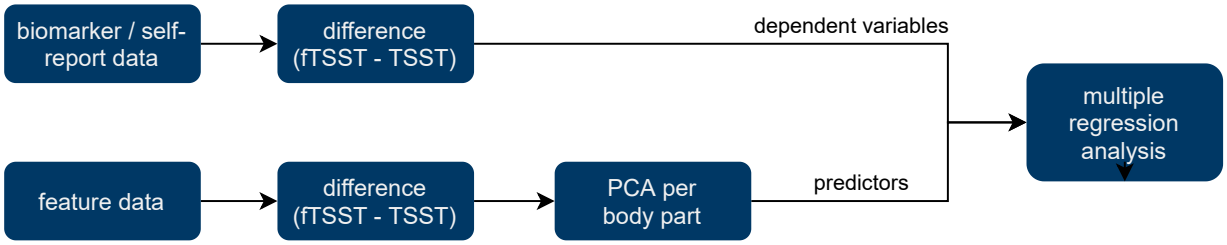

Figure 6.4: Evaluation progress for predicting the biomarkers and self-reports using PCA movement factors.

The data of the extracted movement features were scaled as before. Then the PCA was performed with the maximum number of principal components. Afterwards, the *percentage of the total variance (PotV)* was evaluated as

$$PotV = \frac{1}{\sum_{i=1}^{p} \lambda_i} * \sum_{j \in S} \lambda_j * 100\%, \tag{6.2}$$

where p is the number of original variables, and S is the set of principal components, which explains the percentage of the total variance, and λ are the eigenvalues [Jol16]. The percentage of total variance can be predefined to decide on the number of principal components, for this application a threshold of 80% was chosen. A higher value might overfit the model due to the low number of participants. The number of principal components has been set in a way, that these components account for a percentage of total variation above the given threshold. Before regression, pairwise correlation coefficients were calculated to detect multicollinearity. Additionally, the predictors and the independent variable were again z-transformed for better

[4] pingouin 0.3.12, https://pingouin-stats.org/index.html

interpretability. From this, a backward multiple regression was performed for each self-report and biomarker individually, with the PCA movement factors as predictors and for each regression analysis, one of the self-report scores and biomarkers as the independent variable.

6.3.3 Prediction of Biomarkers and Self-Reports using Movement changes

For the prediction of biomarkers and self-reports by movement changes, the feature data of single body parts was used, to determined which features of single body parts can predict biomarkers or self-report scores. The evaluation process is presented in Figure 6.5. First, the features were divided into one dataset per body part (one dataset for each of head, arms, spine3 and total body). To avoid over-fitting by the prediction of the self-reports and biomarkers by the extracted features of single body parts, just features of the norm were used.

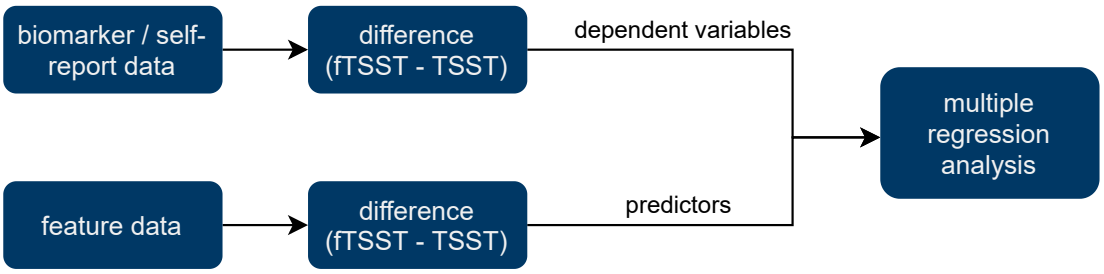

Figure 6.5: Evaluation progress for predicting a PCA movement factor per body part using the biomarkers and self-reports.

For the analysis, the features were first normalized using z-score normalization. Afterwards, pairwise correlation coefficients were calculated to avoid the effect of multicollinearity. Then, the data was z-transformed for standardized regression coefficients. Afterwards, a backward multiple regression was performed for each self-report and biomarker individually, with the feature data of a single body part. For the regression analysis, the feature differences were used as predictors, and one biomarker and self-report score was used as the independent variable.

Chapter 7

Results

This chapter presents the results of the data analysis in this thesis. First, biomarker and self-report responses to the (f-)TSST are presented. Afterwards, the results from assessing the influence of biomarker and self-report changes on movement alteration are given. The last section shows the findings about the relationship between the biomarkers and the movement changes. For the data analysis, the data of one participant had to be excluded, because the recording of the movement data stopped during the TSST, which resulted in missing data. The data analysis was performed on the remaining 20 participants' data.

7.1 Responses to TSST and f-TSST

The responses to the (f-)TSST will be compared based on biomarker features derived from saliva cortisol concentrations and self-report features derived from the state questionnaires PASA, PANAS, and STADI. Both feature types can be linked to psychosocial stress and, thus, to HPA axis activation.

Cortisol Response

Figure 7.1 shows the mean cortisol response of all participants for both TSST and f-TSST. It shows that the initial cortisol levels before the beginning of the (f-)TSST were similar for both conditions, TSST, and f-TSST. During the TSST, the participants showed a noticeable increase in cortisol levels compared to the beginning, which reached its peak 20 minutes after the end of the stress induction. In contrast to this, during the f-TSST, the cortisol concentration after the f-TSST (S2) is continuously decreasing, until the end of the observation (S5).

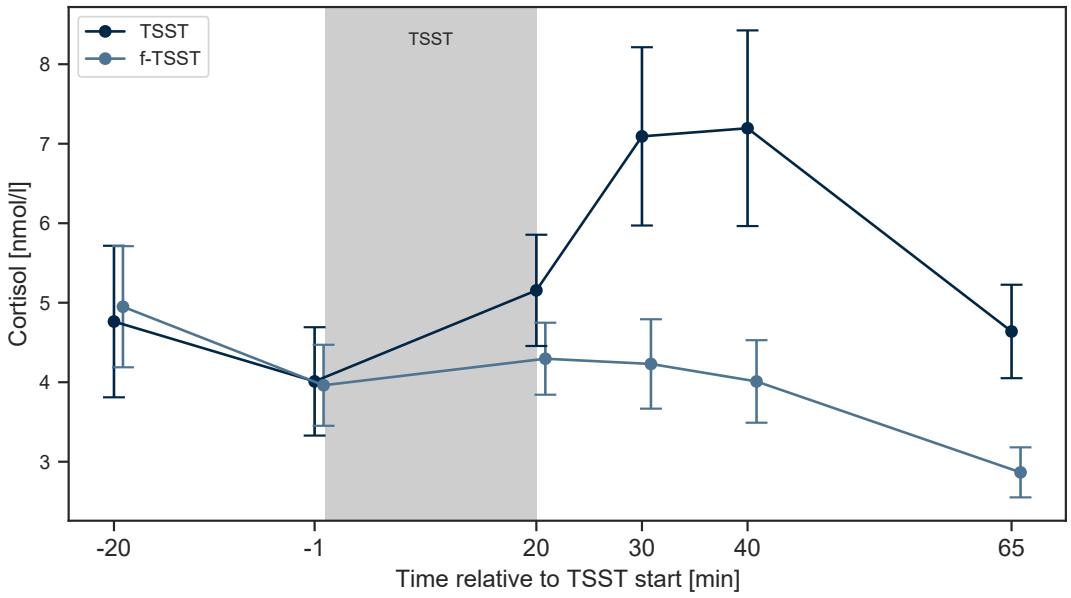

Figure 7.1: Cortisol concentration during TSST / f-TSST, ; values are depicted as mean ± standard error

The results of the biomarker features derived from saliva cortisol concentrations, AUG_g and Δc_{max} are both statistically significant between the two conditions. Both are presented in Figure 7.2. It appears that the stress condition (TSST) caused a significantly higher maximum cortisol increase ($w = 26.0, p = 0.002, g = 0.746$) (Table 7.1). During the TSST, the Δc_{max} of the participants was with $3.50 \pm 5.16\ nmol/l$ (M ± STD) clearly higher than during the f-TSST, with $0.48 \pm 2.17\ nmol/l$. The maximum cortisol increase was observed during the stress condition, with 86.31 % higher values than during the control condition.

Table 7.1: Wilcoxon results for biomarker and self-report features, between TSST and f-TSST, Note: $^{*}p < 0.05$, $^{**}p < 0.01$, $^{***}p < 0.001$, max-inc: maximum increase

Feature	Wilcoxon w	p	Hedge's g
PANAS-NegAffect	8.5	$< 0.001^{***}$	1.696
PANAS-PosAffect	26.0	0.010^{*}	-0.952
AUC-G	31.0	0.004^{**}	0.709
Δc_{max}	26.0	0.002^{**}	0.746

The area under the cortisol curve (AUG_g) of both conditions, was statistically significant higher during the TSST, than during the f-TSST ($w = 31.0, p = 0.004, g = 0.709$). During the TSST the participants had a mean AUG_g of $265.37 \pm 175.81\ nmol/l$, during the f-TSST it was

significantly lower with $165.07 \pm 87.16\, nmol/l$ (Figure 7.2). The Mean $\pm$ Std values are listed in Table 7.3

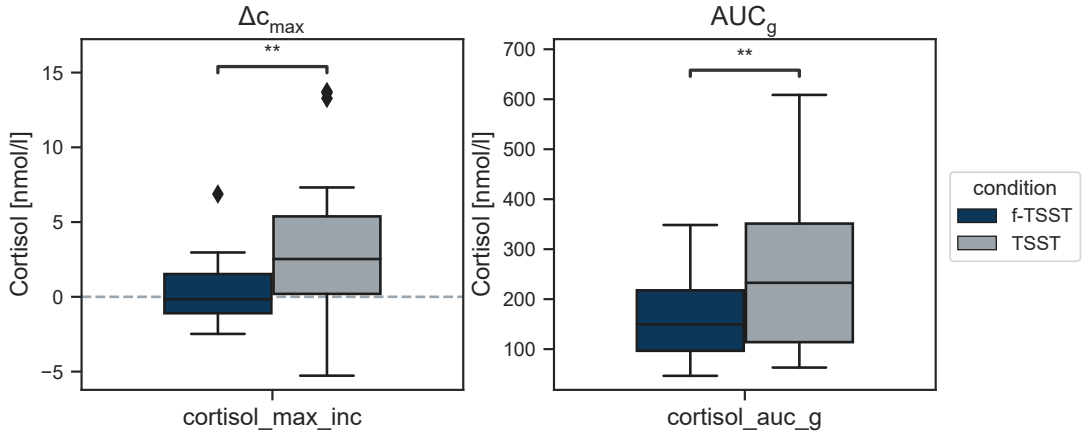

Figure 7.2: Cortisol-derived Features, Δc_{max} and AUG_g ; Note: $^{*}p < 0.05$, $^{**}p < 0.01$, $^{***}p < 0.001$

Self-Reports

Comparing both conditions by the *STADI* questionnaire score, the participants showed a statistically significant lower state of anxiety during the f-TSST than during the TSST ($t(19) = 6.424, p = 0.000, g = 1.618$) (Table 7.2).

Table 7.2: T-test results for self-resport-derived features, betweeen TSST and f-TSST, Note: $^{*}p < 0.05$, $^{**}p < 0.01$, $^{***}p < 0.001$

Feature	T(19)	p	Hedge's g
STADI-State	6.424	0.0^{***}	1.618

During the TSST, the participants declared a mean of 3.6 ± 0.88 for the *PASA-Threat* and a mean value of 4.4 ± 0.61 for the *PASA-Challenge* score. The mean $\pm$ Std changes for al biomarkers and self-reports are listed in Table 7.3.

The *PANAS* questionnaire declared for both scores (Positive-Affect & Negative-Affect) a statistically significant difference between TSST and f-TSST, presented in Figure 7.3. During the TSST condition the participants responded with a statistical significant decrease in positive affect change ($w = 26, p = 0.010, g = -0.952$), presented by Table 7.2.

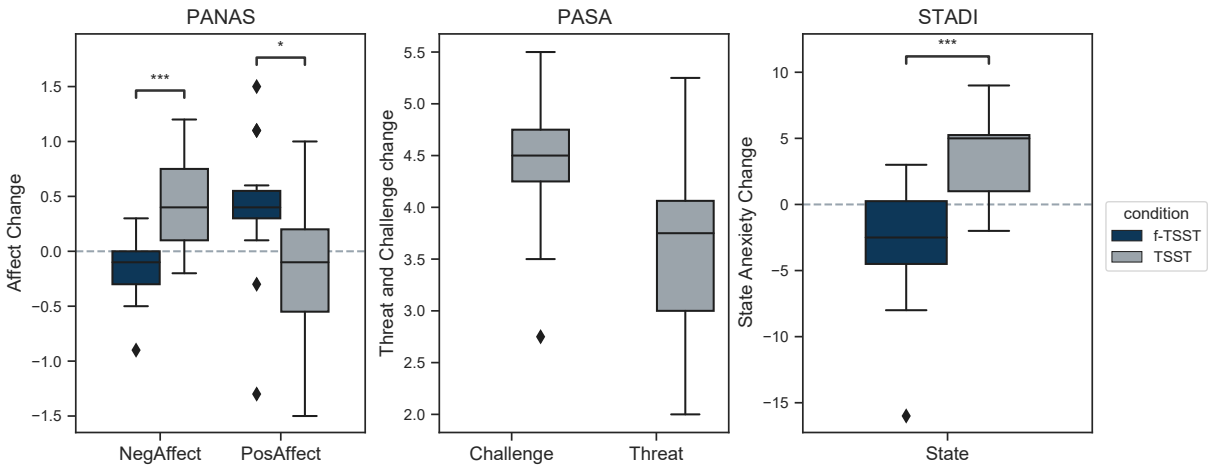

Figure 7.3: Self-report-derived features of PANAS, PASA and STADI, Note: $^{*}p < 0.05$, $^{**}p < 0.01$, $^{***}p < 0.001$

Table 7.3: Biomarker and self-report values of Mean $\pm$ STD changes between TSST andf-TSST

Feature	TSST	f-TSST
STAD-State	3.75 $\pm$ 3.19	-2.75 $\pm$ 4.56
PASA-Challenge	4.40 $\pm$ 0.61	-
PASA-Threat	3.60 $\pm$ 0.88	-
Δc_{max}	3.49 $\pm$ 5.16	0.48 $\pm$ 2.17
cortiso-aucg	265.37 $\pm$ 175.81	165.07 $\pm$ 87.16
PANAS-NegativeAffect	0.45 $\pm$ 0.44	-0.17 $\pm$ 0.26
PANAS-PositiveAffect	-0.17 $\pm$ 0.60	0.39 $\pm$ 0.57

7.2 Psychosocial Stress-induced Movement changes

This section presents the acute psychosocial stress-induced body posture and movement changes. All movement features that showed statistically significant differences between the two conditions, as described in Section 6.3.1, were considered for further analysis.

7.2.1 Generic Movement Features

These sections present the findings of a selection of generic movement features of the following body parts: total-body, trunk, upper-extremity, lower-extremity, head, and spine3 as body sway. The significance values for all evaluated generic features are given in Table A.1 and Table A.2. The mean velocity of all evaluated body parts was statistically significant (p$<$ 0.05) and generally

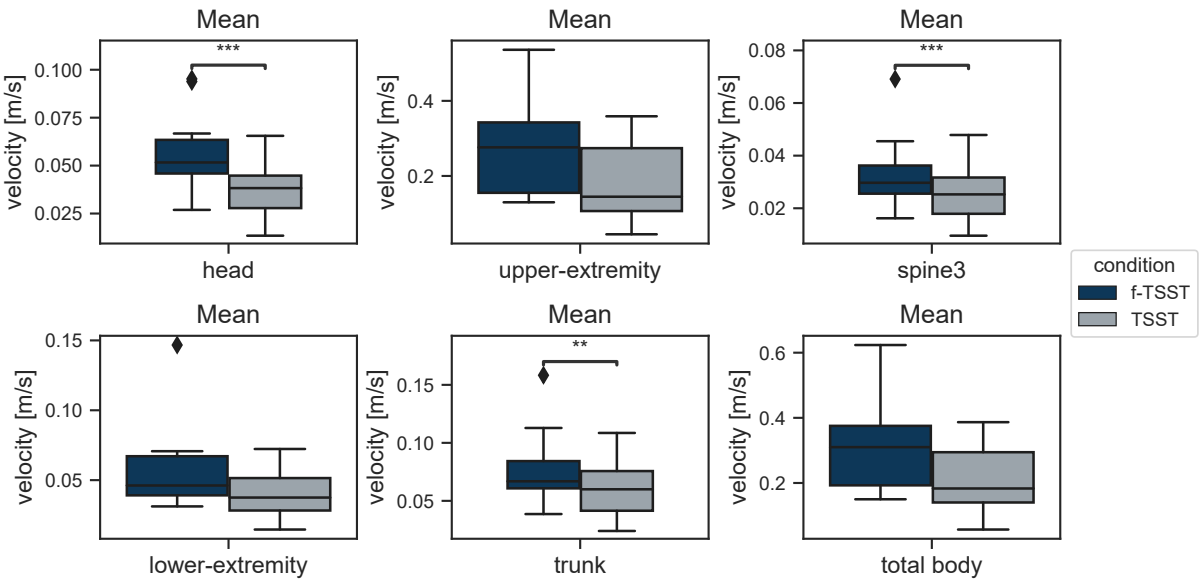

Figure 7.4: Generic Feature mean of norm, Note: $^{*}p < 0.05$, $^{**}p < 0.01$, $^{***}p < 0.001$

lower during the TSST, than during the f-TSST (Table 7.5). During the f-TSST, the mean velocity of all body parts was 26% higher than during the TSST (Figure 7.4). Moreover, the upper-extremity had the most prominent mean velocity difference between the two conditions, with a higher mean velocity of 56.94% ($w = 13, p = 0.001, g = -0.868$). The lowest mean velocity difference was measured for the trunk, with a value of 26.24% ($w = 20, p = 0.003, g = -0.612$). The mean velocity values for the single axes of spine3 (body sway) and the head between the two conditions are shown in Figure 7.5.

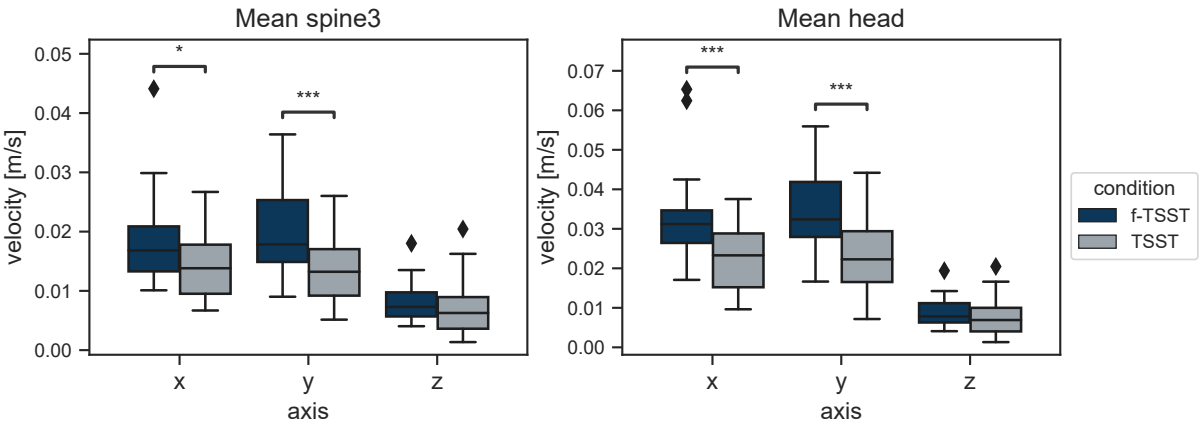

Figure 7.5: Generic feature mean velocity of head and spine3 for the single axes, values showed as mean with standard deviation, Note: $*p < 0.05, **p < 0.01, ***p < 0.001$

For both body parts, the mean velocity of the z-axis showed no statistical differences between the two conditions (spine3: $w = 64, p = 0.194, g = -0.168$; head: $w = 4, p = 0.126, g = -0.993$). In contrast, the other two axis (x, y) were statistically significant between the TSST and f-TSST, for head and spine3 (Table 7.4 and 7.5). Additionally, for spine3 and the head, the mean velocity increase between TSST and f-TSST was higher in the y-axis than in the x-axis. For the head, the increase between the two conditions for the y-axis was 51.24% and for the x-axis 47.73%. The spine3 had an increase of 41.21% for the y-axis and 26.45% for the x-axis, between TSST and f-TSST.

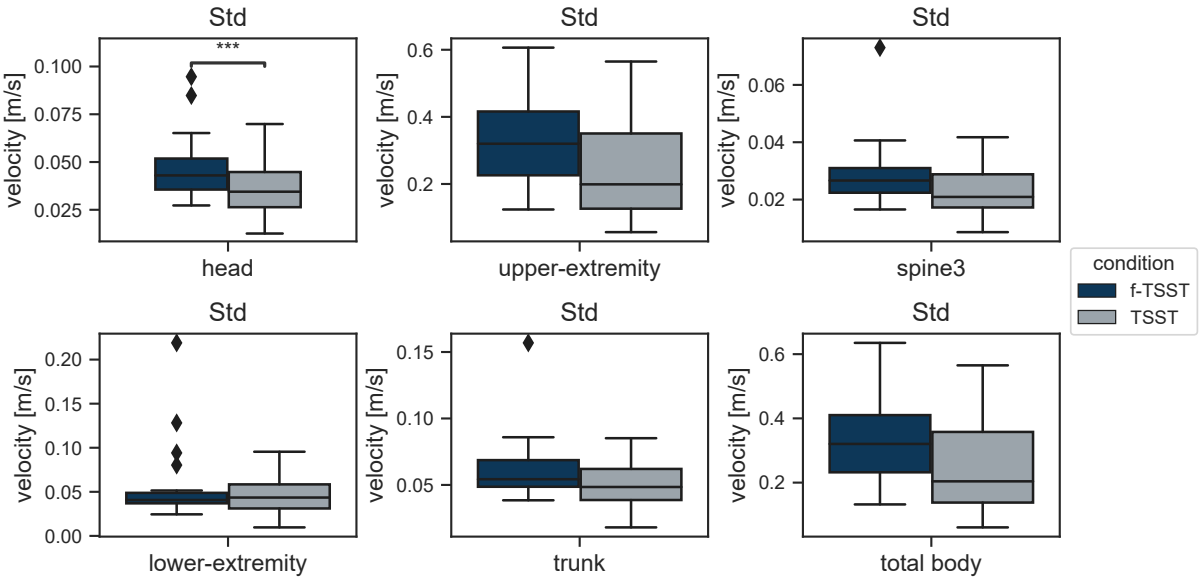

Figure 7.6: Generic features for the Std of the norm, Note: $^{*}p < 0.05, ^{**}p < 0.01, ^{***}p < 0.001$

The standard deviation (Std) difference between (f-)TSST was statistical significant for head ($w = 16, p = 0.002, g = -0.744$), upper-extremity ($T(19) = -4.01, p = 0.003; g = -.672$) and total-body ($T(19) = -3.91, p = 0.004, g = -0.673$) (Table 7.4 and 7.5). The feature Std of the velocity of the three body parts was more than 32% percent higher during f-TSST than TSST. The most noticeable difference between stress and non-stress was again in the upper-extremity with 41.50% ($T(19) = -4.014, p = 0.003, g = -0.672$). The other three body parts (lower-extremity, spine3, trunk) showed no significant difference between the two conditions (Figure 7.6).

The Std feature difference was significantly higher during the f-TSST than during the TSST for both body parts and all axes, respectively. However, the lowest difference for head and spine3 occurred along the z-axis. The head Std of velocity for z-axis was during the f-TSST 30.32% higher ($w = 23, p = 0.017, g = -0.570$) and the spine3 Std 29.20% ($w = 37, p = 0.023, g = -0.534$).

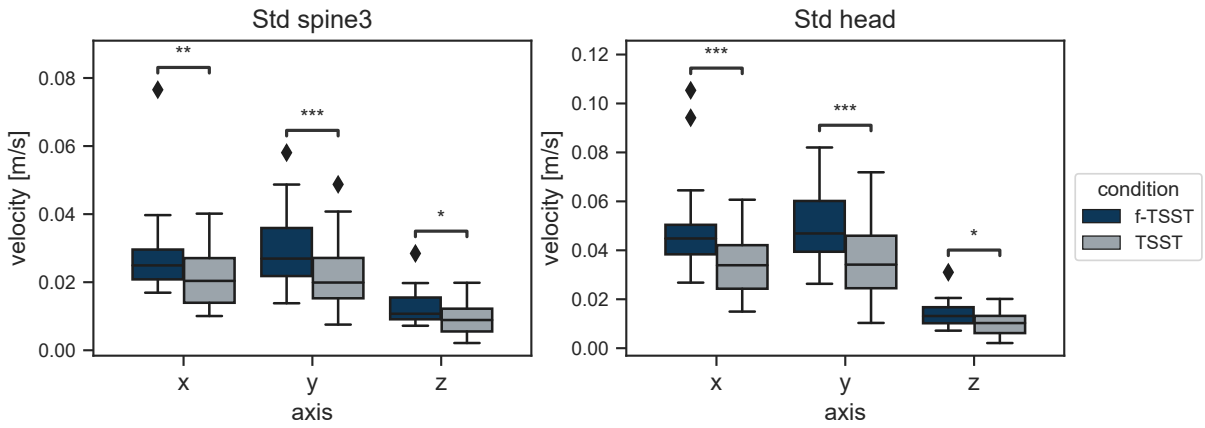

Figure 7.7: Generic feature Std head and spine3 of the single axes, Note: $^{*}p < 0.05$, $^{**}p < 0.01$, $^{***}p < 0.001$

Table 7.4: Wilcoxon results of the generic features, Note: $^{*}p < 0.05$, $^{**}p < 0.01$, $^{***}p < 0.001$

Type	Body-part	Axis	Wilcoxon w	p	Hedge's g
Mean	head	x	4	0.000^{***}	-0.993
		z	56	0.126	-0.247
	trunk	norm	20	0.003^{**}	-0.612
	lower-extrem	norm	31	0.012^{**}	-0.603
	upper-extrem	norm	13	0.001^{**}	-0.868
	spine3	norm	13	0.001^{**}	-0.681
		x	31	0.012^{*}	-0.535
		z	64	0.194	-0.168
SamEn	head	y	1	0.000^{***}	-1.882
Std	spine3	x	21	0.004^{**}	-0.624
		z	37	0.023^{*}	-0.534
	head	z	34	0.017^{*}	-0.570
		x	4	0.000^{***}	-0.884
	lower-extrem	norm	75	0.358	-0.302
	head	norm	16	0.002^{**}	-0.744
	trunk	norm	57	0.130	-0.488
	spine3	norm	50	0.078	-0.534

The last presented generic feature is the Sample Entropy (SamEn) of head rotation. The sample entropy (a measure for the randomness of the data) was statistically significant between the two conditions for both all single axes and the norm, respectively (Table 7.4 and 7.5). The sample entropy was during the f-TSST for all axes more than 50% increased than during the TSST (Figure 7.8). The highest increase of sample entropy between (f-)TSST was observed in the y-axis, with a higher value of 96.53% ($w = 1, p = 0.000 g = -1.882$). The lowest increase between the two conditions was in z-direction with 51.70% ($T(19) = -5.10, p = 0.001, g = -1.238$).

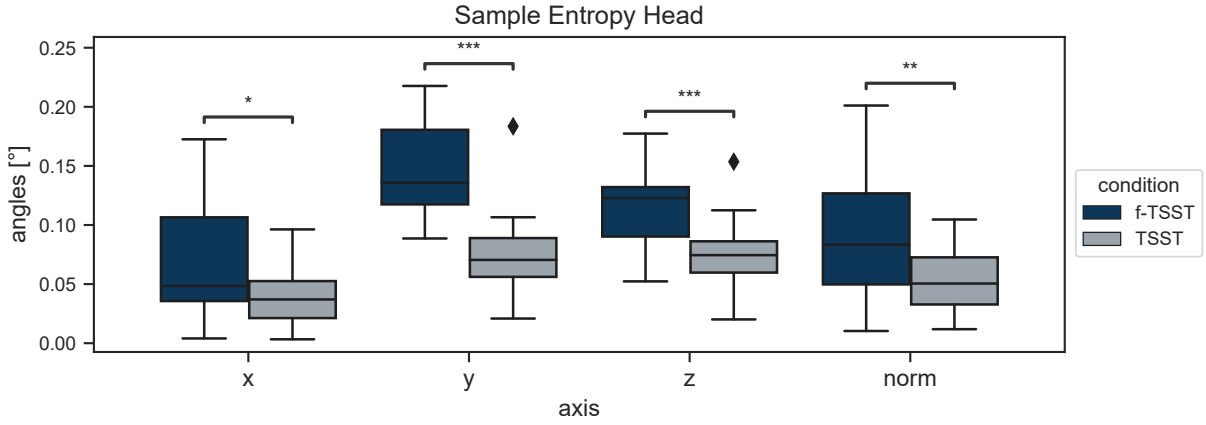

Figure 7.8: Generic feature sample entropy (SamEn) of the rotation, values showed as mean with standard deviation, Note: $^{*}p < 0.05$, $^{**}p < 0.01$, $^{***}p < 0.001$

Table 7.5: T-test results of the generic features, Note: $^{*}p < 0.05$, $^{**}p < 0.01$, $^{***}p < 0.001$; SamEn : Sample Entropy

Type	Body part	Axis	T(19)	p	Hedge's g
Mean	head	norm	-7.0966	0.000^{***}	-1.085
		y	-8.4608	0.000^{***}	-1.196
	spine3	y	-6.0775	0.000^{***}	-0.872
	total-body	norm	-5.0073	0.001^{***}	-0.900
SamEn	head	norm	-3.6477	0.006^{**}	-0.879
		x	-3.0468	0.017^{*}	-0.698
		z	-5.103	$<0.001^{***}$	-1.238
Std	head	y	-6.5344	0.000^{***}	-0.971
	spine3	y	-4.5451	0.001^{**}	-0.673
	total-body	norm	-3.9088	0.004^{**}	-0.673
	upper-extrem	norm	-4.0141	0.003^{**}	-0.672

Table 7.6: Mean and Std of all generic features., Note: Mean ± Std

Type	Body part	Axis	TSST	f-TSST
Std	head	norm	0.036 ± 0.013	0.048 ± 0.017
		x	0.034 ± 0.013	0.049 ± 0.020
		y	0.036 ± 0.014	0.050 ± 0.015
		z	0.011 ± 0.006	0.014 ± 0.006
	spine3	x	0.021 ± 0.009	0.028 ± 0.013
		y	0.022 ± 0.010	0.030 ± 0.011
		z	0.010 ± 0.005	0.013 ± 0.005
	total-body	norm	0.245 ± 0.137	0.342 ± 0.145
	upper-extrem	norm	0.237 ± 0.139	0.336 ± 0.148
mean	head	norm	0.037 ± 0.013	0.054 ± 0.017
		x	0.022 ± 0.008	0.033 ± 0.013
		y	0.023 ± 0.009	0.034 ± 0.010
	lower-extrem	norm	0.041 ± 0.016	0.054 ± 0.026
	spine3	norm	0.025 ± 0.010	0.033 ± 0.012
		x	0.015 ± 0.006	0.019 ± 0.008
		y	0.014 ± 0.006	0.020 ± 0.007
	total-body	norm	0.206 ± 0.102	0.316 ± 0.134
	trunk	norm	0.059 ± 0.023	0.075 ± 0.027
	upper-extrem	norm	0.179 ± 0.099	0.281 ± 0.129
SamEn	head	norm	0.053 ± 0.028	0.090 ± 0.052
		x	0.040 ± 0.026	0.066 ± 0.046
		y	0.074 ± 0.035	0.145 ± 0.039
		z	0.075 ± 0.030	0.114 ± 0.031

7.2.2 Expert Features

Evaluating the expert features, non of the movement features distance and TimeTogether was statistically significant between the two conditions. The significance values of all expert features can be found in Table A.3 and Table A.4.

The absolute movement (AbsMov) feature results are presented in Figure 7.9. The AbsMov was statistical significant between TSST and f-TSST, for all evaluated body parts, expect for the lower-extremity ($w = 59, p = 0.152, g = -0.315$) (Table 7.8 and Table 7.7). The increase of AbsMov value of all observed body parts was during the TSST more than 40% higher than during the f-TSST. The highest AbsMov increase was observed for the trunk, during the f-TSST, the movement was 51.34% higher than during the TSST (Figure 7.9). The detailed Mean ± Std values for all expert features are presented in Table 7.9.

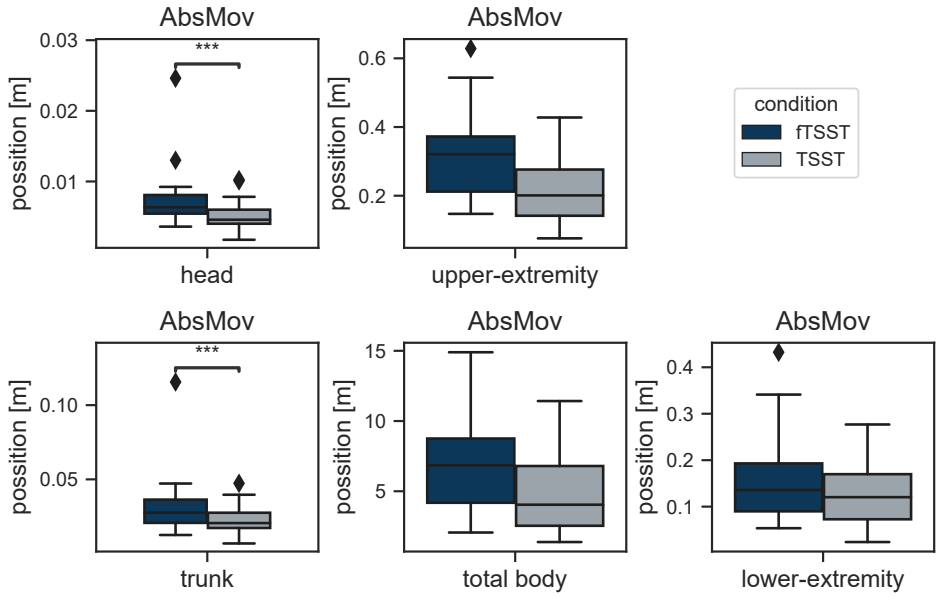

Figure 7.9: Movement change results of the AbsMov feature, Note: $*p < 0.05, **p < 0.01, ***p < 0.001$

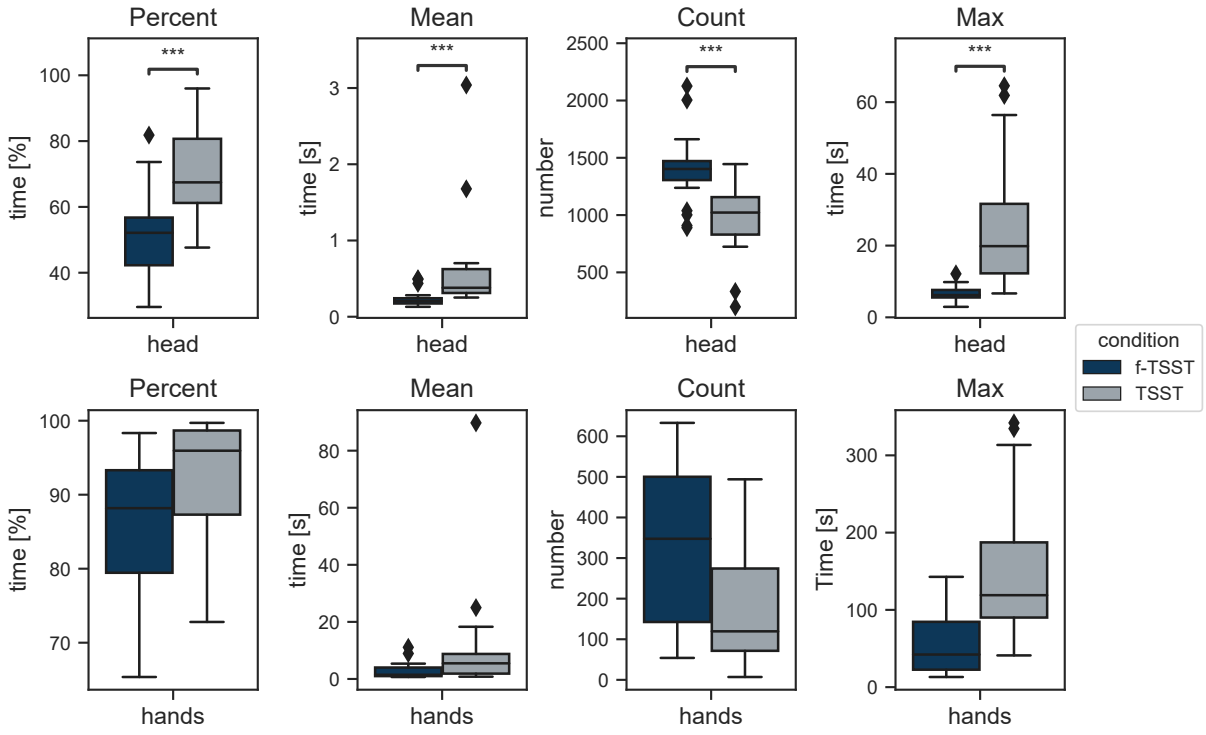

Figure 7.10: Static-moments (StatMom) feature results, values showed as mean with standard deviation, Note: $^{*}p < 0.05,\ ^{**}p < 0.01,\ ^{***}p < 0.001$

In contrast to the AbsMov features, the static moments (StatMom) characteristics were all statistically significant between the two conditions. The StatMom were calculated for the head and the arms. Comparing the percentage of static moments of the two conditions, the head was motionless 69.78% $\pm$ 13.66% of the time during the TSST period and only 51.44% $\pm$ 13.47% of the time during the f-TSST period. The hands were motionless for 92.95% $\pm$ 7.47 of the TSST time and for 86.06% $\pm$ 9.97 of the f-TSST time (Figure 7.10).

Table 7.7: T-test results for the Expert features, Note: $^{*}p < 0.05$, $^{**}p < 0.01$, $^{***}p < 0.001$

Feature	Type	Body part	T(19)	p	Hedge's g
AbsMov	-	total-body	-2.9534	0.021^{*}	-0.652
		upper-extrem	-3.5152	0.007^{**}	-0.763
StatMom	percent	head	10.0672	0.000^{***}	1.325
	count	head	-7.3227	0.000^{***}	-1.361

Table 7.8: Wilcoxon results for the Expert Features, Note: $^{*}p < 0.05$, $^{**}p < 0.01$, $^{***}p < 0.001$

Feature	Type	Body-part	Wilcoxon w	p	Hedge's g
AbsMov	-	head	11	$<0.001^{***}$	-0.663
		lower-extrem	59	0.152	-0.315
		trunk	15	0.002^{**}	-0.631
StatMom	percent	hands	26	0.006^{**}	0.768
	mean	head	0	0.000^{***}	0.788
		hands	26	0.006^{**}	0.544
	count	hands	13	$<0.001^{***}$	-0.919
	max	head	0	0.000^{***}	1.412
		hands	6	0.000^{***}	1.314

For the arms, the mean time without movement (StatMomMean) during TSST was 10.69 $\pm$ 19.62 s, whereas, during f-TSST, it was only 2.91 $\pm$ 2.85 s, so the static moments (StatMom) during TSST were noticeably longer for the arms. Comparing the movement of the head during the two conditions the head had shorter motionless periods during the TSST (TSST: 0.61 $\pm$ 0.65 s, f-TSST: 0.24 $\pm$ 0.11 s) and overall shorter periods than the arms. Considering the maximum motionless periods of the head the longest motionless TSST period was 25.43 $\pm$ 18.33 s, and the f-TSST was only 6.73 $\pm$ 2.12 s. In comparison, the maximum motionless time of the hands was 149.45 $\pm$ 93.03 s during the TSST and only 54.06 $\pm$ 38.36 s during the f-TSST .

The head had 431 static moments more during the f-TSST than during the TSST (StatMom-Count), for the hands, it was only 156 more static moments, but the head (1400 $\pm$ 306.8) has in total more static moments than the arms (325 $\pm$ 135.18) (Figure 7.10).

Table 7.9: Mean and Std of all Expert features., Note: Mean $\pm$ Std

Feature	Type	Body part	TSST	f-TSST
AbsMov	-	head	0.01 $\pm$ 0.0	0.01 $\pm$ 0.0
	-	total-body	4.88 $\pm$ 2.89	7.02 $\pm$ 3.53
	-	trunk	0.02 $\pm$ 0.01	0.03 $\pm$ 0.02
	-	upper-extrem	0.22 $\pm$ 0.1	0.31 $\pm$ 0.13
StatMom	percent	head	69.78 $\pm$ 13.66	51.44 $\pm$ 13.47
		hands	92.95 $\pm$ 7.47	86.06 $\pm$ 9.97
	mean	head	0.61 $\pm$ 0.65	0.24 $\pm$ 0.11
		hands	10.69 $\pm$ 19.62	2.91 $\pm$ 2.85
	count	head	968.95 $\pm$ 306.79	1399.95 $\pm$ 314.04
		hands	169.45 $\pm$ 135.18	325.35 $\pm$ 192.43
	max	head	25.53 $\pm$ 18.33	6.73 $\pm$ 2.12
		hands	149.45 $\pm$ 93.03	54.06 $\pm$ 38.36

7.3 Relationship of Stress-induced variables and Movement

To assess the relationship, a regression analysis was performed for predicting the movement changes by the self-reports and biomarkers. Afterwards, the self-reports and biomarkers are predicted by movement factors of the single body parts. At last, the biomarkers and self-report scores will be predicted by movement features of single body parts.

7.3.1 Prediction of PCA Motion Factor using Biomarkers and Self-Reports

Computing pairwise correlation coefficients revealed (Figure B.1), that the two biomarkers Δc_{max} and AUG_g had a correlation coefficient of $0.88 > 0.80$. For that, reason, AUG_g was excluded from the regression analysis. After evaluating the steps of the stepwise backward multiple linear regression, the best-fitted model is presented in Table 7.10. The only remaining predictor was the PASA-Threat questionnaire score. The predictor explains 19.7% of the variance PCA movement factor. A lower PCA movement factor was predicted by a higher PASA-Threat value ($\beta = 0.494, 95\%CI = [0.034 to 0.955], p = 0.037$). Figure 7.11 shows the relation between the PCA movement factor and the PASA-Threat.

Table 7.10: Best fitted model of the linear regression;
β : regression coefficient σ : standard error, adj : adjusted

Predictors	β	σ	T	p	R^2	adj-R^2	CI[2.5%]	CI[97.5%]
PASA-Threat	-0.494	0.217	-2.274	0.037	0.244	0.197	-0.955	-0.034

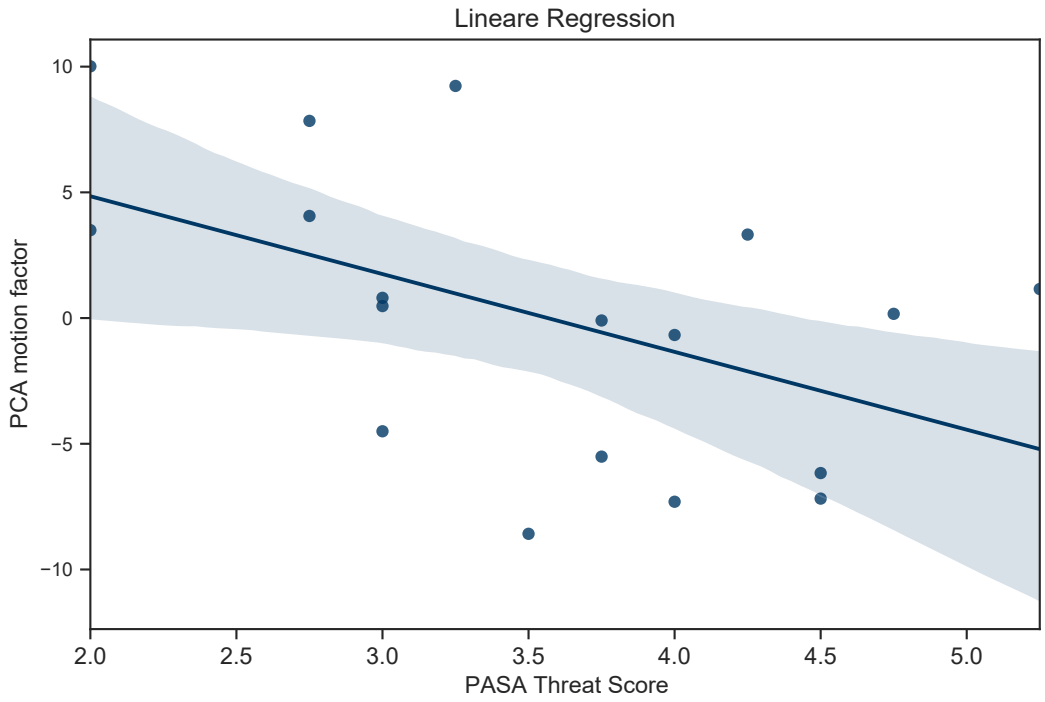

Figure 7.11: Relation between the PCA movement factor and the PASA-Threat.

7.3.2 Prediction of Biomarkers and Self-Reports using PCA Motion Factors

In contrast to the section before, the regression analysis was inverted to examine to which extent traditional stress assessment modalities, such as biomarker and self-reports, can be predicted by PCA movement factors of different body parts. As predictors, the calculated PCA movement factors were used. Due to the low number of significant features, the total body features and also lower extremity features were excluded. Afterwards, the remaining body part's PCA values were evaluated. For the head, using n=5 principal components resulted in an explained variance of 80%. The same explained variance was achieved by n=4 components for arms and only n=2 components for the spine3. Checks for multicollinearity revealed that one of the head components and one of the spine3 components were highly correlated (r = 0.84) (Figure B.2). Thus, the spine3 feature

was excluded from further analysis. As an independent variable for each backward multiple linear regressions, one of the seven biomarker or self-report scores were chosen. As non of the STADI-State and the PASA-Challenge, the Δc_{max}, and the AUG_g were significantly predicted the PCA movement factors, the tables are not presented in the following. The best-fitted model of the STADI-State only included head-pca4 (fifth PCA factor of the head). It explained the STADI-state with 11.9% of the total variance ($\beta = 0.414,\ 95\%CI = [-0.069\ to\ 0.896],\ p = 0.088$). The best-fitted model for the PASA-Challenge explained 12.3% of the total variance of the PASA-Challenge. The Δc_{max} was only predicted by the head-pca4 (p=0.186) with 5.1% of the total variance. For the cortisol AUG_g, the PCA movement factors explained 26.5% of the variance.

The best-fitted model of the PANAS-NegAffect included head-pca1, head-pca3, and arms-pca3. The PCA movement factors explained 26.5% of the variance of the questionnaire. A higher score was significantly predicted by a lower value of the head-pca1 (p=0.028). Also included in the model but not significant were head-pca3 and arms-pca3. The regression result for the PANAS-NegAffect is given in Table 7.11.

Table 7.11: Regression result for predicting the PANAS-NegAffect score;
β : regression coefficient, σ : standard error, adj : adjusted

predictors	β	σ	T	p	R^2	adj-R^2	CI[2.5%]	CI[97.5%]
head-pca1	-0.524	0.214	-2.444	0.028	0.395	0.265	-0.983	-0.064
head-pca3	0.227	0.212	1.071	0.302	0.395	0.265	-0.228	0.683
arms-pca3	-0.276	0.212	-1.302	0.214	0.395	0.265	-0.731	0.179

The PANAS-PosAffect was significantly predicted by head-pca0 (p=0.006), head-pca4 (p=0.013) and arms-pca0 (p=0.009) with 61.9% of the explained variance. The result of the regression can be found in Table 7.12.

Table 7.12: Regression result for predicting the PANAS-PosAffect score;
β : regression coefficient, σ : standard error, adj : adjusted

Predictors	β	σ	T	p	R^2	adj-R^2	CI[2.5%]	CI[97.5%]
head-pca0	0.539	0.163	3.309	0.006	0.708	0.618	0.187	0.891
head-pca1	0.436	0.151	2.881	0.013	0.708	0.618	0.109	0.762
head-pca4	-0.193	0.169	-1.142	0.274	0.708	0.618	-0.557	0.172
arms-pca0	-0.532	0.174	-3.058	0.009	0.708	0.618	-0.907	-0.156

The results for predicting the PASA-Threat are presented in Table 7.13. The PASA-Threat was explained, by the best fitted model with 79.6% of total variance. The model included

significant head-pca0 (p=0.002), head-pca1 (p=0.009), head-pca3 (p=0.011), head-pca4 (p=0.000) and spine3-pca1 (p=0.031). Additional included in the model were head-pca2 (p=0.124) and arms-pca1 (p=0.090).

Table 7.13: Regression result for predicting the PASA-Threat score;
β : regression coefficient, σ : standard error, adj : adjusted

Predictors	β	σ	T	p	R^2	adj-R^2	CI[2.5%]	CI[97.5%]
head-pca0	0.576	0.140	4.126	0.002	0.88	0.796	0.265	0.888
head-pca1	-0.388	0.120	-3.224	0.009	0.88	0.796	-0.656	-0.120
head-pca2	-0.224	0.134	-1.679	0.124	0.88	0.796	-0.522	0.073
head-pca3	0.436	0.141	3.101	0.011	0.88	0.796	0.123	0.749
head-pca4	0.583	0.115	5.056	0.000	0.88	0.796	0.326	0.840
arms-pca1	-0.312	0.166	-1.879	0.090	0.88	0.796	-0.682	0.058
spine3-pca1	-0.350	0.139	-2.508	0.031	0.88	0.796	-0.661	-0.039

For better interpretability, the signs of the PCA factors were multiplied by -1, as all signs of the PCA, scores are arbitrary, and only the sign patterns are meaningful [Jol16]. Additionally, it is known from previous results of the thesis is known, that the subjects reduce their movement during the stressed condition.

7.3.3 Prediction of Biomarkers and Self-Reports using Movement changes

This section presents the regression result of the regression analysis to predict the biomarkers and self-reports by changes of body posture and movement of different body parts. The regression analysis results were grouped by the different body parts. Each subsection presents the regression result for all biomarkers and self-reports. The body part lower extremity was excluded as before as only one feature was significant between the two conditions.

Total body

Checks for multicollinearity revealed (Figure B.5) that the features mean velocity, Std of speed and the AbsMov were highly correlated (r = 0.81 and r = 85). Thus, the mean of the velocity feature was excluded from further analysis which resulted in three predictors for the total body movement. The regression analyses of the total body only included significant features for the prediction of the PANAS-PosAffect and the PASA-Threat questionnaire. A higher PANAS-PosAffect score difference was significantly predicted by a higher value of the AbsMov feature of the total body (p=0.04) with 18.9% of the total variance (see Table 7.14 for detailed results).

Table 7.14: Regression result for predicting the PANAS-PosAffect score by the features of the total body; β : regression coefficient, σ : standard error, adj : adjusted

Predictors	β	σ	T	p	R^2	adj-R^2	CI[2.5%]	CI[97.5%]
AbsMov	0.487	0.218	2.23	0.04	0.237	0.189	0.024	0.95

The PASA-Threat was also significantly predicted by the AbsMov of the total body (p=0.014). It predicted 28.2% of the total variance (detailed results are given in Table 7.15). A lower value of the PASA-Threat score was predicted by a higher value of the AbsMov feature.

Table 7.15: Regression result for predicting the PASA-Threat score by the total body features; β : regression coefficient, σ : standard error, adj : adjusted

Predictors	β	σ	T	p	R^2	adj-R^2	CI[2.5%]	CI[97.5%]
AbsMov	-0.569	0.206	-2.768	0.014	0.324	0.282	-1.005	-0.133

The STADI-State, PANAS-NegAffect, and the biomarker were not significant predicted by features of the total body, but the best-fitted model of the STADI-State included the Std of the velocity (p=0.103) with 4.7% of the total variance. The PANAS-PosAffect was predicted by the absolute movement of the head (p=0.122) with 9%. The best-fitted model of the PASA-Challenge score explained just 3.3% of the total variance, including the Std of the velocity (p=0.275) and the AbsMov feature (p=0.129). The last two linear regressions were performed to predict the biomarkers. The Δc_{max} could not be predicted by the total body features. The best-fitted model for the AUG_g explained the cortisol score with 9.4%, including only the AbsMov feature.

Head

Checks for multicollinearity revealed (Figure B.3) that the mean velocity feature was highly correlated with three other features. Additionally, the absolute-energy feature was excluded, due to a strong correlation with two other head features. Thus, the mean velocity feature was excluded from further analysis which resulted in nine remaining predictors for the regression analysis of the head. The only best-fitted model of the PASA-Challenge was the only one without a significant predictor. It included four variables but was only able to explain 4.1% of the total variance. The containing variables were Std of velocity (p=0.115), CV of speed (p=0.224), percentage of time with static moments (p=0.167), and the maximum time of static moments (p=0.193).

The STADI-State was significantly explained with 40.5% of total variance by the features AbsMov, StatMomPercent, and StatMomMean. Additionally included in the best-fitted model

were the maximum time of static moments and the sample entropy of rotation. The results are presented in Table 7.16. For the STADI-State a higher score was significantly predicted by higher values of the AbsMov, the StatMomPercent and the StatMomMean features, and a lower value of the StatMomMax feature. In addition, higher state anxiety was associated with a higher value of SamEnRotation.

Table 7.16: Regression analysis results predicting the STADI-State by the features of the head; β : regression coefficient, σ : standard error, adj : adjusted

Predictors	β	σ	T	p	R^2	adj-R^2	CI[2.5%]	CI[97.5%]
AbsMov	1.025	0.271	3.779	0.003	0.58	0.405	0.434	1.616
StatMomPercent	0.826	0.295	2.804	0.016	0.58	0.405	0.184	1.468
StatMomMean	0.784	0.313	2.505	0.028	0.58	0.405	0.102	1.466
StatMomMax	-0.688	0.332	-2.069	0.061	0.58	0.405	-1.411	0.036
SamEnRotation	-0.263	0.200	-1.315	0.213	0.58	0.405	-0.698	0.173

The PANAS-NegAffect was significantly explained with 51.9% of total variance by the features Std, AbsMov, CV, StatMomMean, StatMomMax. The best-fitted model also includes the feature SamEnVel (p=0.172). The findings of the regression analysis are given in Table 7.17. In summary, a higher score value was significantly predicted by lower values of the features Std and StatMomMax, and higher values of the features AbsMov, CV, and StatMomMean. The features SamEnVel was additionally included in the model and it was predicted with a higher value.

Table 7.17: Regression analysis results predicting the PANAS-NegAffect score by head features; β : regression coefficient, σ : standard error, adj : adjusted

Predictors	β	σ	T	p	R^2	adj-R^2	CI[2.5%]	CI[97.5%]
Std	-0.905	0.344	-2.634	0.023	0.689	0.519	-1.662	-0.149
AbsMov	0.680	0.279	2.434	0.033	0.689	0.519	0.065	1.294
CV	0.956	0.218	4.393	0.001	0.689	0.519	0.477	1.435
StatMomMean	0.819	0.299	2.737	0.019	0.689	0.519	0.161	1.478
StatMomMax	-1.285	0.366	-3.511	0.005	0.689	0.519	-2.090	-0.479
SamEnRotation	-0.273	0.187	-1.463	0.172	0.689	0.519	-0.684	0.138

The best-fitted model of the PANAS-PosAffect included the features Std and StatMomCount, which explained 69.4% of the total variance. Additionally, the features StatMomPercent and StatMomMean were included in the best-fitted model. The detailed results are given in Table 7.18. A higher PANAS-PosAffect score was significantly predicted by a lower value of the Std and a higher value of the StatMomCount.

Table 7.18: Regression analysis results predicting the PANAS-PosAffect score by head features; β : regression coefficient, σ : standard error, adj : adjusted

Predictors	β	σ	T	p	R^2	adj-R^2	CI[2.5%]	CI[97.5%]
Std	-0.903	0.242	-3.727	0.003	0.766	0.694	-1.427	-0.380
StatMomPercent	-0.491	0.251	-1.956	0.072	0.766	0.694	-1.033	0.051
StatMomMean	0.205	0.170	1.202	0.251	0.766	0.694	-0.163	0.572
StatMomCount	0.581	0.176	3.311	0.006	0.766	0.694	0.202	0.961

The PASA-Threat score was explained significantly with 61.4% of total variance by the features Std, StatMomCount, StatMomMax, and SamEnVel. Further included in the best-fitted model was the feature AbsMov (p=0.147). The detailed regression results are presented in Table 7.19. Looking at the relationship of the PASA-Threat score and the movement features higher values of the PASA-Threat score were significantly predicted by lower values in Std, StatMomCount, StatMomMax, and SamEnVel.

Table 7.19: Regression analysis results predicting the PASA-Threat score by head features; β : regression coefficient, σ : standard error, adj : adjusted

Predictors	β	σ	T	p	R^2	adj-R^2	CI[2.5%]	CI[97.5%]
Std	-0.820	0.258	-3.176	0.008	0.728	0.614	-1.382	-0.258
AbsMov	0.351	0.227	1.551	0.147	0.728	0.614	-0.142	0.845
StatMomCount	-0.479	0.182	-2.629	0.022	0.728	0.614	-0.876	-0.082
StatMomMax	-0.456	0.193	-2.357	0.036	0.728	0.614	-0.877	-0.034
SamEnVel	-0.515	0.190	-2.718	0.019	0.728	0.614	-0.928	-0.102

For the prediction of the biomarkers by the head movement features, both cortisol-derived features were significantly predicted. The cortisol-derived features Δc_{max} was significantly predicted by the features Std, StatMomMean, and StatMomMax with 44.4% of variance explained. Also included in the model were the features AbsMov (p=0.095) and CV (p=0.119). These results can be found in Table 7.20. A higher cortisol increase (Δc_{max}) was significantly predicted by lower values of Std and StatMomMax and higher values of StatMomMean.

The cortisol-derived feature AUG_g was predicted by the same features as Δc_{max}, but in addition, the AbsMov feature (p=0.049) was significant. A higher AbsMov value predicted higherAUG_g values. The AUG_g value could be explained by the movement features of the head with 48.3% of the total variance. Detailed results are listed in Table 7.21.

Table 7.20: Regression analysis results predicting the Δc_{max} by head features;
β : regression coefficient, σ : standard error, adj : adjusted

Predictors	β	σ	T	p	R^2	adj-R^2	CI[2.5%]	CI[97.5%]
Std	-0.936	0.428	-2.189	0.049	0.444	0.212	-1.868	-0.004
AbsMov	0.643	0.356	1.809	0.095	0.444	0.212	-0.131	1.418
CV	0.467	0.278	1.677	0.119	0.444	0.212	-0.140	1.073
StatMomMean	1.030	0.379	2.717	0.019	0.444	0.212	0.204	1.857
StatMomMax	-1.420	0.466	-3.048	0.010	0.444	0.212	-2.435	-0.405

Table 7.21: Regression analysis results predicting the AUG_g score by head features;
β : regression coefficient, σ : standard error, adj : adjusted

Predictors	β	σ	T	p	R^2	adj-R^2	CI[2.5%]	CI[97.5%]
Std	-1.107	0.412	-2.684	0.020	0.483	0.267	-2.006	-0.208
AbsMov	0.751	0.343	2.192	0.049	0.483	0.267	0.004	1.498
CV	0.521	0.268	1.942	0.076	0.483	0.267	-0.063	1.106
StatMomMean	1.071	0.366	2.929	0.013	0.483	0.267	0.274	1.868
StatMomMax	-1.432	0.449	-3.190	0.008	0.483	0.267	-2.411	-0.454

Spine3 (body sway)

For the prediction of the self-reports and biomarkers by the spine3 movement features, non of the features was significant. Due to the low number of the spine3 norm features, the movement features of the single axes were also included. Before performing the regression, the predictors were tested for multicollinearity using pairwise correlation coefficients revealed (Figure B.4). Thus, the feature Abs energy (of the x-and y-axis) and the feature mean velocity (of the y-axis) were excluded, because of high correlation with other features. Only the PASA-Challenge was explained by a higher percentage of the variance than 10%. The score was explained by 13.5% of the total variance. The best-fitted model included only the mean velocity in the x-direction (p=0.074).

Arms

Checks for multicollinearity revealed (Figure B.3) that the mean velocity feature was highly correlated with four other features. Thus, the mean velocity feature of the upper extremity was excluded from further regression analysis, as this feature was highly correlated with four of the other arm features. The regression analysis was performed based on the remaining 11 arm

features. All biomarker and self-report values could be predicted significantly by features of the arms. First, the result of the regression analysis for the STADI-State questionnaire is presented in Table 7.22. The STADI-States score was significantly predicted with 28.4% by the features Std of Left forearms rotation (LFaSTDrotation) and StatMomCount. The best-fitted model included additionally the following features: CV of Left forearms rotation (LFaCVrotation), max of Left forearms rotation (LFaMaxRotation), StatMomPercent and StatMomMax. A higher value of the STADI-State was significantly predicted by higher values of LFaSTDrotation and a lower value of StatMomCount.

Table 7.22: Regression analysis results predicting the STADI-State by arm features; β : regression coefficient, σ : standard error, adj : adjusted

Predictors	β	σ	T	p	R^2	adj-R^2	CI[2.5%]	CI[97.5%]
Std	0.917	0.525	1.748	0.111	0.579	0.284	-0.252	2.086
LFaSTDrotation	1.042	0.376	2.774	0.020	0.579	0.284	0.205	1.878
LFaCVrotation	-0.481	0.291	-1.651	0.130	0.579	0.284	-1.129	0.168
LFaMaxRotation	-0.691	0.312	-2.212	0.051	0.579	0.284	-1.386	0.005
StatMomPercent	-0.742	0.571	-1.300	0.223	0.579	0.284	-2.015	0.530
StatMomCount	-1.879	0.662	-2.838	0.018	0.579	0.284	-3.355	-0.404
StatMomMax	0.611	0.342	1.786	0.104	0.579	0.284	-0.151	1.374

The PANAS-NegAffect was explained by 24.2% of the total variance of the PANAS score. A higher score value was significantly predicted by a higher value of the StatMomCount feature. Additionally, included in the best-fitted model are the features Std, CV of Right forearms rotation (RFaCVrotation), LFaMaxRotation and StatMomPercent. All were linked with a higher PANAS-NegAffect score. The detailed results are listed in Table 7.23.

Table 7.23: Regression analysis results predicting the PANAS-NegAffect by arm features; β : regression coefficient, σ : standard error, adj : adjusted

Predictors	β	σ	T	p	R^2	adj-R^2	CI[2.5%]	CI[97.5%]
Std	0.397	0.374	1.060	0.310	0.465	0.242	-0.418	1.212
RFaCVrotation	0.422	0.280	1.507	0.158	0.465	0.242	-0.188	1.033
LFaMaxRotation	-0.367	0.245	-1.498	0.160	0.465	0.242	-0.901	0.167
StatMomMax	-0.890	0.657	-1.355	0.201	0.465	0.242	-2.323	0.542
StatMomCount	-1.432	0.561	-2.551	0.025	0.465	0.242	-2.655	-0.209

The result of the regression analysis predicting the PANAS-PosAffect is presented in Table 7.24. A higher PANAS-PosAffect score was significant predicted by lower values of LFaSTDrota-

tion and StatMomMax and a higher value of StatMomCount. The best-fitted model included also the features Std and StatMomPercent. With the regression analysis, 55.6% of the total variance of the PANAS-PosAffect could be explained.

Table 7.24: Regression analysis results predicting the PANAS-PosAffect by arm features; β : regression coefficient, σ : standard error, adj : adjusted

Predictors	β	σ	T	p	R^2	adj-R^2	CI[2.5%]	CI[97.5%]
Std	-0.527	0.333	-1.584	0.139	0.556	0.371	-1.253	0.198
LFaSTDrotation	-0.603	0.262	-2.303	0.040	0.556	0.371	-1.174	-0.032
StatMomPercent	0.694	0.521	1.332	0.207	0.556	0.371	-0.441	1.830
StatMomCount	1.458	0.534	2.731	0.018	0.556	0.371	0.295	2.622
StatMomMax	-0.663	0.294	-2.256	0.044	0.556	0.371	-1.304	-0.023

The PASA-Challenge score was only predicted significantly by arm features. The score was explained by 55.7% of variance by lower value of LFaCVrotation and higher values of Std, RFaCVrotation, and StatMomPercent. The result of the regression analysis is depicted in Table 7.25.

Table 7.25: Regression analysis results predicting the PASA-Challenge by arm features; β : regression coefficient, σ : standard error, adj : adjusted

Predictors	β	σ	T	p	R^2	adj-R^2	CI[2.5%]	CI[97.5%]
Std	1.144	0.315	3.631	0.003	0.688	0.557	0.458	1.831
LFaCVrotation	-0.726	0.236	-3.072	0.010	0.688	0.557	-1.240	-0.211
RFaCVrotation	0.599	0.221	2.709	0.019	0.688	0.557	0.117	1.082
StatMomPercent	0.956	0.312	3.067	0.010	0.688	0.557	0.277	1.636
StatMomMax	0.205	0.194	1.060	0.310	0.688	0.557	-0.217	0.627

The PASA-Threat score was only predicted significantly by the AbsMov features. The PASA-Threat score could be explained by 37.5% of the total variance. Also included in the best-fitted model were LFaCVrotation and StatMomMean, lower values were associated with higher values of the score. The findings of the regression analysis can be found in Table 7.26. The result of the prediction of the Δc_{max} are presented in Table 7.27. Higher values of feature Δc_{max} were significantly explained by 58.3% of variance by lower values of AbsMov, StatMomPercent, and StatMomCount, and higher values of LFaSTDrotation and StatMomMean. Also a higher value of the features LFaCVrotation was associated with a higher cortisol increase.

Table 7.26: Regression analysis results predicting the PASA-Threat by arm features; β : regression coefficient, σ : standard error, adj : adjusted

Predictors	β	σ	T	p	R^2	adj-R^2	CI[2.5%]	CI[97.5%]
AbsMov	-0.606	0.193	-3.138	0.007	0.485	0.375	-1.021	-0.192
LFaCVrotation	-0.318	0.210	-1.510	0.153	0.485	0.375	-0.769	0.134
StatMomMean	-0.433	0.210	-2.058	0.059	0.485	0.375	-0.885	0.018

Table 7.27: Regression analysis results predicting the Δc_{max} by the features of the arms; β : regression coefficient, σ : standard error, adj : adjusted

Predictors	β	σ	T	p	R^2	adj-R^2	CI[2.5%]	CI[97.5%]
AbsMov	-1.761	0.398	-4.429	0.001	0.73	0.583	-2.636	-0.886
LFaSTDrotation	0.644	0.240	2.688	0.021	0.73	0.583	0.117	1.171
RFaCVrotation	0.508	0.232	2.191	0.051	0.73	0.583	-0.002	1.019
StatMomPercent	-2.912	0.601	-4.848	0.001	0.73	0.583	-4.234	-1.590
StatMomMean	0.692	0.214	3.241	0.008	0.73	0.583	0.222	1.162
StatMomCount	-1.162	0.429	-2.708	0.020	0.73	0.583	-2.105	-0.218

$AUG_g$was significantly explained by the features AbsMov and StatMomPercent with 26.1% of total variance. Higher values of AUG_g were significantly predicted by lower values of the AbsMov and StatMomPercent features. The detailed results are given in Table 7.28.

Table 7.28: Regression analysis results predicting the cortisol AUG_g by arm features; β : regression coefficient, σ : standard error, adj : adjusted

Predictors	β	σ	T	p	R^2	adj-R^2	CI[2.5%]	CI[97.5%]
AbsMov	-1.187	0.506	-2.344	0.037	0.479	0.261	-2.290	-0.084
LFaSTDrotation	0.492	0.319	1.543	0.149	0.479	0.261	-0.203	1.187
StatMomPercent	-1.759	0.646	-2.725	0.018	0.479	0.261	-3.166	-0.352
StatMomMean	0.497	0.271	1.833	0.092	0.479	0.261	-0.094	1.089
StatMomCount	-0.868	0.538	-1.613	0.133	0.479	0.261	-2.042	0.305

Summary

The following Table 7.29 presents the adj-R^2 results of all regressions of the subsection, which included significant predictors.

Table 7.29: Summary of the regression analysis results (adj-R^2)

Independent variable	Head	Arms	Total body	Spine3	pca-bodypart-factors
STADI-State	40.5%	28.5%			
PANAS-NegAffect	51.9%	24.4%			26.5%
PANAS-PosAffect	69.4%	37.1%	18.9%		61.8%
PASA-Threat	61.4%	37.5%	28.2%		79.6%
PASA-Challenge		55.7%			
Δc_{max}	21.2%	58.3%			
AUG_g	26.7%	26.1%			

Chapter 8

Discussion

This chapter discusses the previously presented results. First, the TSST and f-TSST responses are evaluated, afterwards, the stress-induced movement changes. At last, the relationship between stress-induced movement alteration and the traditional assessment modalities biomarker and self-reports is presented.

8.1 Responses to TSST and f-TSST

The comparison of cortisol responses to the f-TSST and TSST, respectively, show that stress induction was successful and resulted in effective HPA axis activation. This is supported by a considerably increased cortisol concentration after the TSST compared to the f-TSST. On average, participants reached their maximum cortisol levels 20 min after the end of the TSST whereas no cortisol increase was observed after the f-TSST. These findings are supported by previous work [All14, Kud07]. These results are confirmed by the statistically significant differences in Δc_{max} and AUG_g values. Previous work with both conditions (TSST and f-TSST), as the one of Wiemers et al. 2013 [Wie13a] supports the results.

Comparing self-report variables with findings of other TSST studies, where the PASA was collected, a similar increase of the subscores PASA-Threat and PASA-Challenge was observed [Sto07, Wir07]. Comparing the STADI-State scores of the TSST and f-TSST, during the TSST, the score increased, which leads to an increased anxiety state during the stress condition. In contrast, the anxiety state during the f-TSST decreased. These findings fit with the observed cortisol response as a positive correlation between the cortisol response and state anxiety is expected [Osw04]. For the PANAS self-report, both scores were statistically significant between the two conditions. The TSST resulted in a decrease in positive affect, whereas the negative affect

increased as a response to the TSST. In contrast, the f-TSST caused an increase in positive affect and a slight decrease in negative affect. Both results indicate that the TSST leads to an effective induction of acute psychosocial stress, whereas the f-TSST did not [Wie15, Wie13b, Wie13a]. The previously discussed results indicate that the TSST and the f-TSST were carried out successfully and reproduced the results from the literature.

8.2 Psychosocial Stress-induced Movement changes

In addition to utilizing traditional assessment methods, such as biomarkers and self-reports, for measuring the response to acute psychosocial stress, the goal of this thesis was to examine whether changes in body posture and movement can be used for stress assessment. In general, the features extracted from the motion data show strong differences between TSST and f-TSST indicating that acute stress considerably affects body posture and movement. The mean velocity feature showed a significant reduction in all measured body parts between TSST and f-TSST. The velocity reduction leads to the assumption that the velocity of the motion was lower or fewer movements occurred during the stress condition. The significant STD features showed that the participants have fewer changes in the speed of their movements during the TSST condition.

Lower Extremity Movement changes

When comparing features extracted from lower extremity movement between TSST and f-TSST only the mean feature and the absolute movement features were significant for differentiating between the conditions of the lower extremities. For the mean velocity, the lower extremities feature had a low increase between TSST and f-TSST with just 31.85%. For the STD of speed feature and AbsMov feature, they were not statistically significant. This leads to the assumption that lower-extremity features may not be strongly affected by acute psychosocial stress. However, it can not be ruled out that differences in lower extremity movement between the two conditions occurred, such as posture changes, and were not reflected well by the choice of features. Alternatively, it might be that the motion capture suit was simply not able to record the, e.g., due to missing accuracy or because the drift compensation pipeline removed these differences from the original data. Another possible explanation might arise from the experiment design itself: During the (f-)TSSTthe participants were instructed to remain standing in front of the microphone. Thus, the participants kept a steady standing position and did not show strong leg movement or even moved around in front of the evaluators.

Upper Extremity Movement changes

When comparing features extracted from upper extremity movement between TSST and f-TSST, a big decrease in mean velocity, Std and AbsMov were observed, which results in slower and lower hand movement. These findings are in line with previous work, as a reduction in arm movement was observed with an IMU sensor under exposure to stress [Pis18]. The number of periods with static moments was lower for the TSST and the percentage of time without movement was higher, which resulted in decreased hand movement during the f-TSST. These findings are supported by the video analysis. In the videos, it was noticeable that the participants either put their hands folded in front of their body or kept their arms straight next to their body. It seems that the positioning of the hands depends on the individual person, as some participants did not bring the hands together in front of the body, whereas some did. The subjects who performed the described movement showed clear differences in the two conditions. The individual differences caused the feature of the hands to be not significantly different between the conditions among all participants. These findings indicate a reduction in arm movement and general slower movements with long periods without movement under the influence of stress.

Spine3 movement changes (body sway

The mean velocity reduction of the spine3 can be interpreted as a reduction in body sway over time, which is in line with previous studies, where the body sway was measured with an IMU attached to the thorax [Zit19]. These findings indicate that it is possible to distinguish between the condition using the IMU data of the spine3.

Total body movement changes

For the total body movements changes between the conditions the features mean of velocity, Std of velocity, and AbsMov were significant. These results indicate, that the subjects moved in general, less, slower, and with a lower variation in velocity during the stressed condition than during the control condition. It could be concluded, that the participants showed a so-called "freezing behavior" under exposure to stress. This confirms the result from literature as a freezing behavior during the TSST was reported [Dou18, Zit19].

Head movement changes

While evaluating the head movement changes between the two conditions a decrease in head velocity, Std of velocity, and AbsMov was noticeable, which results in a lower head movement

with a smaller velocity during the TSST. In the literature was reported, that sadness can be expressed by three types of movements; dropping the head, bringing the hands to the face and crossing arms in front of the body [Atk04]. The features for the head showed a clear reduction in head movement under the influence of stress. This is represented by a lower number of static moments with longer periods without any movement. The same situation applies to the hands as described in the section above. Observations of the video data showed that some participants were dropping their heads and some brought their hands to the face or head, but no features measuring these specific movements were calculated, as the number of participants who performed those certain movements was not sufficient. Based on the video data, those movements may indicate a relationship between sadness and stress. In further work with more participants, specific features for characterizing sadness could be calculated.

The STD of the velocity of the three axes was for all three significant between the two conditions, which shows that the subjects had a lower variation in the movement of the head. This indicates that the participant's movement with low differences in velocity. In addition, the sample entropy (SamEn) feature was evaluated to determine if the subjects had a less random movement pattern during the TSST condition. Due to enhanced dropping of the head, the SamEn features were significant for all three axes and the norm. The most increase of randomness between the TSST and the f-TSST was in the y-direction. In contrast to the velocity, where the z-axis points upwards, for the rotation, the y-axis pointed upwards, as velocity and rotation were measured in different coordinate systems. These findings show that the subjects looked more often to the right and the left. Comparing the mocap results with the video data results indicated, that the participants tried to avoid eye contact, which often resulted in the participants turning their heads diagonally upwards or downwards.

8.3 Relationship of Stress-induced variables and Movement

The last section of the discussion deals with the relationship between biomarkers and self-reports, and the motion changes. First, the prediction of movement changes by biomarkers and self-reports will be discussed. Afterwards, the prediction of the biomarkers and self-reports with the movement changes will be presented.

8.3.1 Prediction of PCA Motion Factor using Biomarkers and Self-Reports

While performing a backward multiple linear regression, it was observed that the PASA-Threat score explained 19.7% of variation of the PCA motion factor. The relationship between psycho-

logical stress and the PASA-Threat score has already been shown in the literature. Gaab et al. conducted a stress study for the validation of the PASA questionnaire, where they observed a significant correlation between PASA-Threat and cortisol AUG_g values. They suggested that threat could be a principal stimulus for the HPA axis from a biological point of view [Gaa05]. These findings support the regression result for the PCA motion factor and support the assumption that stress and movement correlate. In this thesis, the AUG_g was no significant predictor for the PCA motion factor, as it was expected based on the findings of Gaab et al.. They also mentioned that the retrospective perception of a situation is generally not suitable to explain cortisol responses [Gaa05]. A limitation could also be that a high number (81) of significant movement features were represented in only a single PCA motion factor.

The summary of the regression analysis results indicates that the participant's movement was highly influenced by their feelings of threat. These findings suggest that threat-associated movement was measured during the TSST condition. These findings are in line with previous work as threat induced by looking at angry faces or affective films was already brought into connection with a reduction in body sway and a so-called "freezing behavior" [Hag14, Roe10].

8.3.2 Prediction of Biomarkers and Self-Reports using PCA Motion Factors

While performing a stepwise backward multiple linear regression for predicting the biomarkers and self-reports with PCA motion factors for different body parts, only the PANAS-PosAffect (26.5% of variance), PANAS-NegAffect (61.8% of total variance), and the PASA-Threat (79.6% of total variance) were predicted by obtained PCA movement factors.

As PCA factors are abstract linear combinations, it is not possible to explain the linear correlation of the PCA movement factors with the biomarkers and self-reports. It is possible to observe which body parts predict the biomarkers and self-reports. As the only significant predictor for the PANAS-NegAffect was a PCA movement factor of the head, it seems that the negative affect is represented best by head movement changes. The PANAS-PosAffect was predicted significantly by two PCA movement factors of the head and one of the arms. This shows that the positive affect of the participants is also expressed by movements of the head and changes in arm movements, respectively. In contrast to the previous results, the PASA-Threat score was significantly predicted by four PCA factors of the head and one of the spine3. These findings obtain that the expression of threat is strongly visible by observing the head, but also body sway is a reliable indicator.

One of the PCA head movement factors (head-pca1) had a significant influence on all three scores as a regression predictor. Interestingly, it predicted in different directions. Higher values

of the v head movement factor change predicted a higher value of the PANAS-PosAffect score, whereas lower values of the factor predicted higher values of PANAS-NegAffect and PASA-Threat. This draws to the conclusion that the PCA factor predicts threat-associated feelings and negative affected feelings in one direction and positive affected feelings in the other direction. Together with previous findings of the thesis, it can be followed that the participants showed a movement reduction during the exposure to stress. It can be concluded that the positive affect was associated with an increased movement in the head and arms and the negative affect and the threat were associated with a head movement reduction.

Overall, it seems that the features of the head had the greatest influence on the prediction of stress, assessed by stress-related questionnaires. Features of the head significantly influenced the prediction of all three questionnaires, whereas the features of the spine3 and arms only could be linked to one of the three questionnaires.

8.3.3 Prediction of Biomarkers and Self-Reports using Movement changes

The regression results of the features of the body parts showed that the STADI-State was only significantly predicted by features of the head and arms. These features indicated that a higher anxiety state was associated by the head with few large movements, with long times in the same position, and by the arms with a few big movements, but in general less and slower movements.

The PANAS-NegAffect was also only predicted significantly by the features of the head and the arms. The results indicated, that a higher negative affect was associated with a lower number of times without movement of the arms and with a few slow movements and long times without any movement of the head.

The PANAS-PosAffect was predicted significantly by features of the head, the arms, and the total body. The features of the total body indicated that participants with a higher Positive Affect moved in general more. These findings are supported by the features of the head and the arms. The movement features of the arms showed that positive affect was associated with bigger movements, more time without movement and a shorter maximum time without movement, and by the head with more times without movement.

Significantly predictive for the PASA-Threat were features of total body, head, and arms. For the features of total body and arms, a higher threat feeling was indicated by a higher movement reduction, which indicates that the participants showed a freezing behavior, as already described in the sections above. The features of the head indicated a threat association with slower and fewer movements with similar movement patterns and without long periods without movement.

The PASA-Challenge scores were predicted by arm features only. It seems that more chal-

lenged participants showed longer periods without movement, but with a few faster movements of the arms. Unexpected was that the CV of one arm predicted negative and the other one positive. This contrast could be explained by the outlier problem as a deviation of the norm has a tremendous impact due to the small number of participants. In Table 8.1, the two predictors are given. Removing the outlier in the left corner of the right plot would result in a prediction in the same direction.

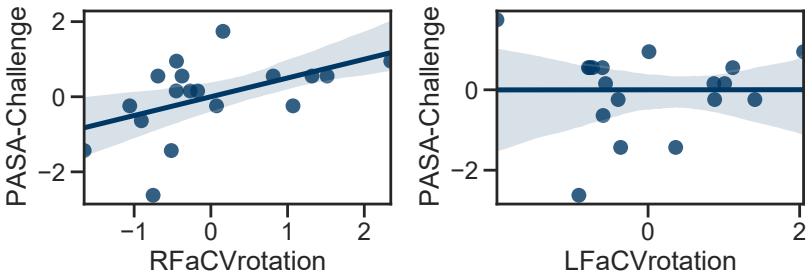

Figure 8.1: Significant predictors RFaCVrotation and LFaCVrotation

It seems like the participant had a higher STD than the mean, which leads to the assumption, that the participants made a few big movements. The analysis of the video data showed, that subjects who were challenged by the TSST condition may bring their arms together more often during the TSST condition, but due to the limited number of participants, further research is necessary for supporting this assumption.

The Δc_{max} was significantly predicted by features of the head and the arms. It seems like that the participants with a higher Δc_{max} showed a reduction in arm movement, with more static moments and a few faster movements. In addition, they showed an increasing STD in the rotation of the left arm, but not for the right one. The result of the head movement change indicates that a higher cortisol increase was associated with slower movement with a longer mean and maximum time of periods without movement.

For the AUG_g, again the head and arm features were significant predictors. The head movement changes indicated lower movements with longer mean time without movement but on average a higher absolute movement, which indicates few bigger movements. The movement change of the arms assumes that participants with a higher value performed a few low movements in the arms, with longer static moment periods. These findings support the freezing behavior under exposure to stress.

The summarised results are shown in Table 7.29. While comparing the adjusted-R^2 values, it seems that the self-report questionnaires were more predictive than the cortisol features. Addi-

tionally, the features of the heads obtained higher adjusted-R^2 values than the other ones. These findings indicate that the movement changes of the head are most suitable to predict psychological stress, measured by biomarkers and self-reports. Overall, arms and head obtained better results than arms, total body, and spine3. A possible explanation could be, that for both body parts, more features were evaluated than for the others. The features of the spine3 were not predictive for any self-report or biomarker. A reason could be those very small movements could not be detected by the mocap suit. Also filtering of the data due to the drift problem may have removed possible predictive movements.

Additionally, it is noticeable that the only significant predictor for the PASA-Challenge score was the movement features of the arms. Maybe the challenge is only expressed by the arms, but this had to be validated with a greater cohort.

Chapter 9

Conclusion and Outlook

The goal of the thesis was to investigate the influence of acute psychological stress on body posture and moment with a motion capture approach containing IMUs. Additionally, investigating whether body posture and movement can be used to predict the magnitude of an endocrinological stress response. For that reason, a stress study was conducted, containing a stress condition (TSST) and a non-stress condition (f-TSST). During the procedure, IMU motion data, saliva samples, and questionnaire data were collected. The collected data was used to develop a body posture and movement analysis pipeline that yielded 81 significant movement characteristics. Afterwards, several backward multiple linear regression analyses were performed to determine the relationship between body posture and movement and the traditional stress assessment modalities, such as biomarkers and self-reports.

Firstly, a backward multiple linear regression was performed to assess whether stress-induced movement alterations can be explained by changes in cortisol and psychological state variables. By predicting a PCA obtained motion factor by the biomarkers and self-report, the PASA-Threat, a threat-associated score, was identified as a significant predictor for the PCA obtained motion factor. The score predicted 19.7% of the total variance of the PCA motion factor. These findings validate the assumption that threat-related movement patterns were measured.

Secondly, the regression analysis was inverted to examine to which extent traditional stress assessment modalities can be predicted by changes of body posture and movement of different body parts. While performing multiple regression analysis, PCA movement factors obtained from different body parts were able to predict the PANAS-Negative-Affect (26.5% of variance), PANAS-Positive-Affect (61.8% of total variance), and the PASA-Threat (79.6% of total variance).

Afterwards, prediction of the self-reports and biomarkers by the extracted features of single body parts showed that the self-reports could be predicted better than the biomarkers. Additionally,

it was obtained, that features of the head were able to predict the highest percentage of the total variance of the self-reports and biomarkers. Just the features of the arms were able to predict all obtained biomarkers and self-reports significantly. With these findings, the study showed that it is possible to predict a psychological stress response assessed by self-reports and biomarkers, just with body posture and movement. Further research has to be conducted to validate these findings.

As a few limits occurred during this work, so there exist a few improvements that could be done in future research for a better understanding of the obtained results. For avoiding the drift problem, possibly using another motion capture system or approach could be helpful. Another room with possibly lower magnetic fields may also yield more precise data. Additionally, a study with more participants should be conducted to confirming or refuting the results of this study, as after excluding some participants due to missing datasets only 19 subjects remained for the analysis. Additionally, this study only measured the body posture and movement changes during the stress condition, and not the consequences of stress afterwards. One possibility for this could be performing a gait test like the TUG (Time up and go), after each condition. Like Lasselin et al. [Las20] did in their study, they obtained the motion changes during inflammation and obtained meaningful results with it.

Appendix A

Additional Tabels

Table A.1: Significance values of all generic features (Wilcoxon test)

Type	Body part	Channel	Axis	T(19)	p	Hedge's g
STD	head	vel	y	-6.534	0.000	-0.971
	left-hand	vel	norm	-3.608	0.006	-0.622
			x	-4.162	0.003	-0.785
	spine3	vel	y	-4.545	0.000	-0.673
	total-body	vel	norm	-3.909	0.003	-0.673
	upper-extrem	vel	norm	-4.014	0.003	-0.672
	head	rotation	norm	0.377	0.735	0.099
			y	2.841	0.024	0.704
			z	-1.673	0.180	-0.291
	right-fore-arm	rotation	norm	-1.587	0.194	-0.348
Mean	head	vel	norm	-7.097	0.000	-1.085
			y	-8.461	0.000	-1.196
	spine3	vel	y	-6.078	0.000	-0.872
	total-body	vel	norm	-5.007	0.000	-0.900
	head	rotation	norm	-0.8	0.521	-0.225
			x	0.391	0.727	0.116
			y	0.839	0.504	0.171
	right-fore-arm	rotation	norm	2.352	0.065	0.493
CV	head	vel	norm	3.242	0.011	0.750

			x	3.384	0.009	0.778
			z	-0.802	0.521	-0.204
	left-hand	vel	x	1.633	0.187	0.366
	right-hand	vel	norm	2.277	0.072	0.439
			x	1.886	0.130	0.402
			y	1.728	0.167	0.404
	spine3	vel	norm	0.971	0.438	0.239
			z	-1.138	0.352	-0.273
	total-body	vel	norm	1.57	0.194	0.330
	trunk	vel	norm	0.746	0.547	0.196
	upper-extrem	vel	norm	1.902	0.129	0.395
	head	rotation	norm	1.407	0.242	0.459
			x	0.792	0.522	0.200
			y	0.727	0.549	0.240
	right-fore-arm	rotation	norm	-3.502	0.006	-0.888
max-abs	left-hand	vel	norm	-1.341	0.266	-0.310
			y	-0.77	0.534	-0.165
			z	-1.885	0.130	-0.399
	right-hand	vel	norm	-1.462	0.230	-0.331
			z	-1.575	0.194	-0.350
	total-body	vel	norm	-0.636	0.599	-0.161
	upper-extrem	vel	norm	-0.798	0.521	-0.200
	head	rotation	y	1.177	0.334	0.268
			z	-3.191	0.014	-0.552
	right-fore-arm	rotation	norm	-1.054	0.391	-0.274
Mean	center-of-mass	-	y	-0.727	0.549	-0.053
CV	center-of-mass	-	z	-1.425	0.237	-0.481
entropy	head	rotation	norm	0.503	0.657	0.166
			x	0.899	0.471	0.262
			y	-0.157	0.891	-0.046
			z	1.117	0.359	0.307
		vel	norm	-0.652	0.592	-0.161
			x	1.232	0.311	0.333

NumCross0	head	vel	norm	NaN	NaN	NaN
			x	1.583	0.194	0.416
			y	1.884	0.130	0.586
			z	-2.37	0.062	-0.611
SamEn	head	vel	norm	-4.702	0.000	-1.126
			x	-2.267	0.072	-0.506
			y	-2.276	0.072	-0.551
		rotation	norm	-3.648	0.006	-0.879
			x	-3.047	0.018	-0.698
			z	-5.103	0.000	-1.238

Table A.2: Significance values of all generic features (t-test)

Type	**Body part**	**Channel**	**Axis**	**p**	**Hedge's g**	**Wilcoxon w**
STD	head	vel	norm	0.000	-0.744	16
			x	0.000	-0.884	4
			z	0.016	-0.570	34
	left-hand	vel	y	0.000	-0.626	17
			z	0.060	-0.464	46
	lower-extrem	vel	norm	0.359	-0.302	75
	right-hand	vel	norm	0.003	-0.717	23
			x	0.003	-0.828	19
			y	0.000	-0.860	12
			z	0.040	-0.538	42
	spine3	vel	norm	0.078	-0.534	50
			x	0.003	-0.624	21
			z	0.022	-0.534	37
	trunk	vel	norm	0.130	-0.488	57
	head	rotation	x	0.657	0.070	91
	left-fore-arm	rotation	norm	0.000	-1.078	10
	left-leg	rotation	norm	0.071	-0.474	48
	right-leg	rotation	norm	0.621	-0.154	89

Mean	head	vel	x	0.000	-0.993	4
			z	0.127	-0.247	56
	left-hand	vel	norm	0.006	-0.721	25
			x	0.000	-0.846	11
			y	0.000	-0.714	13
			z	0.060	-0.470	46
	lower-extrem	vel	norm	0.011	-0.603	31
	right-hand	vel	norm	0.000	-0.868	16
			x	0.000	-0.906	11
			y	0.000	-0.969	7
			z	0.072	-0.541	49
	spine3	vel	norm	0.000	-0.681	13
			x	0.011	-0.535	31
			z	0.194	-0.168	64
	trunk	vel	norm	0.003	-0.612	20
	upper-extrem	vel	norm	0.000	-0.868	13
	head	rotation	z	0.441	0.279	79
	left-fore-arm	rotation	norm	0.190	-0.474	63
	left-leg	rotation	norm	0.194	-0.475	64
	right-leg	rotation	norm	0.704	-0.173	93
CV	head	vel	y	0.003	0.938	22
	left-hand	vel	norm	0.232	0.391	67
			y	0.243	0.421	68
			z	0.232	0.420	67
	lower-extrem	vel	norm	0.325	0.332	73
	right-hand	vel	z	0.097	0.466	53
	spine3	vel	x	0.592	0.066	87
			y	0.072	0.529	49
	head	rotation	z	0.592	0.135	87
	left-fore-arm	rotation	norm	0.000	-0.819	15
	left-leg	rotation	norm	0.745	-0.014	95
	right-leg	rotation	norm	0.258	-0.348	69
max-abs	head	vel	norm	0.477	-0.313	81
			x	0.000	-0.833	4

			y	0.232	-0.394	67
			z	0.908	-0.030	101
	left-hand	vel	x	0.181	-0.384	62
	lower-extrem	vel	norm	0.956	0.049	103
	right-hand	vel	x	0.026	-0.596	38
			y	0.055	-0.437	45
	spine3	vel	norm	0.657	-0.083	91
			x	0.084	-0.602	51
			y	0.621	-0.032	89
			z	0.549	0.133	85
	trunk	vel	norm	0.704	-0.011	93
	head	rotation	norm	0.657	-0.242	91
			x	0.745	-0.267	95
	left-fore-arm	rotation	norm	0.000	-1.095	7
	left-leg	rotation	norm	0.621	-0.071	89
	right-leg	rotation	norm	0.311	-0.244	72
STD	center-of-mass	-	norm	0.163	-0.262	60
			x	0.190	-0.473	63
			y	0.022	-0.581	37
			z	0.194	-0.445	64
Mean	center-of-mass	-	norm	0.644	0.278	90
			x	0.174	-0.450	61
			z	0.608	0.103	88
CV	center-of-mass	-	norm	0.078	-0.353	50
			x	0.621	-0.310	89
			y	0.022	-0.578	37
entropy	head	vel	y	0.223	0.325	66
			z	0.181	0.340	62
abs-energy	head	vel	norm	0.000	-0.772	2
			x	0.000	-0.683	10
			y	0.000	-0.854	3
			z	0.091	-0.256	52
	left-hand	vel	norm	0.011	-0.598	31

			x	0.003	-0.716	20
			y	0.003	-0.465	22
			z	0.084	-0.433	51
	right-hand	vel	norm	0.003	-0.708	22
			x	0.003	-0.668	22
			y	0.000	-0.791	14
			z	0.072	-0.501	49
	spine3	vel	norm	0.003	-0.469	21
			x	0.016	-0.398	33
			y	0.000	-0.529	18
			z	0.097	-0.187	53
	total-body	vel	norm	0.011	-0.561	31
			x	0.011	-0.475	31
			y	0.020	-0.489	36
			z	0.048	-0.519	44
	upper-extrem	vel	norm	0.003	-0.617	22
			x	0.000	-0.638	11
			y	0.003	-0.566	23
			z	0.097	-0.490	53
SamEn	head	vel	z	0.608	-0.025	88
		rotation	y	0.000	-1.882	1

Table A.3: Significance levels of all expert features (t-test)

Feature	**Type**	**Body part**	**Channel**	**Axis**	**T(19)**	**p**	**Hedge's g**
AbsMov	-	total-body	pos-global	norm	-2.953	0.020	-0.652
		upper-extrem	pos-global	norm	-3.515	0.006	-0.763
StatMom	percent	head	vel	norm	10.067	0.000	1.325
	count	head	vel	norm	-7.323	0.000	-1.361

Table A.4: Significance values of all expert features (Wilcoxon test)

Feature	Type	Body-part	Channel	Axis	Wilcoson w	p	Hedges'g
AbsMov	-	head	pos-global	norm	11	0.000	-0.663
		lower-extrem	pos-global	norm	59	0.153	-0.315
		trunk	pos-global	norm	15	0.000	-0.631
StatMom	percent	hands	vel	norm	26	0.006	0.768
	Mean	head	vel	norm	0	0.000	0.788
		hands	vel	norm	26	0.006	0.544
	count	hands	vel	norm	13	0.000	-0.919
	max	head	vel	norm	0	0.000	1.412
		hands	vel	norm	6	0.000	1.314
distance	Mean	hands	pos-global	distance	62	0.181	-0.283
	var	hands	pos-global	distance	80	0.459	-0.131
	STD	hands	pos-global	distance	80	0.459	-0.219
TimeTogether	percent	hands	pos-global	distance	4	0.177	0.329
	count	hands	pos-global	distance	13	0.938	0.030
	Mean	hands	pos-global	distance	3	0.130	0.526
	max	hands	pos-global	distance	1	0.072	0.582

Appendix B

Additional Figures

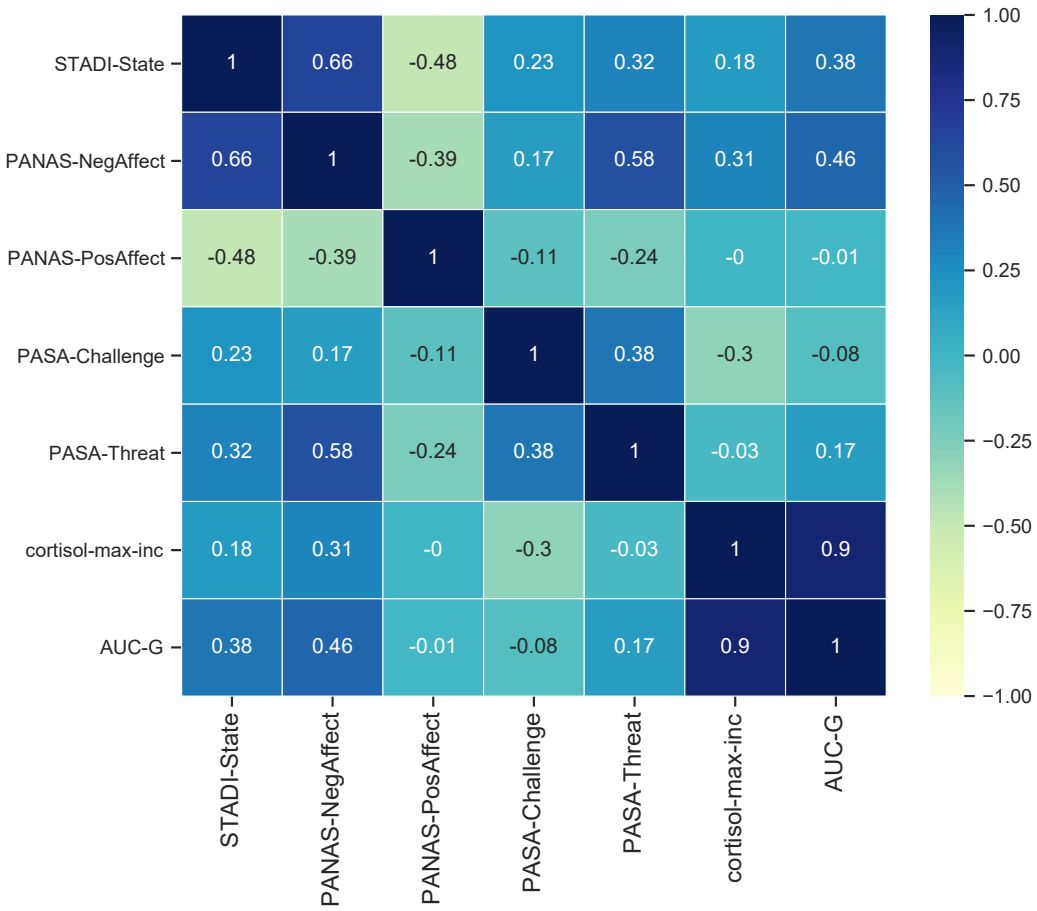

Figure B.1: Correlation heaptmap of the predictors for the regression analysis for predicting a PCA motion factor by biomarkers and self-reports.

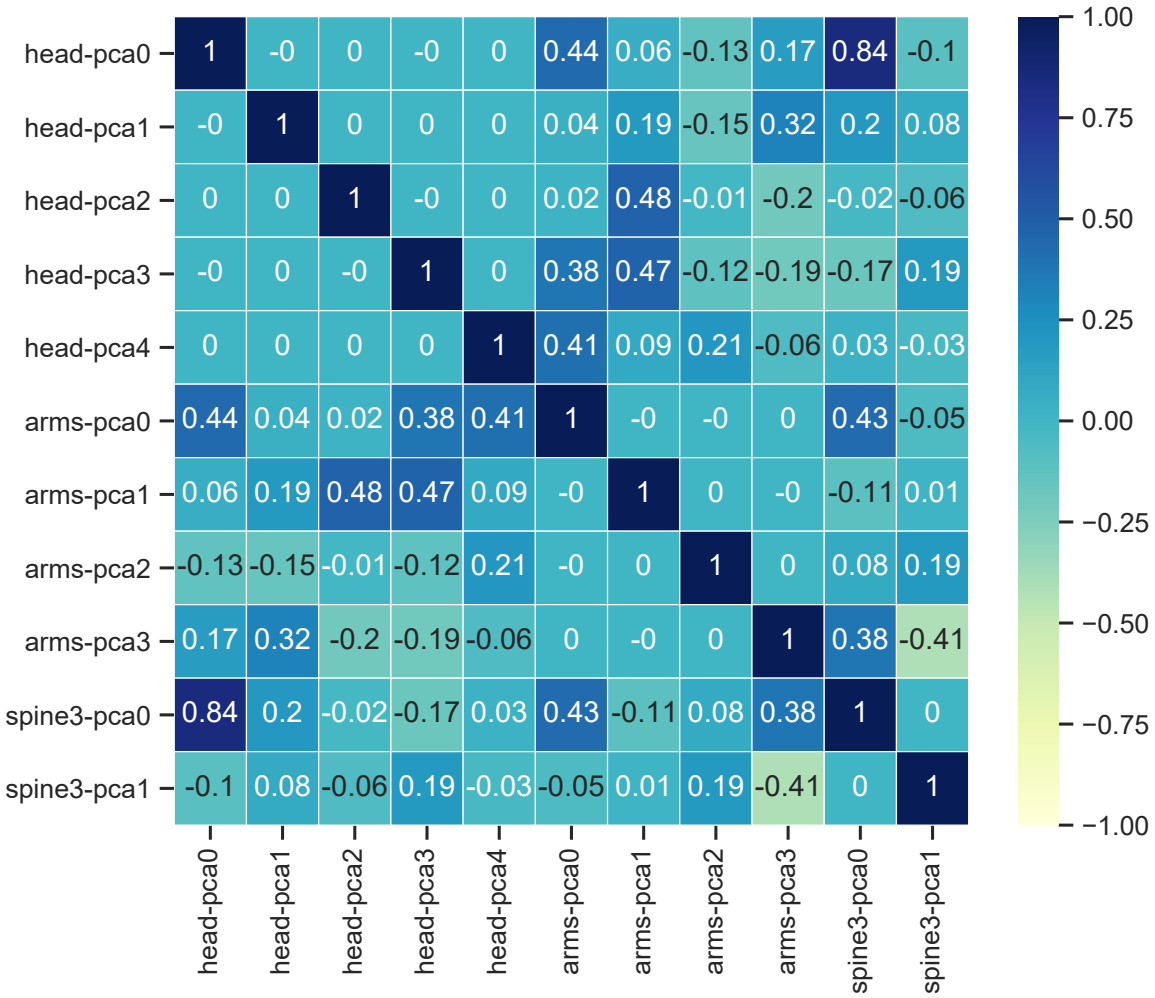

Figure B.2: Correlation heatmap of the predictors for the regression analysis for predicting the biomarker and self-reports using the PCA motion factors per body part.

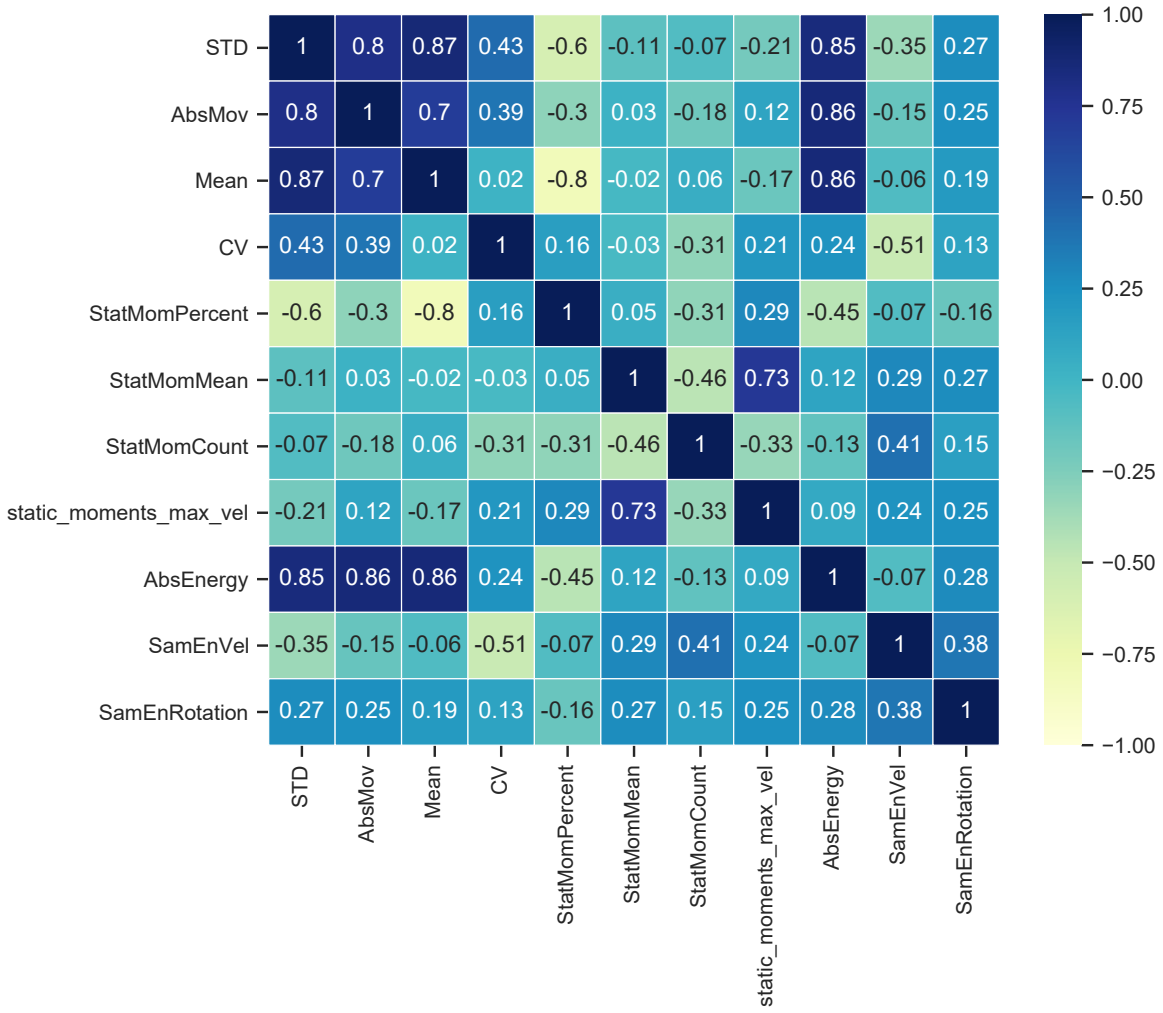

Figure B.3: Correlation heatmap of the predictors for the regression analysis for predicting the biomarker and self-reports using the features of the head.

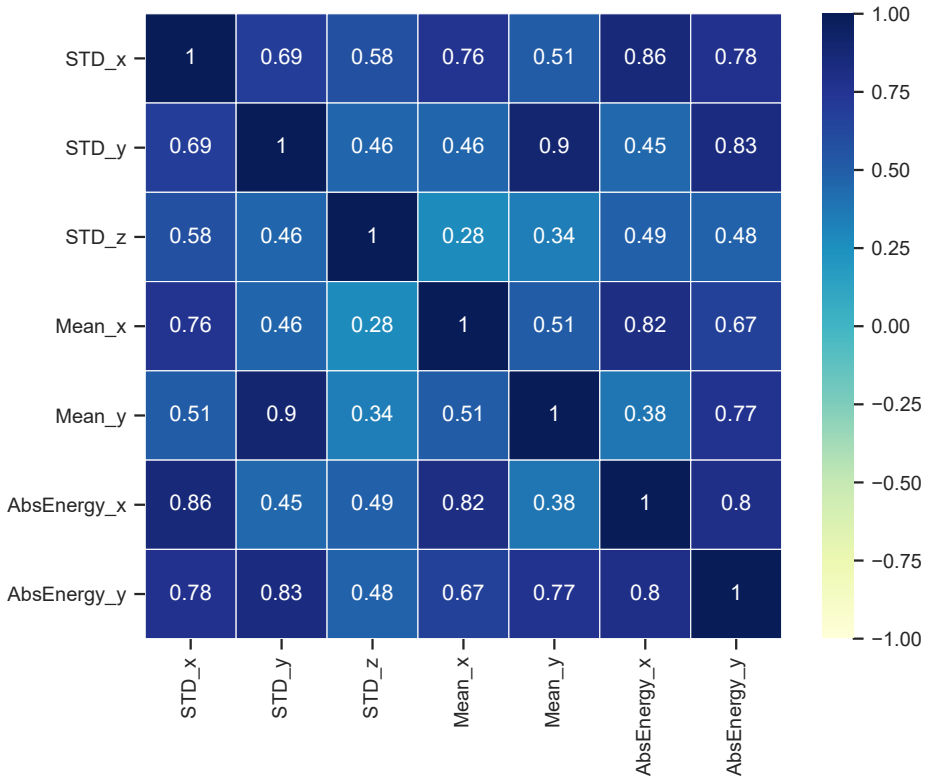

Figure B.4: Correlation heatmap of the predictors for the regression analysis for predicting the biomarker and self-reports the features of the spine3.

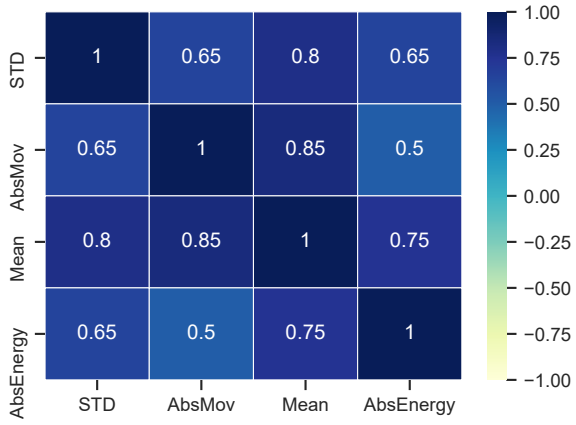

Figure B.5: Correlation heatmap of the predictors for the regression analysis for predicting the biomarker and self-reports the features of the total body.

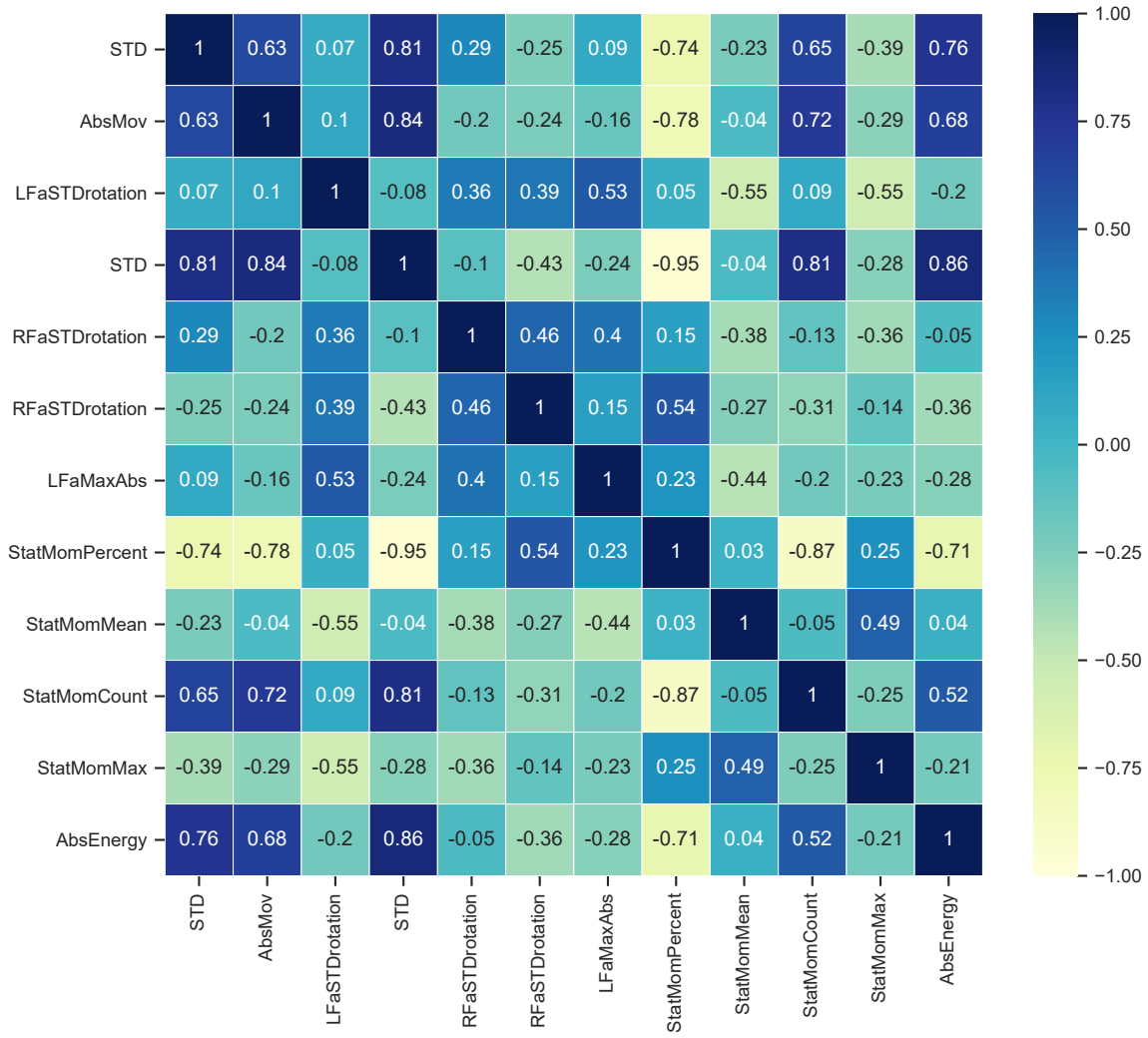

Figure B.6: Correlation heatmap of the predictors for the regression analysis for predicting the biomarker and self-reports the features of the arms.

Glossary

AUG_g area under the curve with respect to ground

Δc_{max} maximum cortisol increase

(f-)TSST f-TSST and TSST

abs-energy absolute energy

AbsMov absolute movement

ACTH adrenocorticotropin hormone

ANS autonomous nervous system

BVH Biovision Hierarchy character animation file format

CALC Calculation file format

CRH corticotropin-releasing hormone

CV coefficient of variation

f-TSST friendly version of the Trier Social Stress Test

HPA hypothalamic-pituitary-adrenocortical

IMU Inertial Measurement Units

LFaCVrotation CV of Left forearms rotation

LFaMaxRotation max of Left forearms rotation

LFaSTDrotation Std of Left forearms rotation

max-abs absolute maximum

MIST Montreal Imaging Stress Task

mocap motion capture

NumCross0 number crossing 0

PANAS Positive and Negative Affect Schedule

PANAS-NegAffect PANAS-Negative-Affect

PANAS-PosAffect PANAS-Positive-Affect

PASA Primary Appraisal Secondary Appraisal Questionnaire

PCA Principal Component Analysis

PSNS parasympathetic nervous system

RFaCVrotation CV of Right forearms rotation

RFaSTDrotation Std of Right forearms rotation

SamEn sample entropy

SNS sympathetic nervous system

STADI State-Trait Anxiety-Depression Inventory

StatMom Static Moments

StatMomCount Static Moments Count

StatMomMax Static Moments Max

StatMomMean Static Moments Mean

StatMomPercent Static Moments Percent

Std standard deviation

TSST Trier Social Stress Test

Wn critical frequency

List of Figures

List of Tables

Listings

Bibliography

[Aig15] Aigrain, Jonathan and Dubuisson, Severine and Detyniecki, Marcin and Chetouani, Mohamed. Person-specific behavioural features for automatic stress detection. In *2015 11th IEEE International Conference and Workshops on Automatic Face and Gesture Recognition (FG)*, pages 1–6, Ljubljana, May 2015. Ieee.

[All14] Allen, Andrew P. and Kennedy, Paul J. and Cryan, John F. and Dinan, Timothy G. and Clarke, Gerard. Biological and psychological markers of stress in humans: Focus on the Trier Social Stress Test. *Neuroscience & Biobehavioral Reviews*, 38:94–124, January 2014.

[Ant17] Antoun, Michael and Edwards, Kate M. and Sweeting, Joanna and Ding, Ding. The acute physiological stress response to driving: A systematic review. *Plos One*, 12(10):e0185517, October 2017.

[Atk04] Atkinson, Anthony P and Dittrich, Winand H and Gemmell, Andrew J and Young, Andrew W. Emotion Perception from Dynamic and Static Body Expressions in Point-Light and Full-Light Displays. *Perception*, 33(6):717–746, June 2004.

[Bal15] Bali, Anjana and Jaggi, Amteshwar Singh. Clinical experimental stress studies: methods and assessment. *Reviews in the Neurosciences*, 26(5):555–579, October 2015.

[Cha05] Charmandari, Evangelia and Tsigos, Constantine and Chrousos, George. Endocrinology Of The Stress Response. *Annual Review of Physiology*, 67(1):259–284, March 2005.

[Che17] Chen, Xuejie and Gianferante, Danielle and Hanlin, Luke and Fiksdal, Alexander and Breines, Juliana G. and others. HPA-axis and inflammatory reactivity to acute stress is related with basal HPA-axis activity. *Psychoneuroendocrinology*, 78:168–176, April 2017.

[Coh07] Cohen, Sheldon and Janicki-Deverts, Denise and Miller, Gregory E. Psychological Stress and Disease. *Jama*, 298(14):1685, October 2007.

[Ded05] Dedovic, Katarina and Renwick, Robert and Mahani, Najmeh Khalili and Engert, Veronika and Lupien, Sonia J and others. The Montreal Imaging Stress Task: using functional imaging to investigate the effects of perceiving and processing psychosocial stress in the human brain. *J Psychiatry Neurosci*, page 7, July 2005.

[Dic04] Dickerson, Sally S. and Kemeny, Margaret E. Acute Stressors and Cortisol Responses: A Theoretical Integration and Synthesis of Laboratory Research. *Psychological Bulletin*, 130(3):355–391, 2004.

[Dou18] Doumas, Michail and Morsanyi, Kinga and Young, William R. Cognitively and socially induced stress affects postural control. *Experimental Brain Research*, 236(1):305–314, January 2018.

[Dut12] Dutta, Tilak. Evaluation of the Kinect sensor for 3-D kinematic measurement in the workplace. *Applied Ergonomics*, 43(4):645–649, July 2012.

[Epe18] Epel, Elissa S. and Crosswell, Alexandra D. and Mayer, Stefanie E. and Prather, Aric A. and Slavich, George M. and others. More than a feeling: A unified view of stress measurement for population science. *Frontiers in Neuroendocrinology*, 49:146–169, April 2018.

[Eur17] European Commission. Safer and Healthier Work for All - Modernisation of the EU Occupational Safety and Health Legislation and Policy, January 2017.

[Fin16] Fink, G. Stress, Definitions, Mechanisms, and Effects Outlined. In *Stress: Concepts, Cognition, Emotion, and Behavior*, pages 3–11. Elsevier, 2016.

[Fol10] Foley, Paul and Kirschbaum, Clemens. Human hypothalamus-pituitary-adrenal axis responses to acute psychosocial stress in laboratory settings. *Neuroscience & Biobehavioral Reviews*, 35(1):91–96, September 2010.

[Gaa05] Gaab, J. and Rohleder, N. and Nater, U.M. and Ehlert, U. Psychological determinants of the cortisol stress response: the role of anticipatory cognitive appraisal. *Psychoneuroendocrinology*, 30(6):599–610, July 2005.

[Hag14] Hagenaars, Muriel A. and Roelofs, Karin and Stins, John F. Human freezing in response to affective films. *Anxiety, Stress, & Coping*, 27(1):27–37, January 2014.

[Het09] Het, S. and Rohleder, N. and Schoofs, D. and Kirschbaum, C. and Wolf, O.T. Neuroendocrine and psychometric evaluation of a placebo version of the 'Trier Social Stress Test'. *Psychoneuroendocrinology*, 34(7):1075–1086, August 2009.

[Igl93] Iglewicz, Boris and Hoaglin, David C. *How to detect and handle outliers*. Number v. 16 in ASQC basic references in quality control. ASQC Quality Press, Milwaukee, Wis, 1993.

[Jan17] Janson, Johanna and Rohleder, Nicolas. Distraction coping predicts better cortisol recovery after acute psychosocial stress. *Biological Psychology*, 128:117–124, September 2017.

[Jol16] Jolliffe, Ian T. and Cadima, Jorge. Principal component analysis: a review and recent developments. *Philosophical Transactions of the Royal Society A: Mathematical, Physical and Engineering Sciences*, 374(2065):20150202, April 2016.

[Kir93] Kirschbaum, Clemens and Pirke, Karl-Martin and Hellhammer, Dirk H. The 'Trier Social Stress Test' - A Tool for Investigating Psychobiological Stress Responses in a Laboratory Setting. *Neuropsychobiology*, 28(1-2):76–81, 1993.

[Kir94] Kirschbaum, Clemens and Hellhammer, Dirk H. Salivary cortisol in psychoneuroendocrine research: Recent developments and applications. *Psychoneuroendocrinology*, 19(4):313–333, January 1994.

[Kud07] Kudielka, Brigitte M and Hellhammer, Dirk H and Kirschbaum, Clemens. Ten years of research with the Trier Social Stress Test (TSST) - revisited. page 36, January 2007.

[Las20] Lasselin, J. and Sundelin, T. and Wayne, P.M. and Olsson, M.J. and Paues Göranson, S. and others. Biological motion during inflammation in humans. *Brain, Behavior, and Immunity*, 84:147–153, February 2020. tex.ids: Lasselin2019 publisher: Elsevier Inc.

[Lew04] Lewis-Beck, Michael and Bryman, Alan and Futing Liao, Tim. Standardized Regression Coefficients. In *The SAGE Encyclopedia of Social Science Research Methods*. Sage Publications, Inc., 2455 Teller Road, Thousand Oaks California 91320 United States of America, 2004.

[Lot13] Lothar Laux and Michael Hock and Ralf Bergner-Köther and Volker Hodapp and Karl-Heinz Renner. *STDI - Das State-Traite-Angst_depression_Inventar*. Hogrefe, 2013 edition, 2013.

[McC07] McCorry, Laurie Kelly. Physiology of the Autonomic Nervous System. *American Journal of Pharmaceutical Education*, page 11, March 2007.

[Mer01] Meredith, M and Maddock, S. Motion Capture File Formats Explained. page 36, January 2001.

[Nae19] Naeemabadi, Mreza and Dinesen, Birthe and Andersen, Ole Kaeseler and Hansen, John. Influence of a Marker-Based Motion Capture System on the Performance of Microsoft Kinect v2 Skeleton Algorithm. *IEEE Sensors Journal*, 19(1):171–179, January 2019.

[Nat21] NaturalPoint, Inc. Opitrack. *https://optitrack.com/*, July 2021. Accessed: 17.07.2021.

[Noi20] Noitom. Axis Neuron User Manual, 2020.

[Noi21] Noitom. Neuron MOCAP. *https://neuronmocap.com/perception-neuron-series*, July 2021. Accessed: 17.07.2021.

[Osw04] Oswald, Lynn M. and Mathena, Joanna R. and Wand, Gary S. Comparison of HPA axis hormonal responses to naloxone vs psychologically-induced stress. *Psychoneuroendocrinology*, 29(3):371–388, 2004.

[P. 16] P. Vatcheva, Kristina and Lee, MinJae. Multicollinearity in Regression Analyses Conducted in Epidemiologic Studies. *Epidemiology: Open Access*, 06(02), 2016.

[Pfi14] Pfister, Alexandra and West, Alexandre M. and Bronner, Shaw and Noah, Jack Adam. Comparative abilities of Microsoft Kinect and Vicon 3D motion capture for gait analysis. *Journal of Medical Engineering & Technology*, 38(5):274–280, July 2014.

[Pis18] Pisanski, Katarzyna and Kobylarek, Aleksander and Jakubowska, Luba and Nowak, Judyta and Walter, Amelia and others. Multimodal stress detection: Testing for covariation in vocal, hormonal and physiological responses to Trier Social Stress Test. *Hormones and Behavior*, 106:52–61, November 2018. tex.ids: Pisanski2018.

[Pru03] Pruessner, Jens C. and Kirschbaum, Clemens and Meinlschmid, Gunther and Hellhammer, Dirk H. Two formulas for computation of the area under the curve represent measures of total hormone concentration versus time-dependent change. *Psychoneuroendocrinology*, 28(7):916–931, October 2003.

[Rea21] Reallusion Inc. Kinect MOCAP. *https://www.reallusion.com/de/iclone/mocap/default.html*, July 2021. Accessed: 17.07.2021.

[Ric00] Richman, Joshua S. and Moorman, J. Randall. Physiological time-series analysis using approximate entropy and sample entropy. *American Journal of Physiology-Heart and Circulatory Physiology*, 278(6):H2039–h2049, June 2000.

[Roe10] Roelofs, Karin and Hagenaars, Muriel A. and Stins, John. Facing Freeze: Social Threat Induces Bodily Freeze in Humans. *Psychological Science*, 21(11):1575–1581, November 2010.

[Roh04] Rohleder, Nicolas and Nater, Urs M. and Wolf, Jutta M. and Ehlert, Ulrike and Kirschbaum, Clemens. Psychosocial Stress-Induced Activation of Salivary Alpha-Amylase: An Indicator of Sympathetic Activity? *Annals of the New York Academy of Sciences*, 1032(1):258–263, December 2004.

[Roh12] Rohleder, Nicolas. Acute and chronic stress induced changes in sensitivity of peripheral inflammatory pathways to the signals of multiple stress systems - 2011 Curt Richter Award Winner. *Psychoneuroendocrinology*, 37(3):307–316, March 2012.

[Ser20] Sers, Ryan and Forrester, Steph and Moss, Esther and Ward, Stephen and Ma, Jianjia and others. Validity of the Perception Neuron inertial motion capture system for upper body motion analysis. *Measurement*, 149:107024, January 2020.

[Sha19] Sharma, Shubham and Verma, Shubhankar and Kumar, Mohit and Sharma, Lavanya. Use of Motion Capture in 3D Animation: Motion Capture Systems, Challenges, and Recent Trends. In *2019 International Conference on Machine Learning, Big Data, Cloud and Parallel Computing (COMITCon)*, pages 289–294, Faridabad, India, February 2019. Ieee.

[Shi16] Shields, Grant S and Sazma, Matthew A and Yonelinas, Andrew P. The effects of acute stress on core executive functions: A meta-analysis and comparison with cortisol. *Neuroscience and biobehavioral reviews*, 68:651–668, September 2016. Edition: 2016/06/28.

[Sto07] Storch, Maja and Gaab, Jens and Küttel, Yvonne and Stüssi, Ann-Christin and Fend, Helmut. Psychoneuroendocrine effects of resource-activating stress management training. *Health Psychology*, 26(4):456–463, 2007.

[Ulr09] Ulrich-Lai, Yvonne M. and Herman, James P. Neural regulation of endocrine and autonomic stress responses. *Nature Reviews Neuroscience*, 10(6):397–409, June 2009.

[van19] van der Zee, Sophie and Poppe, Ronald and Taylor, Paul J. and Anderson, Ross. To freeze or not to freeze: A culture-sensitive motion capture approach to detecting deceit. *Plos One*, 14(4):e0215000, April 2019.

[Vla07] Vlasic, Daniel and Adelsberger, Rolf and Vannucci, Giovanni and Barnwell, John and Gross, Markus and others. Practical motion capture in everyday surroundings. *ACM Transactions on Graphics*, 26(3):35, July 2007.

[Wat88] Watson, David and Anna, Lee and Tellegen, Auke. Development and Validation of Brief Measures of Positive and Negative Affect: The PANAS Scales. page 8, 1988.

[Wie13a] Wiemers, Uta S. and Sauvage, Magdalena M. and Schoofs, Daniela and Hamacher-Dang, Tanja C. and Wolf, Oliver T. What we remember from a stressful episode. *Psychoneuroendocrinology*, 38(10):2268–2277, 2013.

[Wie13b] Wiemers, Uta S. and Schoofs, Daniela and Wolf, Oliver T. A friendly version of the Trier Social Stress Test does not activate the HPA axis in healthy men and women. *Stress*, 16(2):254–260, March 2013.

[Wie15] Wiemers, Uta S. and Wolf, Oliver T. Cortisol broadens memory of a non-stressful social interaction. *Psychopharmacology*, 232(10):1727–1733, May 2015.

[Wik21] Wikipedia. Kinect. *https://upload.wikimedia.org/wikipedia/commons/6/67/Xbox-360-Kinect-Standalone.png*, July 2021. Accessed: 17.07.2021.

[Wir07] Wirtz, Petra H. and Känel, Roland von and Emini, Luljeta and Suter, Tobias and Fontana, Adriano and others. Variations in anticipatory cognitive stress appraisal and differential proinflammatory cytokine expression in response to acute stress. *Brain, Behavior, and Immunity*, 21(6):851–859, August 2007.

[Xse21] Xsens North America Inc. Xsens. *https://www.xsens.com/products/mvn-analyze*, July 2021. Accessed: 17.07.2021.

[Zho08] Zhou, Huiyu and Hu, Huosheng. Human motion tracking for rehabilitation–A survey. *Biomedical Signal Processing and Control*, 3(1):1–18, January 2008.

[Zhu16] Zhu, Xudong and Li, Kin Fun. Real-Time Motion Capture: An Overview. In *2016 10th International Conference on Complex, Intelligent, and Software Intensive Systems (CISIS)*, pages 522–525, Fukuoka, Japan, July 2016. Ieee.

[Zit19] Zito, Giuseppe Angelo and Apazoglou, Kallia and Paraschiv-Ionescu, Anisoara and Aminian, Kamiar and Aybek, Selma. Abnormal postural behavior in patients with functional movement disorders during exposure to stress. *Psychoneuroendocrinology*, 101:232–239, March 2019. tex.ids: Zito2019a.